ΠΑΝΕΠΙΣΤΗΜΙΟ ΘΕΣΣΑΛΙΑΣ

ΠΟΛΥΤΕΧΝΙΚΗ ΣΧΟΛΗ

ΤΜΗΜΑ ΜΗΧΑΝΟΛΟΓΩΝ ΜΗΧΑΝΙΚΩΝ

Διπλωματική Εργασία

Simulation of micropolar fluid flows: validation of numerical results with analytical solutions

Υπό:

Θωμά Μανώλη

Θεοδόση Κουτσούκο

Υπεβλήθη για την εκπλήρωση μέρους των

απαιτήσεων για την απόκτηση του

Διπλώματος Μηχανολόγου Μηχανικού

ΒΟΛΟΣ 2018

Εγκρίθηκε από τα Μέλη της Τριμελούς Εξεταστικής Επιτροπής:

Πρώτος Εξεταστής	**Δρ. Τσιακάρας Παναγιώτης**
(Επιβλέπων)	**Καθηγητής, Τμήμα Μηχανολόγων Μηχανικών, Πανεπιστήμιο Θεσσαλίας**
Δεύτερος Εξεταστής	**Δρ. Χαραλάμπους Γεώργιος**
	Επίκουρος Καθηγητής, Τμήμα Μηχανολόγων Μηχανικών, Πανεπιστήμιο Θεσσαλίας
Τρίτος Εξεταστής	
	_____, Τμήμα Μηχανολόγων Μηχανικών, Πανεπιστήμιο Δυτικής Αττικής

Ευχαριστίες

Αρχικά θα θέλαμε να ευχαριστήσουμε τον κ. Αθανάσιο Παπαθανασίου, καθηγητή στο τμήμα Μηχανολόγων Μηχανικών του Πανεπιστημίου Θεσσαλίας και επιβλέποντα καθηγητή αυτής της εργασίας, για το κίνητρο, την ώθηση και τις συμβουλές που πρόσφερε, καθώς και για την καθοδήγηση για την εκπλήρωση αυτής της εργασίας.

Παράλληλα, θα θέλαμε ολόψυχα να ευχαριστήσουμε τον κ. Ιωάννη Σαρρή, επίκουρο καθηγητή στο Πανεπιστήμιο Δυτικής Αττικής, για τη δημιουργία του, αναγκαίου για αυτήν την εργασία, micropolarFoam solver, αλλά και για τη πολύτιμη βοήθεια που μας πρόσφερε σε αυτή την εργασία.

Επιπλέον, θα θέλαμε να ευχαριστήσουμε τον Ανδρέα Τσιαντή, για την υποστήριξή του και για τις συμβουλές που έδωσε σχετικά με το λογισμικό OpenFOAM, και τον κ Παναγιώτη Τσιακάρα, καθηγητή του τμήματος Μηχανολόγων Μηχανικών του Πανεπιστημίου Θεσσαλίας, για την πολύτιμη βοήθειά του στα τελικά στάδια εκπλήρωσης αυτής της εργασίας.

Τέλος, θα θέλαμε και οι δυο να ευχαριστήσουμε τις οικογένειές που υποστήριξαν τις προσπάθειές μας όλα αυτά τα χρόνια τόσο σε υλικό όσο και ψυχολογικό επίπεδο.

Simulation of micropolar fluid flows: validation of numerical results with analytical solutions

Θεοδόσης Κουτσούκος

Θωμάς Μανώλης

Τμήμα Μηχανολόγων Μηχανικών, Πανεπιστήμιο Θεσσαλίας

Επιβλέπων Καθηγητής: Παναγιώτης Τσιακάρας

Καθηγητής, Τμήμα Μηχανολόγων Μηχανικών, Πανεπιστήμιο Θεσσαλίας

Abstract

In this study, two micropolar fluid flows are simulated using the OpenFOAM software, in order to test the validity of the micropolarFoam solver and to investigate the fluid behavior under changing parameters. For each type of flow, namely Couette and Poiseuille flow, several cases are examined and the numerical results are consistently found to be in agreement with the corresponding analytical solutions. Additionally, the effect of specific micropolar parameters on the flow attributes, is detailed for both flow types through a parametric analysis.

Περιεχόμενα

CHAPTER 1 INTRODUCTION

1.1 Basic concepts

Matter can be found in nature in a solid, liquid or gas state. These are referred to as the three stages of matter. Solids are characterized by having defined shape and volume, liquids can alter their shape but have consistent volume and, finally, gases have the ability to alter both their shape and volume. Gases and liquids deform continuously when subjected to shear stress, they are thus defined as fluids. Fluids are made up of randomly oriented molecules, held together by weak cohesion forces. Flow, the characteristic property of fluids, represents the continuous and irrecoverable change of position of their molecules relative to one another when under shear stress. The degree of deformation that a fluid exhibits when put under stress is dependent on a quantity called viscosity [1]. In science, the discipline that involves the understanding, predicting and controlling the patterns of fluid flow is called Fluid Mechanics. Because it provides an effective methodology for the study of fluids, Fluid Mechanics evidently branches into many scientific fields, like Physics, Astrophysics, Medicine, Biology, Chemistry, Aeronautics, etc {2].

There are several types and categories of fluids, possessing a variety of properties and characterized by varying equations. Fluids in which the viscous shear stress is analogous to the rate of angular deformation, are termed Newtonian; the proportionality constant corresponds to the viscosity of the fluid. In contrast, many fluids do not present a linear relationship between the viscous shear stress and the deformation rate; these are defined as non-Newtonian.

The majority of flow phenomena are described by the standard Navier-Stokes equations. However, many of the parameters involved in the relationships exhibit non-linear behavior; for these, analytical solutions cannot be applied. To overcome this inconvenience,

researchers resort to the application of numerical methods in order to explore the flow phenomena. Computational Fluid Mechanics is the scientific discipline that aims in the study and analysis of systems involving flow (of fluid or heat), along with related phenomena, such as diffusion, convection, dispersion and boundary layers, which are studied through computational simulations. Computational Fluid Mechanics encompasses the development and implementation of methods that employ computational codes as their tool.

A specific category of fluids involves fluids containing microelements and possessing internal microstructure. These materials present properties that cannot be described by the classical Fluid Mechanics. In order to interpret their behavior, it was necessary to develop theoretical concepts that would take into account the geometrical characteristics, deformation phenomena and the intrinsic movement of the material particles. Subsequently, several theories have appeared in the field of Fluid Mechanics, such as, the theory of micropolar fluids, simple microfluids, dipolar fluids, couple stress theory [3], [4] and simple deformable directed fluids.

Eringen [5] first introduced the theory of simple microfluids. According to the theory, the term 'microfluid' refers to a category of fluids exhibiting specific patterns of behavior. These patterns stem from certain spatial characteristics of the internal structure, as well as from micro-movements of the elements contained into the fluid mass. Microfluids have the ability to support stress moments and body moments and are influenced by rotational inertia. Because of the above, the theory of microfluids, along with the mathematical model that describes it, are referred to be highly complicated, especially in cases that the problem under consideration is complex. Consequently, Eringen's theory was refined and subcategories of microfluids were introduced.

Micropolar fluids represent a category of fluids showing micro-rotational phenomena and micro-rotational inertia. The mathematical relationships that arise for this fluid subclass are

simpler in comparison to the rest of microfluids. Micropolar fluids can support couple stresses and body couples only, thus they are simpler than the rest of the microfluids.

Micropolar fluids possess microstructure, as they contain non-deformable solid particles, randomly oriented, and/or spherical, suspended in a viscous medium [6]. Lukaszewicz [7] states that, because of the aforementioned microstructure, micropolar fluids possess a certain degree of polarity. The microstructure within the fluid acts as an additional factor affecting the fluid behavior in various flows. The internal particles may possess varying shape and size, shrink, expand or change their geometry. Additionally, they can rotate individually, apart from the rotation of the fluid, and move independently of the flow volume. Micropolar fluids also belong to a class of fluids with non-symmetrical stress tensor, called polar fluids. [7]

In a physical sense, they can be effectively simulated as fluids containing small-sized bar-like /rod-shaped elements and micro-additives. The behavior of these liquids can be described by the mathematical model for micropolar fluids [8], [9] Examples of such liquids may be liquid crystals, animal blood, liquid suspensions and polymeric liquids.

The concept /theory of micropolar fluids found immediately a plethora of applications in the description of physical phenomena that could not be safely described by the classical fluid mechanics. Examples of these phenomena are Stoke's flow around a spherical geometry, stagnation flow, Taylor-Benard instability, and flow of boundary layers over a horizontal plate. A detailed description of the distinct cases and corresponding equations can be found in the extensive review of Ariman [10], [11].

The experimental data have shown that the solutions resulting from micropolar theory tend to better describe the behavior of physical fluids with microstructure, such as blood,

compared to the classical models. This advantage becomes much more pronounced for smaller values of the characteristic length, i.e. for a smaller scale [7].

1.2 Couette and Poiseuille Flows

Flows inside channels or conduits are of great interest in fluid mechanics, as they constitute a plethora of everyday life applications, Fluids moving through enclosed spaces, are in contact with solid boundaries that may sometimes move and affect the flow characteristics. Practical analysis and exact description of every-day examples is difficult, due to complex geometries and the time it takes for a flow to be fully developed. Because of this, simplified examples using basic geometrical models and steady state flows of ideal fluids, are generally used to understand fluids behavior. Two of the most basic and fundamental examples of movement in a viscous medium are Couette and Poiseuille flow.

The term 'Couette flow', in general, describes the flow of a viscous fluid between two parallel plates caused by the movement of one plate relative to the other; however, the case could also involve an external change in pressure in the direction of the flow. The simplest form of Couette flow is the steady state, two-dimensional, planar Couette flow with no external pressure input. This flow pattern will be examined in the present study.

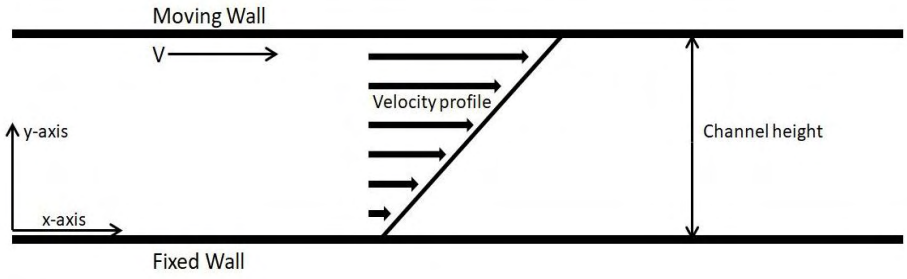

Figure 1.1. Couette flow velocity profile

Mainly, steady viscous fluid flow induced by the existence of pressure difference, is known as Poiseuille flow. It is given its name by Jean Poiseuille (1797-1869), as he was the first to experimentally study it. Although the term describes flows usually taking place inside a long pipe, in the present work the analysis is focused on flows between two infinite long, parallel to each other plates, using Cartesian and not polar coordinates, as shown in Figure 1.2. Poiseuille flow has to be distinguished from previously described, drag induced flow, because of the fact that both of the channel walls are fixed.

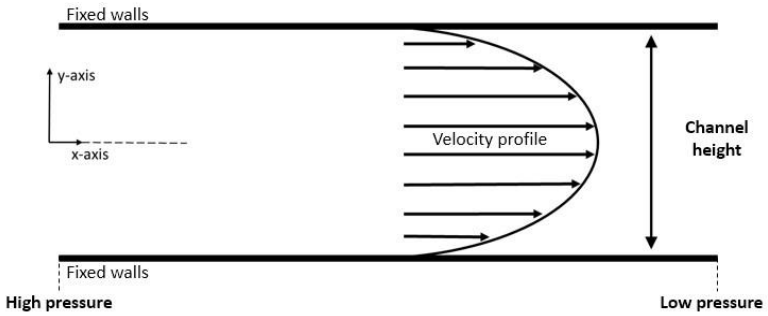

Figure 1.2 Poiseuille flow velocity profile

1.3 Aims and objectives

The aim of the present study was to verify the validity of the micropolar solver and investigate the behaviour of micropolar fluids under specific types of flows.

To pursue this goal, two distinct fluid flows, namely micropolar Couette and Poiseuille flow, were simulated using the OpenFoam software. The results were compared with the corresponding analytical solutions, in order to test their validity. Furthermore, for each type of flow, several cases were examined, aiming to investigate the effect of specific micropolar parameters on the flow attributes.

CHAPTER 2 THEORY

2.1 Introduction

Eringen's model for microfluids and his theory remains the basis for the current knowledge [5]. The theory presents numerous assets; in general, it is recognized as a simple, yet powerful extension of the classic Navier-Stokes equations. In these, a new vector field, the angular velocity field of rotation of particles (microrotation field), is introduced, as well as four additional viscosity coefficients. Of these, the vortex viscosity connects the linear momentum to the existence of microstructure; if this is zeroed, the linear momentum becomes independent of the microstructure [7].

In the present Chapter, the equations describing micropolar fluid flow will be analysed. The fundamental differential equations for the laws of conservation (mass, momentum, etc), and their deviations from the classic Navier-Stokes model, will first be presented. Moreover, new parameters will be introduced through the non-dimensionalization process. The distinct cases of boundary conditions relating to the corresponding physical quantities, more specifically microrotation, will be discussed, along with the limitations governing the viscosity coeffients. Finally, the analytical solutions of micropolar fluid flow, regarding momentum, mass and microrotation, will be analysed.

2.2 Mathematical formulation

In order to describe the general case of a viscous, compressible, micropolar fluid flow we need to utilize the mathematical formulas for the conservation of mass, momentum and microrotation, as well as the corresponding boundary and initial conditions that define each model. We can begin with gathering and defining all the quantities that will be used in the mathematical analysis of this chapter in the following table.

Table 2.1. Quantities used in the mathematical analysis

Symbol	Quantity	Unit
$\boldsymbol{\rho}$	Density	$[kg/m^3]$
$\boldsymbol{p}$	Pressure	$[Pa]$
$\vec{\boldsymbol{\nabla}}$	Del Operator	
$\boldsymbol{t}$	Time	$[s]$
$\vec{\boldsymbol{v}}$	Velocity vector	$[m/s]$
$\boldsymbol{\mu_v}$	Dynamic viscosity	$[Pa \cdot s]$
$\boldsymbol{\lambda_v}$	Second order viscosity	$[Pa \cdot s]$
$\boldsymbol{k_v}$	Vortex viscosity	$[Pa \cdot s]$
$\boldsymbol{\alpha_v}$	Viscosity Coefficient	$[m^4/s]$
$\boldsymbol{\beta_v}$	Viscosity Coefficient	$[m^4/s]$
$\boldsymbol{\gamma_v}$	Spin gradient viscosity	$[m^4/s]$
$\vec{\boldsymbol{l}}$	Body Moment per unit mass	$[m/s^2]$
$\vec{\boldsymbol{f}}$	Body Force per unit mass	$[m^2/s^2]$
$\boldsymbol{j}$	Microinertia	$[m^2]$
$\vec{\boldsymbol{N}}$	Microrotation Vector	$[s^{-1}]$

For the case of an isothermal fluid flow, the following micropolar equations are presented:

$$\frac{\partial \rho}{\partial t} + \nabla(\rho \vec{v}) = 0 \tag{1}$$

$$\rho \frac{D\vec{v}}{Dt} = -\vec{\nabla}p + (\lambda_v + 2\mu_v + k_v)\vec{\nabla}\vec{\nabla} \cdot \vec{v} - (\mu_v + k_v)\vec{\nabla} \times \vec{\nabla} \times \vec{v} + k_v \vec{\nabla} \times \vec{N} + \rho \vec{f} \tag{2}$$

$$\rho j \frac{D\vec{N}}{Dt} = (\alpha_v + \beta_v + \gamma_v)\vec{\nabla}\vec{\nabla} \cdot \vec{N} - \gamma_v \vec{\nabla} \times \vec{\nabla} \times \vec{N} + k_v \vec{\nabla} \times \vec{v} - 2k_v \vec{N} + \rho \vec{l} \tag{3}$$

[12]

Equations (1) to (3) formulate the laws of conversation of mass, momentum, and microrotation respectively. Scalar quantities ρ and j are fluid density and microinertia; in this specific case they are considered constant parameters. Vector fields $\vec{v}$, $\vec{f}$, $\vec{l}$, $\vec{N}$ which mark fluid velocity, body forces per unit mass, body couple per unit mass, and microrotation respectively, may change with respect to location. Variables λ_v, μ_v, k_v denote different viscosity types and similarly, a_v, β_v, γ_v denote viscosity coefficients. Those aforementioned

viscosities and viscosity coefficients do not take arbitrary values, but are instead bound to the following inequalities:

$$3\lambda_v + 2\mu_v + k_v \geq 0, \;\; \gamma_v \geq 0, \;\; |\beta_v| \leq \gamma_v, \;\; 3a_v + \beta_v + \gamma_v \geq 0,$$

[13]

An attentive observation is that for $k_v = a_v = \beta_v = \gamma_v = 0$ and the withdrawal of vectors $\vec{f}$ and $\vec{l}$, microrotation is nullified and equation (2) reduces to the classical Navier-Stokes equation. Moreover, with the elimination of just k_v, microrotation phenomena do not affect the velocity field [13]

Considering equations (1) to (3) presented above, the following assessments and assumptions can be made: Differential operator $\frac{\mathrm{D}(\cdot)}{\mathrm{D}t} = \frac{\partial(\cdot)}{\partial t} + \left(\vec{v} \cdot \vec{\nabla}\right)(\cdot)$, marks the Stokes material derivative. Both types of flow under study are steady state, fully developed laminar flows of an incompressible micropolar fluid. Mass density as well all micropolar fluid properties (λ_v, μ_v, k_v, a_v, β_v, γ_v, j) remain constant and vectors $\vec{f}$ and $\vec{l}$ are set to zero. Therefore, using vector algebra $\vec{\nabla} \times \vec{\nabla} \times \vec{F} = \vec{\nabla}\left(\vec{\nabla} \cdot \vec{F}\right) - \Delta\vec{F}$, the equation system can further be simplified as follows:

$$\vec{\nabla} \cdot \vec{v} = 0 \tag{4}$$

$$\rho \frac{D\vec{v}}{Dt} = -\vec{\nabla}p + (\mu_v + k_v)\Delta\vec{v} + k_v\vec{\nabla} \times \vec{N} \tag{5}$$

$$\rho j \frac{D\vec{N}}{Dt} = \gamma_v \Delta\vec{N} + k_v\vec{\nabla} \times \vec{v} - 2k_v\vec{N} \tag{6}$$

[12]

2.3 Dimensional Analysis of the flow field equations

In fluid mechanics non-dimensionalization is the conversion of a modeling equation to a non-dimensional form. When dexterously performed, this eases the analysis of the problem by reducing the free parameters. The magnitude of certain dimensionless parameters indicate the importance of the corresponding terms in the equations. Scaling, refers to the process of selecting the proper scales to be used in the non-dimensionalization of the flow equation. Since the resulting equations need to be dimensionless, a suitable combination of parameters and constants has to be found. As a result of this procedure, the number of analyzed parameters is reduced and the results are obtained in terms of the scaled variables.

In the vast majority of published literature, a non-dimensional form of the equations describing conservation laws is used, as it tends to better describe the effects of the parameters involved. The main purpose of this Chapter is to present the effects of the non-dimensional quantities, resulting as a combination of geometrical and micropolar parameters, on the behavior of the fluid flow.

For a start, it is assumed that, for a particular flow, the characteristic quantities L_0, t_0, are respectively a set characteristic length and time. Also v_0 is used to denote the maximum velocity of the fluid. Symbols with asterisk (*) are used to showcase non-dimensional variables:

$$\vec{x}^* = \frac{\vec{x}}{L_0} \qquad t^* = \frac{t}{t_0} \qquad \vec{v}^* = \frac{\vec{v}}{v_0}$$

$$J = \frac{j}{{L_0}^2} \qquad \vec{N}^* = \frac{\vec{N} L_0}{v_0} \qquad p^* = \frac{p L_0}{(\mu_v + k_v) v_0}$$

By substituting these into (4) - (6) and applying the standard method of dimensional analysis, the governing equations may be written again.

For equation (4), introducing the non-dimensional variables and expanding, results in:

$$\vec{\nabla} \cdot \vec{v} = 0 \Leftrightarrow$$

$$\frac{v_0}{L_0}\vec{\nabla}^* \cdot \vec{v}^* = 0 \Leftrightarrow$$

$$\vec{\nabla}^* \cdot \vec{v}^* = 0 \tag{7}$$

Following the same approach for equation (5):

$$\rho \frac{D\vec{v}}{Dt} = -\vec{\nabla}p + (\mu_v + k_v)\Delta\vec{v} + k_v\vec{\nabla} \times \vec{N} \Leftrightarrow$$

$$\rho\left(\frac{\partial \vec{v}}{\partial t} + (\vec{v} \cdot \vec{\nabla})\vec{v}\right) = -\vec{\nabla}p + (\mu_v + k_v)\Delta\vec{v} + k_v\vec{\nabla} \times \vec{N} \Leftrightarrow$$

$$\rho\frac{v_0}{t_0}\frac{\partial \vec{v}^*}{\partial t^*} + \rho\frac{{v_0}^2}{L_0}(\vec{v}^* \cdot \vec{\nabla}^*)\vec{v}^* = -\frac{(\mu_v + k_v)v_0}{{L_0}^2}\vec{\nabla}^*p^* + \frac{(\mu_v + k_v)v_0}{{L_0}^2}\Delta^*\vec{v}^* + \frac{k_v v_0}{{L_0}^2}\vec{\nabla}^* \times \vec{N}^* \Leftrightarrow$$

$$\frac{\rho v_0 L_0}{(\mu_v + k_v)}\left[\frac{L_0}{t_0 v_0}\frac{\partial \vec{v}^*}{\partial t^*} + (\vec{v}^* \cdot \vec{\nabla}^*)\vec{v}^*\right] = -\vec{\nabla}^*p^* + \Delta^*\vec{v}^* + \frac{k_v}{(\mu_v + k_v)}\vec{\nabla}^* \times \vec{N}^* \tag{8}$$

And finally for the microrotation equation (6):

$$\rho j\frac{D\vec{N}}{Dt} = \gamma_v\Delta\vec{N} + k_v\vec{\nabla} \times \vec{v} - 2k_v\vec{N}$$

$$\rho j\left(\frac{\partial \vec{N}}{\partial t} + (\vec{v} \cdot \vec{\nabla})\vec{N}\right) = \gamma_v\Delta\vec{N} + k_v\vec{\nabla} \times \vec{v} - 2k_v\vec{N}$$

$$\frac{\rho J v_0 L_0}{t_0}\frac{\partial \vec{N}^*}{\partial t^*} + \rho J {v_0}^2(\vec{v}^* \cdot \vec{\nabla}^*)\vec{N}^* = \frac{\gamma_v v_0}{{L_0}^3}\Delta^*\vec{N}^* + \frac{k_v v_0}{L_0}\vec{\nabla}^* \times \vec{v}^* - \frac{2k_v v_0}{L_0}\vec{N}^*$$

$$\frac{\rho J {L_0}^4}{t_0\gamma_v}\frac{\partial \vec{N}^*}{\partial t^*} + \frac{\rho J v_0 {L_0}^3}{\gamma_v}(\vec{v}^* \cdot \vec{\nabla}^*)\vec{N}^* = \Delta^*\vec{N}^* + \frac{k_v {L_0}^2}{\gamma_v}\vec{\nabla}^* \times \vec{v}^* - \frac{2k_v {L_0}^2}{\gamma_v}\vec{N}^*$$

$$\frac{\rho J v_0 {L_0}^3}{\gamma_v}\left[\frac{L_0}{v_0 t_0}\frac{\partial \vec{N}^*}{\partial t^*} + (\vec{v}^* \cdot \vec{\nabla}^*)\vec{N}^*\right] = \Delta^*\vec{N}^* + \frac{k_v {L_0}^2}{\gamma_v}\vec{\nabla}^* \times \vec{v}^* - \frac{2k_v {L_0}^2}{\gamma_v}\vec{N}^* \tag{9}$$

At this step, taking into consideration the non-dimensional form of the aforementioned field equations, we need to differentiate and adapt the terms for each flow case separately. Substantial differences in the definition of classical counterparts of the non-dimensional quantities, mainly present in the classical Navier-Stokes equations, will be presented, and new quantities will be introduced.

2.3.1 Dimensional analysis for Couette flow

The complete form for the non-dimensional differential flow equations regarding Couette flow, can be acquired by following the mathematical process below. Relationships (8) and (9) for velocity and microrotation respectively, are considered as a starting point.

Initially, for the velocity equation, the following is derived:

$$\frac{\rho v_0 L_0}{(\mu_v + k_v)}\left[\frac{L_0}{t_0 v_0}\frac{\partial \vec{v}^*}{\partial t^*} + (\vec{v}^* \cdot \vec{\nabla}^*)\vec{v}^*\right] = -\vec{\nabla}^* p^* + \Delta^* \vec{v}^* + \frac{k_v}{(\mu_v + k_v)}\vec{\nabla}^* \times \vec{N}^* \Leftrightarrow$$

$$\frac{L_0}{t_0 v_0}\frac{\partial \vec{v}^*}{\partial t^*} + (\vec{v}^* \cdot \vec{\nabla}^*)\vec{v}^* = -\frac{\mu_v + k_v}{\rho v_0 L_0}\vec{\nabla}^* p^* + \frac{\mu_v + k_v}{\rho v_0 L_0}\Delta^* \vec{v}^* + \frac{k_v}{\rho v_0 L_0}\vec{\nabla}^* \times \vec{N}^*$$

This is a steady state and fully developed flow, therefore $\frac{\partial \vec{v}^*}{\partial t^*} = 0$. If relationship (7) is taken into account, the velocity equation is simplified to:

$$-\frac{\mu_v + k_v}{\rho v_0 L_0}\vec{\nabla}^* p^* + \frac{\mu_v + k_v}{\rho v_0 L_0}\Delta^* \vec{v}^* + \frac{k_v}{\rho v_0 L_0}\vec{\nabla}^* \times \vec{N}^* = 0$$

In order to gather more information from the above expression, the micropolar parameters need to be isolated. As a result, quantity A is introduced.

$$A = \frac{\mu_v}{k_v}$$

Subsequently, A is extracted from each term, while vortex viscosity $k_v$is absorbed in the process.

$$-\frac{\mu_v\left(1+\frac{1}{A}\right)}{\rho v_0 L_0}\vec{\nabla}^* p^* + \frac{\mu_v\left(1+\frac{1}{A}\right)}{\rho v_0 L_0}\Delta^*\vec{v}^* + \frac{\frac{\mu_v}{A}}{\rho v_0 L_0}\vec{\nabla}^* \times \vec{N}^* = 0$$

In this particular analysis, the Reynolds number is defined as follows:

$$Re = \frac{\rho v_0 L_0}{\mu_v} \tag{10}$$

This format for producing the Reynolds number has also been attested and used by previous research, more specifically by Kim [14]. Finally, with the involvement of Re, the relationship takes a final form:

$$-\frac{\left(1+\frac{1}{A}\right)}{Re}\vec{\nabla}^* p^* + \frac{\left(1+\frac{1}{A}\right)}{Re}\Delta^*\vec{v}^* + \frac{1}{Re\cdot A}\vec{\nabla}^* \times \vec{N}^* = 0 \tag{11}$$

Evidently, a high value on A is negated on the first two terms, but it does affect the third term expressing the influence of the Microrotation. A low value on the other hand, influences all terms of the relationship.

Next, the microrotation equation is examined in a similar manner.

$$\frac{\rho J v_0 {L_0}^3}{\gamma_v}\left[\frac{L_0}{v_0 t_0}\frac{\partial\vec{N}^*}{\partial t^*} + \left(\vec{v}^*\cdot\vec{\nabla}^*\right)\vec{N}^*\right] = \Delta^*\vec{N}^* + \frac{k_v {L_0}^2}{\gamma_v}\vec{\nabla}^* \times \vec{v}^* - \frac{2k_v {L_0}^2}{\gamma_v}\vec{N}^*$$

$$\frac{L_0}{v_0 t_0}\frac{\partial\vec{N}^*}{\partial t^*} + \left(\vec{v}^*\cdot\vec{\nabla}^*\right)\vec{N}^* = \frac{\gamma_v}{\rho J v_0 {L_0}^3}\Delta^*\vec{N}^* + \frac{k_v}{\rho J v_0 L_0}\vec{\nabla}^* \times \vec{v}^* - \frac{2k_v}{\rho J v_0 L_0}\vec{N}^*$$

Akin to the velocity analysis, utilizing relationship (8) and $\frac{\partial\vec{N}^*}{\partial t^*} = 0$, as a result of a fully developed flow, the equation is simplified to:

$$\frac{\gamma_v}{\rho J v_0 {L_0}^3}\Delta^*\vec{N}^* + \frac{k_v}{\rho J v_0 L_0}\vec{\nabla}^* \times \vec{v}^* - \frac{2k_v}{\rho J v_0 L_0}\vec{N}^* = 0$$

For the purpose of isolating the spin gradient viscosity γ_v, non dimensional quantity B is introduced.

$$B = \frac{4\mu_v {L_0}^2}{\gamma_v}$$

With the inclusion of B, the microrotation equation takes the concluding form presented below:

$$\frac{4\mu_v}{\rho J v_0 L_0}\frac{1}{B}\Delta^*\vec{N}^* + \frac{\mu_v}{\rho J v_0 L_0}\frac{1}{A}\vec{\nabla}^* \times \vec{v}^* - \frac{2\mu_v}{\rho J v_0 L_0}\frac{1}{A}\vec{N}^* = 0$$

$$\frac{4}{JRe}\frac{1}{B}\Delta^*\vec{N}^* + \frac{1}{JRe}\frac{1}{A}\vec{\nabla}^* \times \vec{v}^* - \frac{2}{JRe}\frac{1}{A}\vec{N}^* = 0 \qquad (12)$$

B appears only in the first term of the equation, while A directly influences the other two. It is apparent that both quantities play a more direct role in the outcome of microrotation that that of velocity, although A can still affect velocity independently. For $A \to \infty$ ($k_v \to 0$), microrotation may exist, but the connection between the two vector fields is severed, and thus, the velocity equation reverts back to the classic Navier Stokes model.

2.3.2 Dimensional analysis for Poiseuille flow

Following the same steps, the non dimensional form of the equations regarding Poiseuille flow can easily be obtained. Consider the final form of eq(7) - (9) above. Term $\frac{\rho v_0 L_0}{(\mu_v + k_v)}$ refers to the definition of Reynolds -Re- number, with some minor adjustments to the classical one, as it can clearly be seen that the term of micro-rotation viscosity k_v is taking place. There are many cases in literature, where the term $(\frac{L_0}{t_0 v_0})^{-1}$ is denoted as the Strouhal [15] number. Due to the fact that the case studied here, involves a steady state – fully developed flow, all time dependent terms can be successfully ignored. Besides classical counterparts of the non-dimensional parameters previously arose, there occur many new non dimensional parameters:

a) N- is a combination of kinematic viscosity and viscosity of microrotation, mathematically denoted as $N = \sqrt{\frac{k_v}{\mu_v + k_v}}$.

b) k- is denoted as the material parameter $\frac{k_v}{\mu_v}$, and as it can be seen is part of the previously mentioned parameter N.

c) L- is the ratio of characteristic length L_0 over l, $L = \frac{L_0}{l}$, where $l = \sqrt{\frac{\gamma_v}{4\mu_v}}$.

Generally speaking, after taking into consideration all the aforementioned quantities, mathematical expressions (8) - (9) can be transformed into the following ones:

$$\boldsymbol{Re}\left[\frac{1}{\boldsymbol{St}}\frac{\partial \vec{v}^*}{\partial t^*} + \left(\vec{v}^* \cdot \vec{\nabla}^*\right)\vec{v}^*\right] = -\vec{\nabla}^* p^* + \Delta^* \vec{v}^* + \boldsymbol{N}^2\left(\vec{\nabla}^* \times \vec{N}^*\right) \Leftrightarrow$$

$$0 = -\vec{\nabla}^* p^* + \Delta^* \vec{v}^* + \boldsymbol{N}^2\left(\vec{\nabla}^* \times \vec{N}^*\right) \tag{13}$$

and

$$\frac{\rho J v_0 {L_0}^3}{\gamma_v}\left[\frac{L_0}{v_0 t_0}\frac{\partial \vec{N}^*}{\partial t^*} + \left(\vec{v}^* \cdot \vec{\nabla}^*\right)\vec{N}^*\right] = \Delta^* \vec{N}^* + \frac{k_v {L_0}^2}{\gamma_v}\vec{\nabla}^* \times \vec{v}^* - \frac{2k_v {L_0}^2}{\gamma_v}\vec{N}^* \Leftrightarrow$$

$$\boldsymbol{ReJL^2}\frac{(1+\boldsymbol{k})}{4}\left[\frac{L_0}{v_0 t_0}\frac{\partial \vec{N}^*}{\partial t^*} + \left(\vec{v}^* \cdot \vec{\nabla}^*\right)\vec{N}^*\right] = \Delta^* \vec{N}^* + \frac{k_v {L_0}^2}{\gamma_v}\frac{\boldsymbol{4\mu_v}}{\boldsymbol{4\mu_v}}\vec{\nabla}^* \times \vec{v}^* - \frac{2k_v {L_0}^2}{\gamma_v}\frac{\boldsymbol{2\mu_v}}{\boldsymbol{2\mu_v}}\vec{N}^* \Leftrightarrow$$

$$\boldsymbol{0} = \Delta^* \vec{N}^* + \frac{\boldsymbol{L^2 k}}{4}\vec{\nabla}^* \times \vec{v}^* - \frac{\boldsymbol{L^2 k}}{2}\vec{N}^* \tag{14}$$

Taking into consideration every aspect of the aforementioned analysis, a sufficient conclusion about the effects of dimensionless parameters can be conducted. On the one hand, dimensionless parameter N is taking place only in the equation of momentum (13). It can clearly be seen that in case of $N = 0$, equations become independent of each other. In other words it is safe to say that, the bigger the value of N, the more perceptible the microrotational effects should be. On the other hand, dimensionless parameter L, is a

combination of the characteristic length L_0 with l. Parameter l, has dimension of length and its value is indicative of the size of fluid particles[7,16,17→* [15].

As a result, in contrast to parameter N, it should be mentioned that, the smaller the value of L, the greater the non-newtonian effects, as the particle size increases.

It is a necessity, to represent the actual behavior of dimensionless parameters as a function of fluid properties. Specifically, it is appropriate to say that $N = N(k_v)$ and $L = L(\gamma_v)$. For different values of k_v and γ_v, their representation is on Figures 2.1 and 2.2, below.

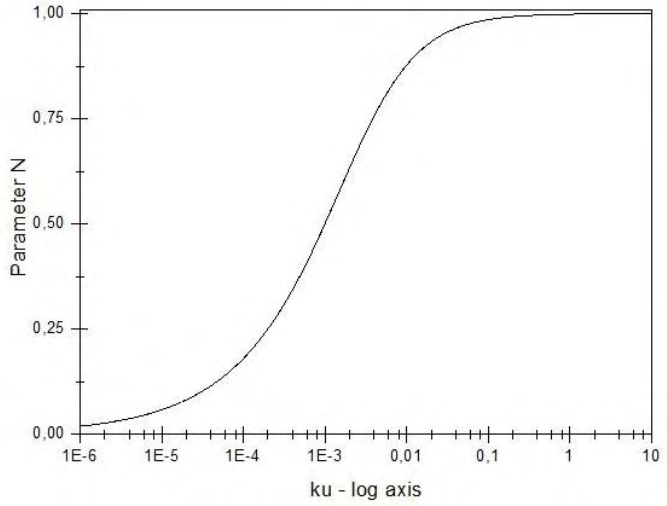

Figure 2.1. Change of N with respect to k_v

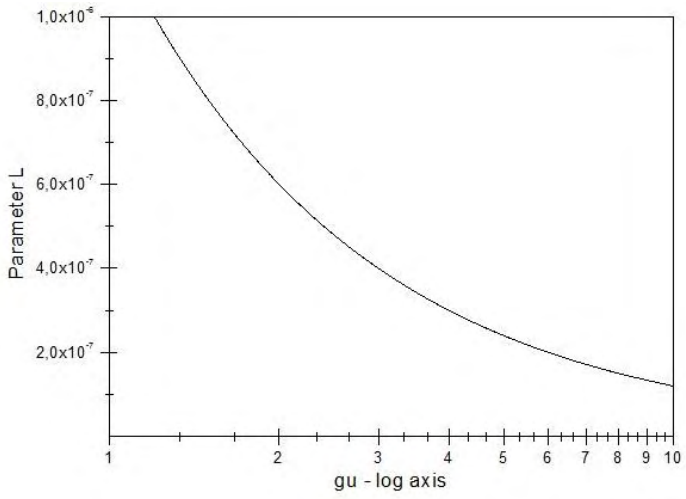

Figure 2.2. Change of L with respect to γ_v

2.4 Theory behind different types of boundary conditions

Every micropolar fluid flow problem analyzed is governed by some set of the partial differential field equations (4) to (6). Under appropriate initial and boundary conditions, these equations are capable of predicting in full the behavior of such fluids. Boundary conditions mathematically define the case geometry, a subset of the three-dimensional Euclidean space $\mathbb{R}^3$ that comprises the location for the problem. Let Ω be such a subset and ∂Ω its boundary. Concerning stationary problem modeling, Dirichlet boundary conditions for the unknown functions of v and N,(i.e. $v = v_b$ and $N = N_b$) on ∂Ω are assumed.

Expressing exact boundary conditions depends on the geometrical, static and dynamic aspects of each case. The inclusion of microrotation raises the issue of the behavior of the fluid, and more specifically the microrotation vector, near solid walls. A general type of boundary condition used for the microrotation field on ∂Ω, was presented by Rees & Basson [16]:

$$N_{\partial\Omega} = -n\frac{\partial v_x}{\partial y}, \qquad 0 \leq n \leq 1 \tag{15}$$

It should be noted that for $n = 0$, microrotation becomes zero at the boundary walls. This correlates to substantial particle density near the wall surface, hence disabling the rotation of microelements [16]. The value $n = \frac{1}{2}$ denotes weak particle concentration and indicates the vanishing of the anti-symmetrical part of the stress tensor. [17] Finally, cases where $n = 1$ are indicative of turbulent boundary layers [16], and are naturally used for modeling turbulent layer flows [18]. Any condition involving $n \neq 0$ implies that the influence of microstructure is exceptionally weak in the vicinity of a solid boundary, since the particles are limited in approaching the boundary by their radius. This in turn, results in the microrotational field being unaffected by microstructure and the only rotational effects exhibited are due to fluid shear.

Regarding velocity, boundary conditions really depend on the modeling problem. The cases of Poiseuille and Couette flow are mathematically characterized by different boundary conditions in both velocity and pressure. Additionally, the well-known no-slip and no-penetration boundary conditions are assumed for both cases. The microrotation boundary condition is considered zero, which aligns with the aforementioned general type of microrotation boundary condition for $n = 0$ [19].

2.3.1 Couette flow

Simple, two-dimensional Couette Flow is mathematically described by the following boundary conditions. Pressure is assumed to be the same in the inlet and the outlet of the flow:

$$P_{inlet} = P_{outlet}$$

Following the no-slip condition, velocity at the boundary walls is considered as:

$$\vec{v}_{motionless\ wall} = (0,0,0)$$

$$\vec{v}_{moving\ wall} = (V,0,0)$$

Where V represents the velocity value of the upper wall.

2.3.2 Poiseuille flow

As it was previously mentioned, Poiseuille is mainly a pressure driven flow. This indicates that the pressure along the flow should gradually decline.

Thus:

$$P_{inlet} > P_{outlet}$$

Regarding velocity, the first one, can be expressed as $\vec{v}_{\partial\Omega} = (v_1, v_2, v_3) = (0, 0, 0)$ and states that that there is no velocity component near the solid boundary. In other words the fluid near the surface cannot be moved. The second one, states that the fluid can only flow parallel to the solid wall and not penetrate it, which mathematically can be shown as $\vec{v} \cdot \hat{n} = 0$, where $\hat{n}$ is the unit normal to the boundary $\partial\Omega$.

2.5 Exact solutions

Under common geometrical and dynamical assumptions made in classical cases (e.g., symmetry, linearization of the equations), the micropolar fluid flow equations can be explicitly solved. This is due to the mathematical simplicity of the micropolar model. Strictly speaking, the derived equations will only be applicable to the studied flow cases. Solving the differential field equations (4) to (6) and acquiring exact solutions has already been accomplished by various researchers, among them Verma [8] and Ariman [20]. The analytical solutions that were used in the present thesis are based on the examples of exact solutions given by Lukaszewicz [7], and aid the comparison with numerical data.

The differential equations used by Lukaszewicz differ from (5) and (6) at specific points. The modified formulas are presented as follows:

$$\frac{\partial \rho}{\partial t} + \vec{v} \cdot \vec{\nabla} \rho = 0 \tag{16}$$

$$\rho \left(\frac{\partial \vec{v}}{\partial t} + (\vec{v} \cdot \vec{\nabla}) \vec{v} \right) = -\vec{\nabla} p + (\mu_v + k_v) \Delta \vec{v} + 2k_v (\vec{\nabla} \times \vec{N}) + \rho \vec{f} \tag{17}$$

$$\rho j \left(\frac{\partial \vec{N}}{\partial t} + (\vec{v} \cdot \vec{\nabla}) \vec{N} \right) = 2k_v (\vec{\nabla} \times \vec{v} - 2\vec{N}) + (c_0 + c_d - c_a) \vec{\nabla} (\vec{\nabla} \cdot \vec{N}) + (c_a + c_d) \Delta \vec{N} + \rho \vec{l} \tag{18}$$

It is apparent that a difference in mathematical denotation exists between (17), (18) and (5), (6). The material time derivative of (2) and (3) has been expanded and additional alterations have been made. By comparing the equations, the following correlation is derived:

$$\gamma_v = ca + cd \tag{19}$$

To avoid unneeded confusion, the γ_v symbolism was adopted.

An additional difference between the mathematical expressions is that the vortex viscosity (k_v) is multiplied by 2 in equations (17) and (18). This occurs in all terms, except within the parenthesis that multiplies the Laplacian of velocity in equation (17). For a better understanding of this divergence, we contrast the relationships (5) and (17). The difference in the 2nd and 3rd terms of the 2nd part of the equations becomes evident and can be seen below:

$$5)\ \rho \frac{D\vec{v}}{Dt} = -\vec{\nabla}p + (\mu_v + k_v)\Delta\vec{v} + k_v\vec{\nabla} \times \vec{N}$$

$$17)\ \rho\left(\frac{\partial\vec{v}}{\partial t} + \left(\vec{v} \cdot \vec{\nabla}\right)\vec{v}\right) = -\vec{\nabla}p + (\mu_v + k_v)\Delta\vec{v} + 2k_v\left(\vec{\nabla} \times \vec{N}\right) + \rho\vec{f}$$

This difference is fundamental in the mathematical analysis of Lukaszewicz and should be always taken into account in any attempt to compare results.

Bearing in mind that the flow under study is fully developed and incompressible, the time derivatives can be disregarded and the equations can be divided by density, thus producing a corresponding change in the coefficients. Also, microinertia (j) becomes equal to 1, for simplification. Consequently, from (16), (17) and (18) we respectively arrive at:

$$\vec{\nabla} \cdot \vec{v} = 0 \tag{20}$$

$$-(\nu + ku)\Delta\vec{v} + \left(\vec{v} \cdot \vec{\nabla}\right)\vec{v} + \vec{\nabla}p = 2ku\left(\vec{\nabla} \times \vec{N}\right) + \vec{f} \tag{21}$$

$$-gu\Delta\vec{N} + \left(\vec{v} \cdot \vec{\nabla}\right)\vec{N} - (c_0 + c_d - c_a)\vec{\nabla}\left(\vec{\nabla} \cdot \vec{N}\right) + 4ku\vec{N} = 2k_v\left(\vec{\nabla} \times \vec{v}\right) + \vec{l} \tag{22}$$

An important observation concerning the above equations is that the viscosity coefficients refer to quantities that are now divided by density. This can be seen in ν and ku which now correspond to kinematic viscosity (ν) and kinematic vortex viscosity (ku), but it also applies

to c_0, c_a, c_d, gu and p. In his book, Lukaszewicz chooses not to divide the equations by density, but to set $\rho = 1$ for simplicity. This differentiation ultimately does not affect the final analytical result.

2.5.1 Exact Couette Flow

For a final solution to the Couette flow problem, the parameters involved need to be strictly defined. Hence, for two-dimensional Couette flow between two parallel plates, we can assume the following:

There are 2 plates in Cartesian space:

$$\Gamma_i = \{(x, y, z) \in \mathbb{R}^3 : \ y = (i-1)h\}, \qquad i = 1,2$$

where h represents the distance between them. The plate set at level Γ_2 moves with a stable velocity V_0 in the direction of the x-axis. The forces and moments per unit mass are considered equal to zero. Because the analysis involves a two-dimensional flow on the x-y level, velocity, microrotation and pressure are considered as:

$$\vec{v} = (v(y), 0, 0), \ \ \vec{N} = \big(0, 0, N(y)\big), \ \ p = p(y)$$

Applying the above adjustments, relationships (21) and (22) are modified as follows:

$$(\nu + ku)\frac{d^2 v}{dy^2} + 2ku\frac{dN}{dy} = 0 \tag{23}$$

$$gu\frac{d^2 N}{dy^2} - 2ku\left(2N + \frac{dv}{dy}\right) = 0 \tag{24}$$

The boundary conditions of Couette flow for velocity are mathematically expressed as:

$$v(0) = 0, \ \ v(h) = V \tag{25}$$

For microrotation, the boundary condition assumes the following general expression:

$$N(0) = N(h) = \frac{\alpha}{2} rot(v) \tag{26}$$

The above condition is a direct equivalent of the Rees & Basson [16] microrotation boundary condition already presented. The coefficient $\frac{\alpha}{2}$ is directly analogous to n.

The general analytical solution deriving from the above differential equations, (23) and (24), accompanied with the specific boundary conditions (25) and (26), is presented in the relationships (26) and (28).

$$v(y) = \frac{V}{K} \times \left[\frac{1 - cosh(\lambda)}{sinh(\lambda)} \left(1 - cosh\left(\lambda \frac{y}{h} \right) \right) - sinh\left(\lambda \frac{y}{h} \right) + \lambda \frac{\nu + ku(1-a)}{ku(1-a)} \frac{y}{h} \right] \tag{27}$$

$$N(y) = \frac{V\lambda}{2hK} \frac{\nu + ku}{ku} \times \left[cosh\left(\lambda \frac{y}{h} \right) + \frac{1 - cosh(\lambda)}{sinh(\lambda)} sinh\left(\lambda \frac{y}{h} \right) - \frac{\nu + ku(1-\alpha)}{(\nu + ku)(1-\alpha)} \right] \tag{28}$$

Numbers λ and K in the above relationships can be calculated with the formulas:

$$\lambda^2 = \frac{ku}{\nu + ku} \frac{4\nu}{gu} h^2 \tag{29}$$

$$K = \lambda \frac{\nu + ku(1-\alpha)}{ku(1-\alpha)} + 2 \frac{1 - cosh(\lambda)}{sinh(\lambda)} \tag{30}$$

A short representative example of an analytical solution is presented below. Firstly, the values for the coefficients and variables are given:

$$V = 0{,}003\ m/s$$

$$\nu = 0{,}003\ m^2/s$$

$$ku = 0{,}006\ m^2/s$$

$$gu = 0{,}00016\ m^4/s$$

$$h = 0{,}01\ m$$

Within the limits of the study, microrotation at the plate walls is set to zero. This boundary condition can be expressed mathematically by setting $\alpha = 0$.

Using the above values, the non-dimensional variables A and B can be calculated:

$$A = \frac{\nu}{ku} = \frac{0{,}003}{0{,}006} = 0{,}5$$

$$B = \frac{4\nu {L_0}^2}{gu} = \frac{4\nu h^2}{gu} = \frac{4x0{,}003x0{,}01^2}{0{,}00016} = 0{,}0075$$

The Reynolds number is determined based on the maximum flow velocity, that is, the speed of the upper plate V:

$$Re = \frac{V \times h}{\nu} = \frac{0{,}003 \times 0{,}01}{0{,}003} = 0{,}01$$

Through A and B, the variables λ and K can be transformed as:

$$\lambda = \sqrt{\frac{h^2 \cdot B}{A+1}} = \sqrt{\frac{0{,}01^2 \cdot 75}{0{,}5+1}} = 0{,}07071$$

$$K = \lambda\left[\frac{A}{(1-\alpha)} + 1\right] + 2\frac{1-\cosh(\lambda)}{\sinh(\lambda)} =$$

$$= 0{,}07071\left[\frac{0{,}5}{1} + 1\right] + 2\frac{1-\cosh(0{,}07071)}{\sinh(0{,}07071)} = 0{,}03538$$

Finally, the velocity and microrotation relations can likewise be expressed as:

$$u(y) = \frac{V}{K} \times \left[\frac{1-\cosh(\lambda)}{\sinh(\lambda)}\left(1-\cosh\left(\lambda\frac{y}{h}\right)\right) - \sinh\left(\lambda\frac{y}{h}\right) + \lambda\left(\frac{A}{1-\alpha}+1\right)\frac{y}{h}\right]$$

$$\omega(y) = \frac{V\lambda}{2hK}(A+1) \times \left[\cosh\left(\lambda\frac{y}{h}\right) + \frac{1-\cosh(\lambda)}{\sinh(\lambda)}\sinh\left(\lambda\frac{y}{h}\right) - \frac{A+1-\alpha}{(A+1)(1-\alpha)}\right]$$

The solution is clearly shown in the following diagrams (Figures 2.3, 2.4):

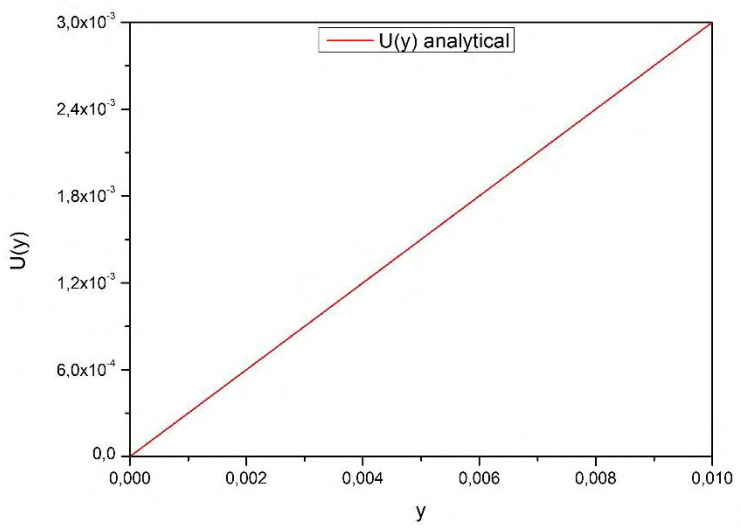

Figure 2.3. Micropolar couette flow velocity profile for $A = 0{,}5$ and $B = 0{,}075$

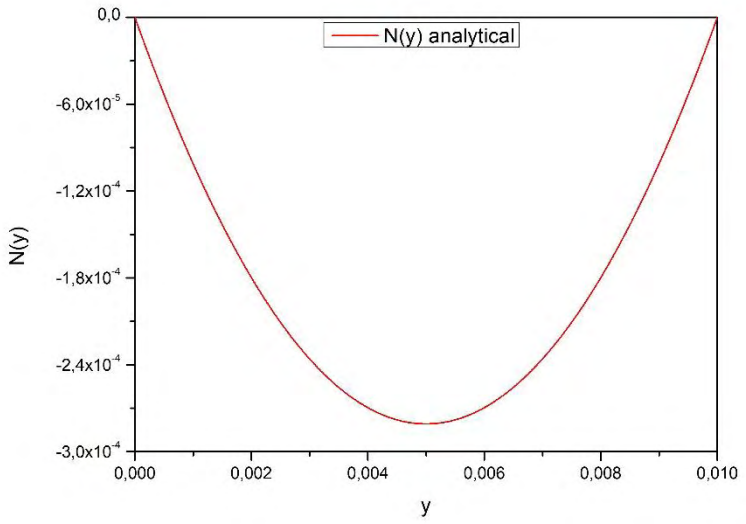

Figure 2.4. Micropolar couette flow microrotation profile for $A = 0{,}5$ and $B = 0{,}075$

2.5.2 Exact Poiseuille Flow

As a final step, the flow of micropolar fluids between two infinite-parallel and stationary planes at distance 2h, is considered. Mathematically described as:

$$\Gamma_i = \{(x, y, z) \in \mathcal{R}^3 : \ y = (-1)^i h\}\ ,\ i = 1, 2$$

Assuming that the fluid initially was at rest, flow was suddenly induced by a constant gradient of pressure $\frac{dp}{dx}$, in sheer absence of body moments and mass forces ($\vec{f} = \vec{l} = 0$). Using cartesian coordinates, with x-axis located at the plane of symmetry, parallel to the flow and y-axis normal to the plates, the case is graphically illustrated in Figure 2.5.

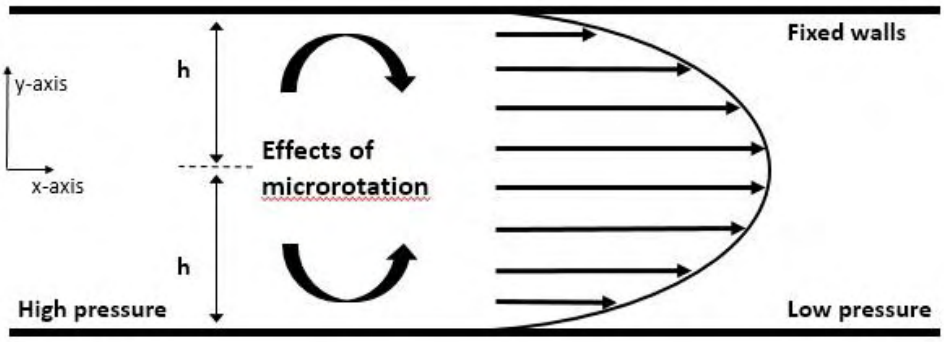

Figure 2.5. Characteristics of micropolar poiseuille flow

Due to the assumption of infinitely long plates, setting $\vec{v} = (v(y), 0, 0)$, $\vec{N} = \big(0, 0, N(y)\big)$ and $p = p(x)$, in the aforementioned equations of motion (11) – (13), formulation of the problem is slightly transformed into the following form:

$$(\nu + k_v)\frac{d^2 v}{dy^2} + 2k_v \frac{dN}{dy} = \frac{dp}{dx} \tag{31}$$

$$g_v \frac{d^2 N}{dy^2} - 2k_v \left(2N + \frac{dv}{dy}\right) = 0 \tag{32}$$

Equations (31) - (32), can simultaneously be solved for unknown quantities $v(y), \omega(y)$. They ought to be treated, as a system of ordinary differential equations with constant coefficients. To fully define the set of equations, several types of boundary conditions need to be established at $y = \pm h$.

For convenience it is assumed, that:

$$v = 0 \qquad \text{at} \qquad y = \pm h \tag{33}$$

$$N = 0 \qquad \text{at} \qquad y = \pm h \tag{34}$$

Taking into account formulas (33) - (34), a solution to the following system of differential equations, need to be derived:

$$\frac{d^2v}{dy^2} + \frac{2k_v}{v + k_v}\frac{dN}{dy} = \frac{dp}{dx}\frac{1}{v + k_v} \tag{35}$$

$$\frac{d^2N}{dy^2} - \frac{2k_v}{g_v}\frac{dv}{dy} - \frac{4k_vN}{g_v} = 0 \tag{36}$$

Setting $a = \frac{2k_v}{v+k_v}$, $A = \frac{dp}{dx}\frac{1}{v+k_v}$, $b = \frac{2k_v}{g_v}$, $B = \frac{4k_v}{g_v}$, differentiation of eq (35), finally gives:

$$\frac{d^2v}{dy^2} = -\alpha\frac{dN}{dy} + A \tag{37}$$

$$\frac{d^2N}{dy^2} - b\frac{dv}{dy} - BN = 0 \xrightarrow{(d(\cdot)/dy)} \frac{d^3N}{dy^3} - b\frac{d^2v}{dy^2} - B\frac{dN}{dy} = 0$$

Substitution of the $\frac{d^2v}{dy^2}$ term, into the 3rd order differential equation, provides the following:

$$\frac{d^3N}{dy^3} + \frac{dN}{dy}[b \cdot a - B] - b \cdot A = 0$$

Using the method of undetermined coefficients and summing up the complementary and particular parts of the solution, the general analytical form of $\omega(y)$ is presented:

$$N(y) = \frac{A\ b\ y}{ab - B} + \frac{e^{\sqrt{-ab+B}\cdot y}}{\sqrt{-ab+B}} \cdot c_1 - \frac{e^{-\sqrt{-ab+B}\cdot y}}{\sqrt{-ab+B}} \cdot c_2 + c_3$$

Calculation of constant parameters involved in the eq (--) can easily be achieved by setting $N(-h) = N(0) = N(h) = 0$. Thus, the following expressions regarding c_1, c_2 and c_3 arise

$$c_1 = \frac{A\ b\ e^{\sqrt{-ab+B}\cdot h} \cdot h}{\sqrt{-ab+B} \cdot (-1 + e^{\sqrt{-ab+B}\cdot h}) \cdot (1 + e^{\sqrt{-ab+B}\cdot h})},$$

$$c_2 = c1,\ c_3 = 0$$

Bear in mind that $B = 2b,\ \sinh(x) = e^{x} - e^{-x}$ and also $G = \sqrt{-ab + B}$, the expression of microrotation, can further be simplified to:

$$N(y) = \frac{A\,y}{(a-2)} - \frac{A\,h}{(a-2)} \cdot \frac{\sinh(G\cdot\ y)}{\sinh(G\cdot\ h\,)} \tag{38}$$

Regarding equation (38), it is clearly seen that an exact expression for the flow velocity equation can be derived using the same principles, as previously described. The final form of the differential equation is presented below:

$$\frac{d^2v}{dy^2} = A - \frac{A\ \ a}{(a-2)} + \frac{A\,a\,h\,G\,\cosh\,(G\cdot\ y)}{(a-2)\,\sinh\,(G\cdot h)}$$

As far as it is concerned, constant parameters c_1 and c_2, can be established using the expressions for the velocity boundary conditions, at $y = \pm h$. Needless to say, that following the steps described, the general form of the velocity flow equation is described as:

$$v(y) = c_1 + y\,c_2 + \frac{A\ \ a}{(a-2)} + \frac{A\,a\,h\cosh(G\cdot\ y)\ \mathrm{csch}\,(G\cdot\ h) - \ A\,y^2G}{G(a-2)}$$

Where:

$$c_1 = \frac{A\,(-B\,G\,h^2 + 2a\,b\,h\coth(G\cdot h))}{2b\,(a-2)\,G}, \quad c_2 = 0$$

Substituting c_1, c_2 into the previous form, the final equation for the velocity is derived:

$$v(y) = \frac{A\,[2b\,G\,(h-y)(h+y) - 2a\,b\,h\,(\cosh(G\cdot h) - \cosh\,(\,G\cdot y))\ \mathrm{csch}\,(G\cdot\ h)]}{2b\,(a-2)\,G} \tag{39}$$

An interesting yet significant observation, regarding the previous analysis, focuses on deeper understanding of all the aforementioned parameters. For start, a new coefficient m, is

introduced, which is a combination of the channel pressure drop dp and kinematic viscosity ν, defined as:

$$m = \frac{A\,h^2}{(a-2)} = \frac{-\frac{dp}{dx}\;h^2}{2\nu}$$

Considering that change, the final form of the exact solutions of microrotation and velocity are reconstructed. The main purpose of the rearrangement of the terms, is to show the level of similarities within the equations proposed by Lukaszewicz [7].

Following the process detailed below, the velocity and microrotation profiles can be acquired:

VELOCITY PROFILE

$$v(y) = \frac{A\,h^2(1-\left(\frac{y}{h}\right)^2)}{(a-2)} - \frac{a\,A\,h\,(\cosh(G\cdot h)-\cosh\,(\,G\cdot y))\,\mathrm{csch}\,(G\cdot\,h)}{(a-2)\,G} \Leftrightarrow$$

$$v(y) = \frac{A\,h^2(1-\left(\frac{y}{h}\right)^2)}{(a-2)} - \frac{a\,A\;\,h^2\,(\cosh(G\cdot h)-\cosh\,(\,G\cdot y))\,\mathrm{csch}\,(G\cdot\,h)}{G\,(a-2)\,h} \Leftrightarrow$$

$$v(y) = \frac{A\,h^2}{(a-2)}[1-\left(\frac{y}{h}\right)^2 - \frac{a\,(\cosh(G\cdot h)-\cosh\,(\,G\cdot y))}{\mathrm{G\;h\;sinh}\,(G\cdot\,h)}] \Leftrightarrow$$

$$v(y) = \frac{-\frac{dp}{dx}\;h^2}{2\nu}\left[1-\left(\frac{y}{h}\right)^2 - \frac{a\,(\cosh(G\cdot h)-\cosh\,(\,G\cdot y))}{\mathrm{G\;h\;sinh}(G\cdot\,h)}\right] \qquad (40)$$

$$v(y)^{\mathrm{Lukaszewiczz}^*} = \frac{-2\nu\,v(y)}{\frac{dp}{dx}\;h^2} = 1-\left(\frac{y}{h}\right)^2 - \frac{a\,(\cosh(G\cdot h)-\cosh\,(\,G\cdot y))}{\mathrm{G\;h\;sinh}(G\cdot\,h)} \qquad (41)$$

MICROROTATION PROFILE

$$N(y) = \frac{A\,y}{(a-2)} - \frac{A\,h}{(a-2)} \cdot \frac{\sinh(G\cdot\ y)}{\sinh(G\cdot\ h\,)} \Leftrightarrow$$

$$N(y) = \frac{A\,h^2}{(a-2)} \left[\frac{y}{h^2} - \frac{1}{h} \cdot \frac{\sinh(G\cdot\ y)}{\sinh(G\cdot\ h\,)} \right] \Leftrightarrow \tag{42}$$

$$N(y)^{\text{Lukaszewicz}} = \frac{(a-2)N(y)}{A\,h^2} = \frac{y}{h^2} - \frac{1}{h} \cdot \frac{\sinh(G\cdot\ y)}{\sinh(G\cdot\ h\,)} \tag{43}$$

The final form of the equations is in complete agreement with the solutions of Lukaszewicz. The velocity term of equation (40) appears in a non-dimensional form, since in the book it is multiplied with the term $\frac{-\frac{dp}{dx}\,h^2}{2\nu} = 1$, which uses velocity measurement units.

Additionally, the microrotation field resulting from the above process, ends up using $[1/m]$ measurement units. Importantly, the normal parabolic profile appears in the formula and the second term of the parenthesis reduces the classical parabola, based on the parameter values involved in the equation

Derivation of exact solutions for planar poiseuille flow of Newtonian fluids

Let us consider again the geometry of the problem mentioned in the previous section. To start with, we are taking into account the same boundary conditions for the velocity field. Further, the flow is considered far downstream from the entrance so that it can be treated as fully-developed. Using continuity equation, it leads to the conclusion that the only component is $u_x = u_x(y)$. Also, $u_y = u_z = 0$, and gravity is neglected. The momentum equations in the respective direction reduces as follows;

$$y - momentum\colon \frac{\partial p}{\partial y} = 0$$

$$z-momentum:\ \frac{\partial p}{\partial z}=0$$

$$x-momentum:\ \rho\left[\frac{\partial u}{\partial t}+u_x\frac{\partial u_x}{\partial x}+u_y\frac{\partial u_x}{\partial y}+u_z\frac{\partial u_x}{\partial z}\right]=\rho\cdot g_x-\frac{\partial p}{\partial x}+$$

$$+\mu\left[\frac{\partial^2 u_x}{\partial x^2}+\frac{\partial^2 u_x}{\partial y^2}+\frac{\partial^2 u_x}{\partial z^2}\right]\ \Rightarrow\ \mu+\frac{\partial^2 u_x}{\partial y^2}=\frac{\partial p}{\partial x}$$

By integrating the last equation with respect to $y\in[-h,h]$, and using the previously known boundary conditions we obtain a formula for $u(y)$;

$$u(y)=\frac{1}{2\mu}\left(\frac{\partial p}{\partial x}\right)(y^2-h^2) \qquad (44)$$

SIMPLE CASE ILLUSTRATION

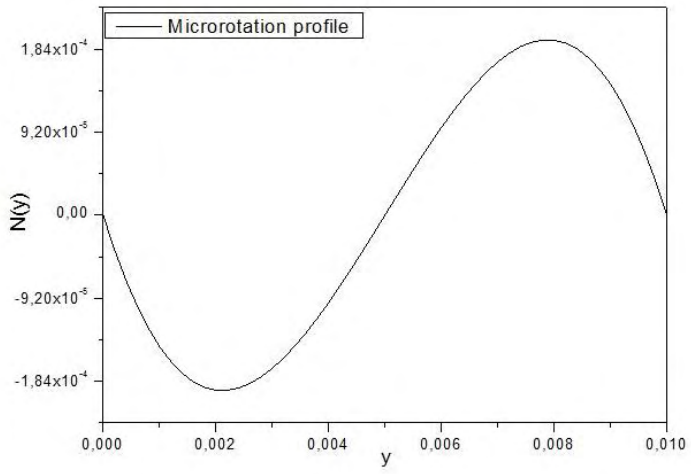

Figure 2.6. Micropolar poiseuille flow microrotation profile

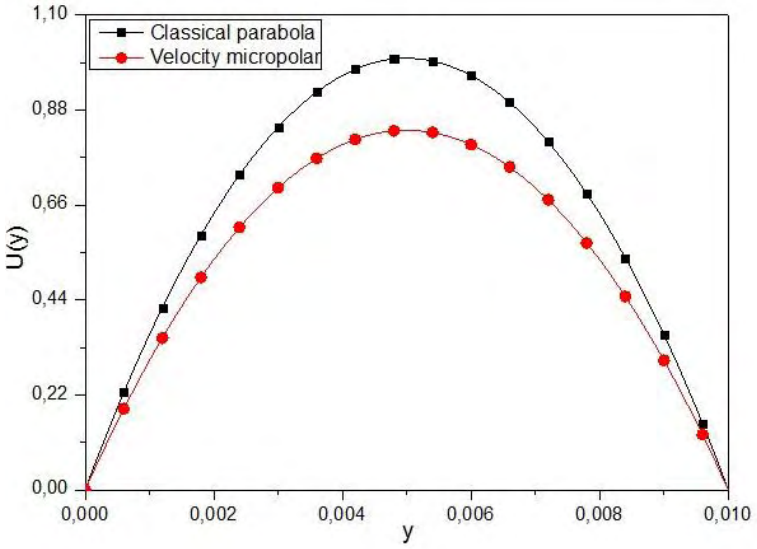

Figure 2.7. Newtonian and Micropolar poiseuille flow velocity profiles

CHAPTER 3 OPEN FOAM

3.1 Introduction

All the simulations were carried out using OpenFOAM. It is an open source CFD software released and developed primarily by OpenCFD Ltd since 2004. OpenFOAM is predominately a framework for developing executables, named applications, that use packaged functionality contained within a collection of C++ libraries. The applications fall under two major categories: Solvers, which are designed to solve a specific problem of fluid (continuum) mechanics, and utilities, which are designed to perform tasks that involve data manipulation. [21]

Users can develop a direct relationship with the software, as they are given the option to create additional solvers and utilities. The software also offers pre- and post-processing environments that aid in the setup and analysis of the problem.

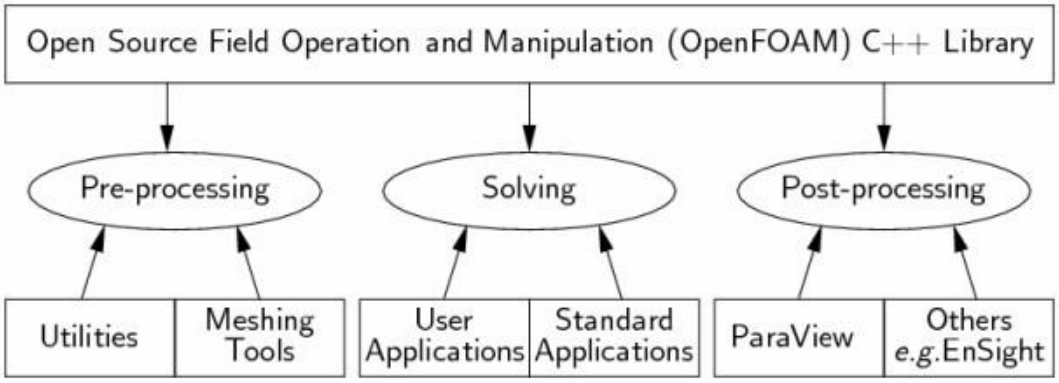

Figure 3.1. OpenFoam structure (openfoam user guide)

The software is accompanied by numerous tutorials and instructions which aim to make the environment familiar to the users. Visualization of all scientific data-sets is performed by using ParaView, an open source multiple platform application, designed for interactive data analysis by means of qualitative and quantitative techniques. An additional advantage of the platform is the plethora of problems of different scientific fields that can be simulated. Each

application solver corresponds to a distinct set of problems. The range of cases that these solvers are applicable to, is presented below:

- Compressible – incompressible – multiphase flows
- Direct numerical simulations
- Combustion – heat transfer – electromagnetism problems
- Stress analysis of solids
- Molecular dynamic methods
- Finance

3.2 Preprocessing Case Geometry and Mesh Generation

Pre-processing involves all the necessary steps made in the simulation preparation. Cases are set up in OpenFoam by creating, editing or using existing case files. Data for mesh, fluid physical properties, boundary and initial conditions, fields, as well as all control parameters need to be in agreement with the simulated case.

3.2.1 Mesh Generation

The OpenFoam software perceives physical geometry as a defined mesh or grid, comprised by cells. Every mesh generated is acknowledged by the software as a 3D entity, even in cases of 2D simulations. In such-2D cases, the third dimension is specified by the user and does not interfere with the result.

OpenFoam is supplied with a mesh generator, which creates a mesh using an input file, blockMeshDict, located in the case directory. In this file, the mesh details, including corner points, cell shape and cell number, are specified. This process is launched by the command *blockMesh* (Figure 3.2).

```
FoamFile
{
    version     2.0;
    format      ascii;
    class       dictionary;
    object      blockMeshDict;
}
// * * * * * * * * * * * * * * * * * * * * * * * * * * * * * * * * * * * * * * * * * * * * //

convertToMeters 1.0;

vertices
(
    (0 0 0)
    (0.1 0 0)
    (0.1 0.01 0)
    (0 0.01 0)
    (0 0 0.01)
    (0.1 0 0.01)
    (0.1 0.01 0.01)
    (0 0.01 0.01)
);

blocks
(
    hex (0 1 2 3 4 5 6 7) (50 50 3) simpleGrading (1 1 1)
);

edges
(
);
```

Figure 3.2. OpenFoam blockMeshDict file

In both cases examined in the present work, the focus was placed on the construction of a 3 dimensional space that could effectively simulate the ideal conditions of Couette and Poiseuille flow. The derived mesh which was uniformly transformed, outlines a closed channel with a square cross section. The block structure is shown in Figure 3.3.

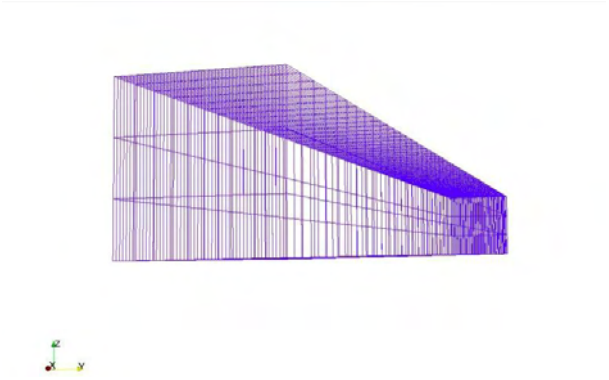

Figure 3.3. OpenFoam case Mesh

3.2.2 Boundary Conditions

After the geometry of the problem has been defined and the mesh has been generated, a boundary description must be provided. This again takes place within the *blockMeshDict* file of the case directory. For the current case geometry, 5 boundary sets, or patches, needed to be specified, namely:

- *inlet*: The boundary where the flow enters the channel
- *outlet*: The boundary where the flow exits the channel
- *top*: The top wall boundary
- *bottom*: The bottom wall boundary
- *frontAndBack*: The side surfaces perpendicular to the flow

In the case of Poiseuille flow, there is no need for a special distinction between the top and low wall boundaries. Thus, they were replaced by *fixedWalls* (Figure 3.4).

```
boundary
(
    inlet
    {
        type wall;
        faces
        (
            (0 4 3 7)
        );
    }
    outlet
    {
        type wall;
        faces
        (
            (1 2 6 5)
        );
    }
    top
    {
        type wall;
        faces
        (
            (3 2 6 7)
        );
    }
    bottom
    {
        type wall;
        faces
        (
            (0 1 5 4)
        );
    }
    frontAndBack
    {
        type wall;
        faces
        (
            (0 3 2 1)
            (4 5 6 7)
        );
    }
);

mergePatchPairs
(
);
```

Figure 3.4. OpenFoam blockMeshDict file

The special variable values in the aforementioned boundary surfaces are given in the *0* folder. There, a field file is assigned to all main problem variables, in this case microrotation, pressure and velocity. Both the boundary and the initial conditions for the problem are

expressed in subdirectories within the corresponding files. Boundary conditions in particular, are designated by specific entries in the *type* line; the most useful in this case are:

- *fixedvalue*: where variable value is directly given
- *movingWallVelocity*: where the boundary moves at a constant, pre-specified velocity
- *zeroGradient*: where the gradient of the variable is zero

3.2.3 Physical Properties

The physical properties of a fluid, also known as mechanical properties, play a crucial role in the field of fluid mechanics, as they determine aspects of the flow behavior. In an OpenFoam case, the physical properties of fluids are defined in the *transportProperties* file.

In order to solve a micropolar flow problem, the relevant parameters, such as the kinematic fluid viscosity (nu), as well as the added micropolar parameters j, gu, and ku have to be specified (Figure 3.5).

```
FoamFile
{
    version     2.0;
    format      ascii;
    class       dictionary;
    location    "constant";
    object      transportProperties;
}
// * * * * * * * * * * * * * * * * * * * * * * * * * * * * * * * * * * * * * * * * * * * * //

nu              [0 2 -1 0 0 0 0] 0.003;

ku              [0 2 -1 0 0 0 0] 0.1;

gu              [0 4 -1 0 0 0 0] 0.016;

j               [0 2 0 0 0 0 0] 1;

// ************************************************************************* //
```

Figure 3.5. OpenFoam transportProperties file

The scope of the study involved examining the behavior of the flow profiles as the micropolar parameters k_v and γ_v change values. Microinertia j remains constant at $1\ m^2$.

Along with the parameter values, the units of measurement for each quantity are specified. This functions through a combination of seven basic measurement units in S.I. outlined in the bracket before each quantity value. Each number denotes the power in which the measurement unit is set at. The correspondence between the units and the bracket positions is shown in Table 3.1:

Table 3.1. Correspondence between the units and the bracket positions

Position	Quantity	Measurement Unit
1	Mass	kg
2	Length	m
3	Time	s
4	Temperature	K
5	Amount of Substance	mol
6	Electric Current	A
7	Luminous Intensity	cd

The values for the new quantities introduced must be given in the S.I units specified. These are m^2/s for ku, m^4/s for gu and m^2 for j.

3.2.4 Control

The execution of flow simulations requires input data relating to time control and general output control. These, as well as other information regarding the resulting solution, are given in the *controlDict* dictionary.

Start and end times for the solver along with the timestep, are set in subdictionaries within the file. These values are not the same for every case but instead vary from case to case (Figure 3.5).

```
application     micropolarFoam;
startFrom       startTime;
startTime       0;
stopAt          endTime;
endTime         0.01;
deltaT          0.000005;
```

Figure 3.6. OpenFoam controlDict file

Aside from time control, *controlDict* also specifies important output information. These mainly include information about recording and storing the results (Figure 3.6).

```
writeControl    timeStep;
writeInterval   200;
purgeWrite      0;
writeFormat     ascii;
writePrecision  6;
writeCompression off;
timeFormat      general;
timePrecision   6;
runTimeModifiable true;
```

Figure 3.7. OpenFoam controlDict file

3.3 MicropolarFoam solver

The application solver used in the study is micropolarFoam and it was created by modifying one of the preexisting solvers provided with the OpenFoam software. As the name implies,

MicropolarFoam has been developed with the aim to provide numerical solutions for problems of micropolar flow. The solver uses essentially the basic differential equations of velocity (5) and microrotation (6) for micropolar fluids referred by Zadravec [Zadravec2008]. These simplified differential equations are not applied unchanged. Instead, some notable modifications have been implemented. These are:

- Contrary to (5) and (6), the solver equations are divided by density. Consequently, fluid viscosity is kinematic and not dynamic. Likewise, solver vortex viscosity ku and pressure p are divided by density and refer to kinematic vortex viscosity and $\frac{p}{\rho}$ respectively. Finally, the spin gradient viscosity (gu) is also divided by density.
- The solver is designed to take into account the effects of temperature on the fluid flow. That is achieved by including one more differential equation, while adding one more variable, temperature (T), and two more entry data, $T0$ and a coefficient of thermal expansion $beta$. The analytical equations for Couette and Poiseuille flow employed in the later comparisons, do not take into account the temperature effects. Thus, the solver was simplified in order to produce comparable results.
- There exists a fundamental difference in the micropolar equations between the methods of Zadravec and Lukaszewicz. It involves the multiplication of k_v by two in some, but not all, equation terms, and it is explained in more detail in the subchapter “Exact Solutions” of Chapter 2. In order to fix this asymmetry, the solver was modified to include the extra multipliers for ku in the key terms (Figure 3.7).

```
// Microrotation concervation equation

fvVectorMatrix NEqn
(
      j*fvm::ddt(N)
    + j*fvm::div(phi, N)
    - fvm::laplacian(gu, N)
    - 2*ku*fvc::curl(U)
    + 4*ku*N
);
NEqn.solve();

// Temperature

//      fvScalarMatrix TEqn
//      (
//          fvm::ddt(T)
//        + fvm::div(phi, T)
//        - fvm::laplacian(a, T)
//      );
//      TEqn.solve();


// Momentum predictor

fvVectorMatrix UEqn
(
    fvm::ddt(U)
  + fvm::div(phi, U)
  - fvm::laplacian(nu+ku, U)
  - 2*ku*fvc::curl(N)
//    + beta*(T - T0)*g
);
```

Figure 3.8. OpenFoam micropolarFoam file

3.4 Numerical schemes

In order to calculate certain equation terms, for example a derivative in the form of a gradient or divergence, OpenFoam employs a collection of numerical schemes. These schemes refer, fundamentally, to calculation techniques used to approximate a result value. They are selected and assigned in the *fvSchemes* file, to specified term categories.

Time derivatives, gradient derivatives, laplacians and others, constitute term categories in need of a specified numerical scheme, so as to be effectively calculated. Within the *fvSchemes* file, a scheme is appointed to a term set in a given subdirectory (Figure 3.8).

```
ddtSchemes
{
    default         Euler;
}

gradSchemes
{
    default         Gauss linear;
    grad(p)         Gauss linear;
}

divSchemes
{
    default         none;
    div(phi,U)      Gauss linear;
    div(phi,N)      Gauss linear;
}

laplacianSchemes
{
    default         Gauss linear orthogonal;
}

interpolationSchemes
{
    default         linear;
}

snGradSchemes
{
    default         orthogonal;
}
```

Figure 3.9. OpenFoam fvschemes file

Concerning time derivatives, time schemes include *steadyState, Euler, backward, CrankNicolson* and *localEuler*. MicropolarFoam is based on the transient IcoFoam solver, and the equations include a first order time derivative. *Euler* functions best in this setting and was thus chosen as time scheme (Figure 3.9).

```
ddtSchemes
{
    default         Euler;
}
```

Figure 3.10. Time scheme sub dictionary

Terms that require interpolation of values use *interpolationSchemes*. By far the most common such scheme, and the one chosen, is *linear* (Figure 3.10).

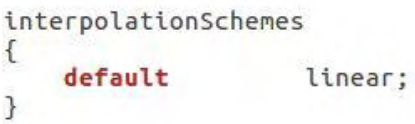

Figure 3.11. Interpolation sub dictionary

Gradient schemes refer to schemes involved in the calculation of gradient derivatives. *Gauss linear* is the most commonly used scheme for this task. *Gauss* signifies the standard finite volume discretisation of Gaussian integration, and the scheme for the interpolation is given by the entry *linear.* Occasionally in more complex tasks, other options, such as *leastSquares* or *Gauss cubic*, are used (Figure 3.11).

Figure 3.12. Grad Scheme sub dictionary

Similarly, Divergence schemes usually involve *Gauss linear* or some variation of it, depending on the given case. The *none* entry in *default* requires the scheme for each divergence term to be defined individually (Figure 3.12).

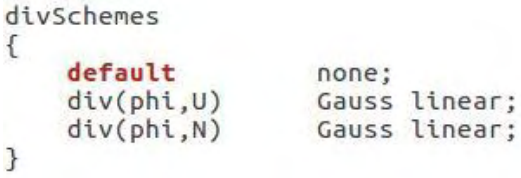

Figure 3.13. Div scheme sub dictionary

For surface normal gradient schemes (*snGradScheme)*, possible entries are: *corrected, limited corrected 0.33, limited corrected 0.5, orthogonal* and *uncorrected*. In this case the *orthogonal* scheme was selected (Figure 3.13).

```
snGradSchemes
{
    default         orthogonal;
}
```

Figure 3.14. snGrad scheme sub dictionary

To calculate Laplacian terms, corresponding laplacian schemes were utilized. These schemes exhibit a specific pattern involving the *Gauss* scheme, as well as an *interpolationScheme* and a *snGradScheme*. Following the previous entries, *Gauss linear orthogonal* was selected (Figure 3.14).

```
laplacianSchemes
{
    default         Gauss linear orthogonal;
}
```

Figure 3.15. Laplacian scheme sub dictionary

3.5 Linear solvers and algorithms

Application solvers, like *icoFoam*, solve a comprehensive and complex problem that may include multiple equations and variables. The task of solving the simple matrix equations during the solution process, for each distinct system equation, is designated to the linear solvers. OpenFoam includes five different linear solvers:

- ***PCG/PBiCGStab***
- ***PCG/PBiCG***
- ***smoothSolver***
- ***GAMG***
- ***diagonal***

Linear solvers may function exclusively with asymmetrical matrixes, symmetrical matrixes or both. When a symmetric solver is incorrectly appointed to a process involving an asymmetric

matrix, an error message stops the task. Linear solvers are designated by the user within the *fvSolutions* file, in the appropriate subdictionary. Multiple solvers were tested for each main variable, in order to sufficiently reduce the calculation time of the application solver. The tolerance for each individual case was selected separately, since a small tolerance is necessary for a correct result in the extreme cases, but tends to increase overall calculation time (Figure 3.15).

```
solvers
{
    p
    {
        solver          PCG;
        preconditioner  FDIC;
        tolerance       1e-07;
        relTol          0.05;
    }

    pFinal
    {
        $p;
        relTol          0;
    }

    U
    {
        solver          smoothSolver;
        smoother        symGaussSeidel;
        tolerance       1e-07;
        relTol          0;
    }

    N
    {
        solver          smoothSolver;
        smoother        symGaussSeidel;
        tolerance       1e-07;
        relTol          0;
    }

}
```

Figure 3.16. OpenFoam fvsolutions file

The coupling of solver equations, and specifically mass conservation and momentum equations, can be accomplished by three algorithms. These are PISO and PIMPLE, applied in transient cases, and SIMPLE applied in steady state cases. The selection of the algorithm takes place in the corresponding subdirectory of the *fvSolutions* file. *MicropolarFoam*, like

icoFoam, is designed to solve a transient problem, so, in this case, the *PISO* algorithm was selected (Figure 3.16).

```
PISO
{
    nCorrectors     2;
    nNonOrthogonalCorrectors 0;
    pRefCell        0;
    pRefValue       0;
}
```

Figure 3.17. PISO sub dictionary

3.5 Post Processing

After the ending of the simulations, all results are successfully retrieved and stored to time directories. Visualization of the case results can be achieved with the help of the reader module ParaView, provided with the software. ParaView uses the Visualization Toolkit (VTK) as its data processing and rendering engine and can therefore read any data in VTK format. The generated mesh can be viewed only in ParaView, since there is no other suitable pre-processing tool. There is a plethora of tools, each and every one for a specific kind of task.

The *plot over line* option was used repeatedly for the visualization of the velocity and microrotation fields in order to extract 2-D profiles. The utility was applied perpendicular to the flow direction in the middle of the x axis.

3.6 Experimental settings

The main focus of the following chapters is the presentation and analysis of numerical results, derived from the OpenFoam micropolar solver, as well as their comparison with the corresponding analytical equations, presented in Chapter 2. For the two distinct cases under study, namely Couette and Poiseuille flow, fixed geometries of similar scale were tested. The micropolar parameters ku and gu, were selected as the independent variables, in order to confirm the validity of the solver and also to test their effect on the numerical results.

Throughout this process, all other variables, such as fluid viscosity, microinertia or, in the case of Couette flow, wall speed, remained constant. This setting constituted a clear and solid framework for understanding the effects of the aforementioned micropolar coefficients on the behavior of the fluid

CHAPTER 4 RESULTS PRESENTATION AND COMPARISON FOR COUETTE FLOW

4.1 Introduction

This chapter is devoted to the presentation and analysis of the Couette flow results. Initialy the case is formulated and the parameters are defined. Following that, the number of cells is established through the mesh refinement process and the results are categorized, presented and analyzed.

4.2 Case Format

For Couette flow, the problem needs to be accurately formulated and the parameters clearly set. The guiding intention in this task is to conclusively produce a low Reynolds number for the flow, in order to approximate the behavior of a highly viscous fluid.

For the present experiment the parameters that were set are presented below:

- The parallel plates were placed at a distance $h = 0{,}01\ m$ from each other.
- The velocity of the upper plate was $V = 0{,}003\ m/s$.
- The kinematic fluid viscosity was set at $\nu = 0{,}003\ m^2/s$
- Microinertia was set at $j = 1\ m^2$.
- The boundary condition for microrotation was considered to be $N_{wall} = 0$.

The Reynolds number for Couette flow was estimated according to the expression (10) presented as part of the non dimensionalisation process.

$$Re = \frac{\rho v_0 L_0}{\mu_v}$$

The characteristic length L_0 is the distance h between the two plates and the maximum speed was decided to be the wall speed V. Hence, Re becomes:

$$Re = \frac{Vh}{\nu} = \frac{0{,}003\ m/s \times 0{,}01\ m}{0{,}003\ m^2/s} = 0{,}01$$

Since parameters V, h and ν remain constant throughout the cases, the value of the Reynolds number is unaffected and remains steady.

This small value for the Reynolds number can be attributed to the high kinematic viscosity of the fluid. High values of kinematic viscosity can be attested in numerous fluids, especially in low temperature environments. Motor oils provide a good example as they are often used in subzero temperatures. A 5W engine oil at -25℃ exhibits a viscosity of roughly $3500\ cP$. This, taking into account a mean oil density of $900\ kg/m^3$, correlates to a kinematic viscosity of $0{,}0039\ m^2/s$. Another similar example is glycerol at low temperatures.

In order to obtain a comparison with the exact solutions, a matching model needed to be established, using the analytical equations and parameters presented in Chapter 2. By attributing appropriate values for fluid viscosity, microinertia, wall velocity and, additionally, by setting microrotation boundary coefficient α to zero, the constant elements of the analytical model were defined. For the independent variables, the correspondence between the two models was implemented via the non dimensional quantities A and B.

4.3 Mesh Refinement

Refining the mesh is an important step in ensuring that the numerical results produced are sufficiently accurate. After this task was concluded the total number of cells, used in all subsequent cases, was set. The process involved testing the solvers response for different grid densities, in one individual case. More specifically, the resulting values of microrotation were compared with the analytical model, for all grids. The case selected was for non

dimensional parameters $A = 0{,}06$ and $B = 2{,}4 \times 10^{-4}$. It represents a typical example of the cases examined.

Starting from a coarse mesh of 20x20, or 1200 cells, the grid is gradually thickened until the numerical results provide an adequate approximation of the analytical profile. The third, depth dimension remained unchanged at three cells. The visual change is depicted in the diagrams that follow (Figure 4.1):

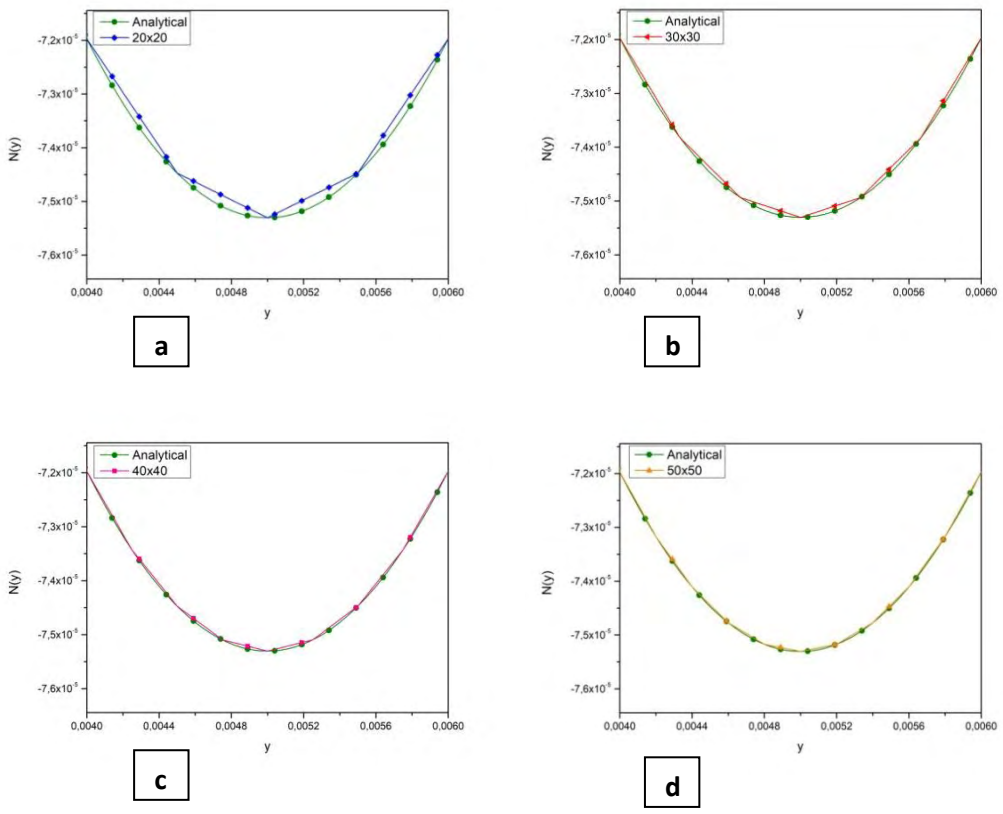

Figure 4.1. Numerical results and analytical profile for the meshes 20x20 (a), 30x30 (b), 40x40 (c) and 50x50 (d)

It is obvious that as the mesh becomes finer, the analytical and numerical profiles converge. It is also evident that for every mesh, there is a visible error that diminishes as the total cell number increases. This error can be quantified using the following formula:

$$ER = \frac{\sum_i N_{i\ numerical} - N_{i\ analytical}}{n}$$

Where n is the total number of points selected.

With this error definition applied, a comparison of ER values can take place (Table 4.1):

Table 4.1. ER values for the meshes used.

Mesh	$\boldsymbol{ER}$
20x20	$1{,}24989 \times 10^{-7}$
30x30	$5{,}55672 \times 10^{-8}$
40x40	$3{,}12084 \times 10^{-8}$
50x50	$1{,}99553 \times 10^{-8}$

The quantitative analysis confirms the visual observations. As the mesh becomes denser, the error decreases. A 50x50 mesh correlates to 7.500 cells in total. For this number, the relative error, that is the error compared to the value scale of microrotation for the same case (10^{-5}), is considered sufficiently small ($\sim 10^{-3}$). Consequently, this is the mesh density used in the following examples.

4.4 Presentation of results

4.4.1 Ahmadi formula

The numerical results and the comparisons were grouped based on the interchanging variable. Initially, using a formula proposed by Ahmadi [22],

$$\gamma_v = \left(\mu_v + \frac{k_v}{2}\right) j$$

which connects vortex viscosity k_v, microinertia j and spin gradient viscosity γ_v, the two independent variables were interlinked. Thus, a change in the value of A produces a change in the value of B.

The results of our measurements are presented in Figures 4.2 – 4.3

Figures 4.2 and 4.3 present the change in profiles of microtation for varying values of the independent variable A.

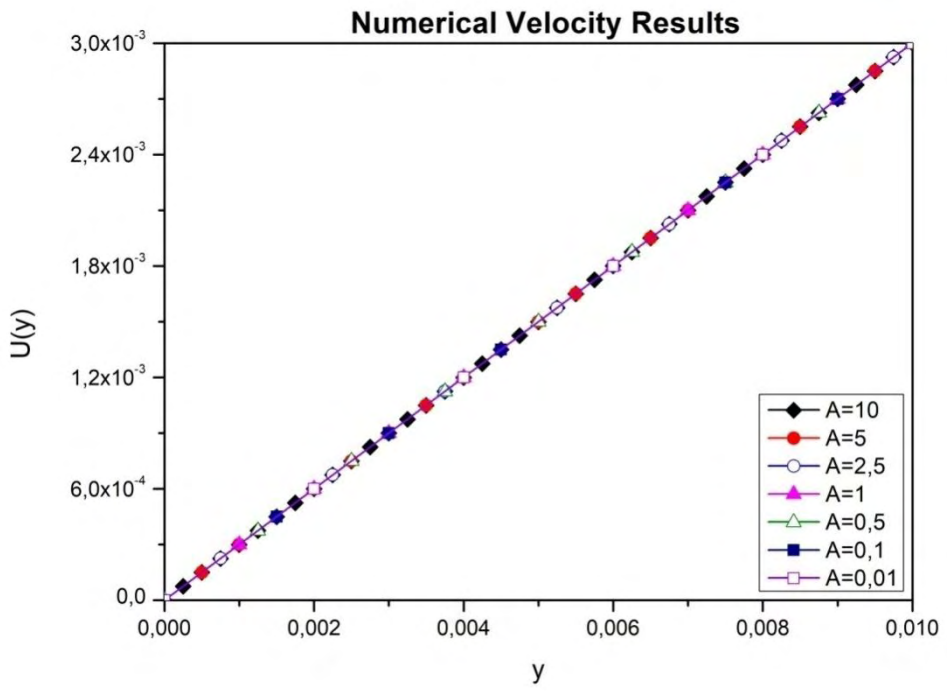

Figure 4.2. Numerical velocity for various values of variable A. Units: y in $[m]$, $U(y)$ in $[m/s]$

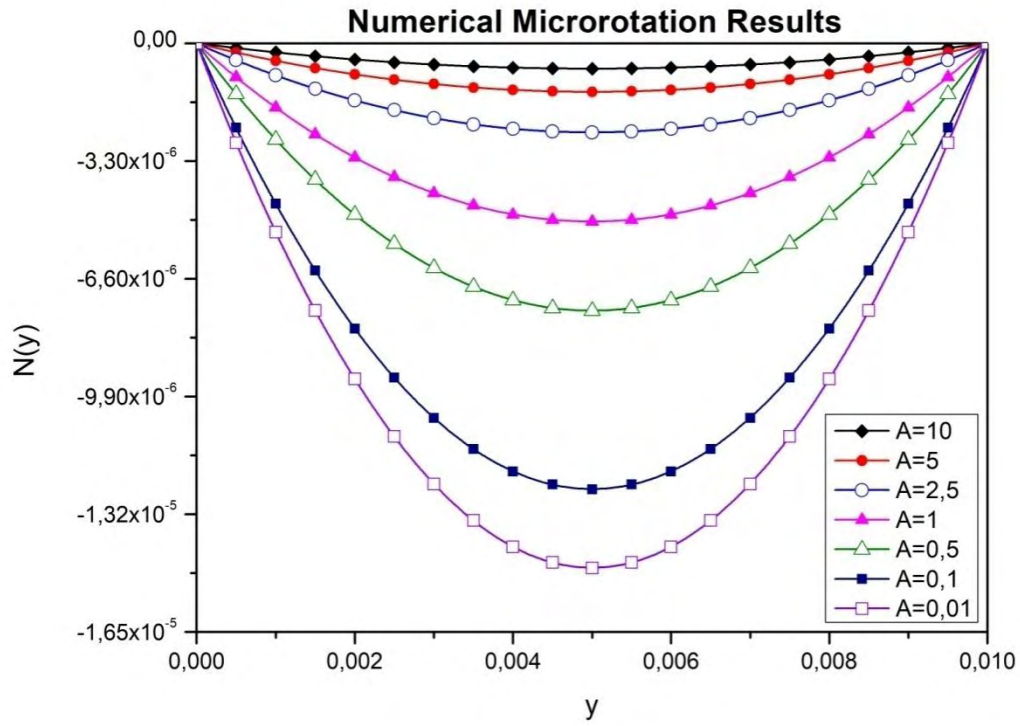

Figure 4.3. Numerical microrotation for various values of variable A. Units: y in $[m]$, $N(y)$ in $[s^{-1}]$

Even though A is given a wide range of values, the range of microrotation values remains contained. As A decreases, the absolute value of microrotation respectively increases. However this rate of change is not analogous to the rate of change in A. Instead there seems to be a diminishing effect in microrotation as A decreases further. This is due to the Ahmadi formula ensuring that as A decreases, B also decreases and counters the effect.

The velocity profiles remain seemingly unchanged. This can be explained by the low overall values of microrotation, which have a very little effect on the velocity profile.

The velocity and microrotation profiles of each individual case, along with their corresponding solutions predicted by the analytical equations, are presented below (Figures 4.4 - 4.10). For all following profiles the units are: y in $[m]$, $U(y)$ in $[m/s]$, $N(y)$ in $[s^{-1}]$.

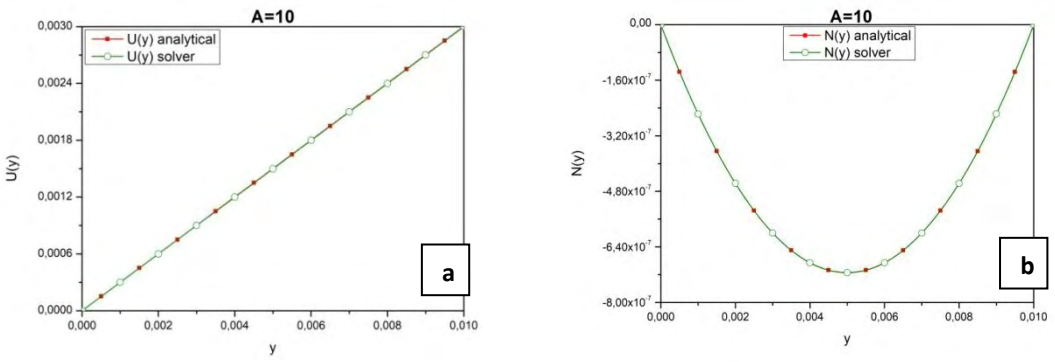

Figure 4.4. Solver and analytical profiles for velocity (a) and microrotation (b), case A=10

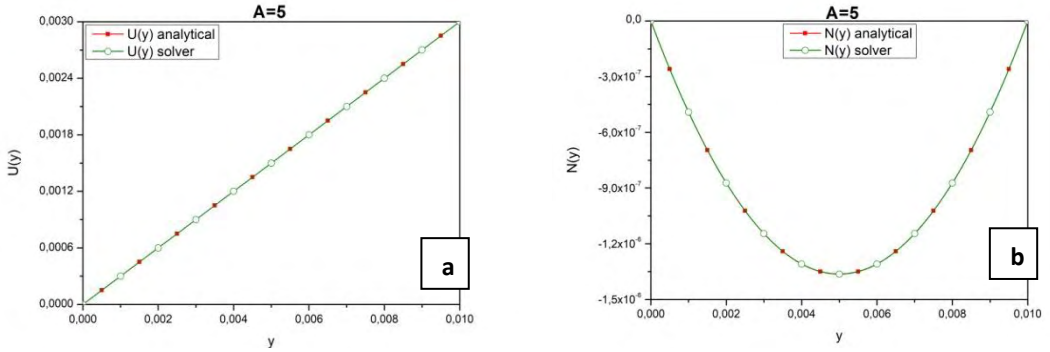

Figure 4.5. Solver and analytical profiles for velocity (a) and microrotation(b), case A=5

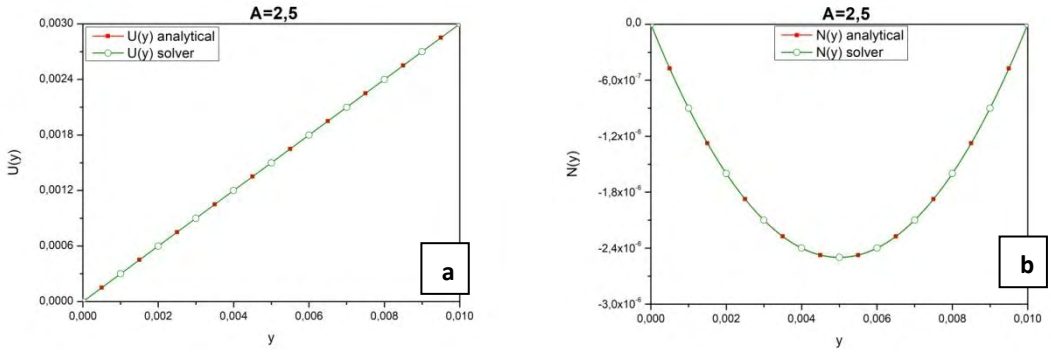

Figure 4.6. Solver and analytical profiles for velocity (a) and microrotation(b), case A=2,5

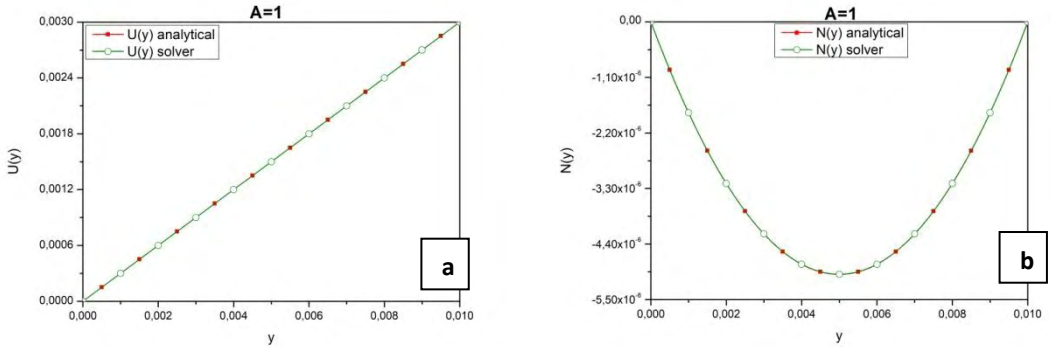

Figure 4.7. Solver and analytical profiles for velocity (a) and microrotation(b), case A=1

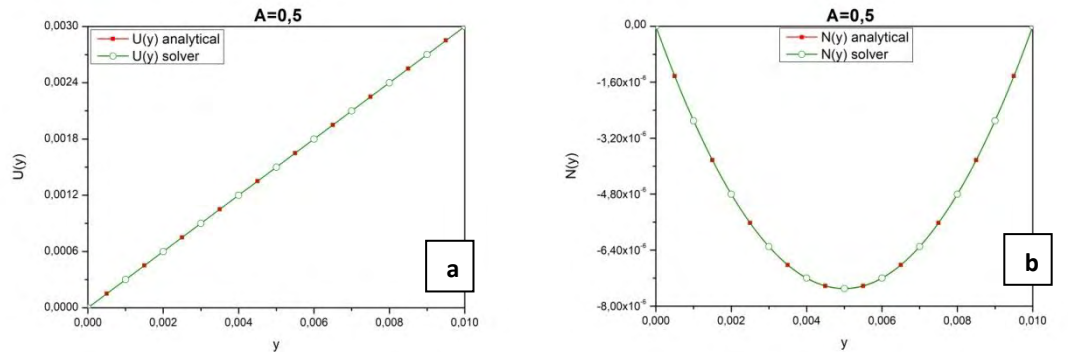

Figure 4.8. Solver and analytical profiles for velocity (a) and microrotation(b), case A=0,5

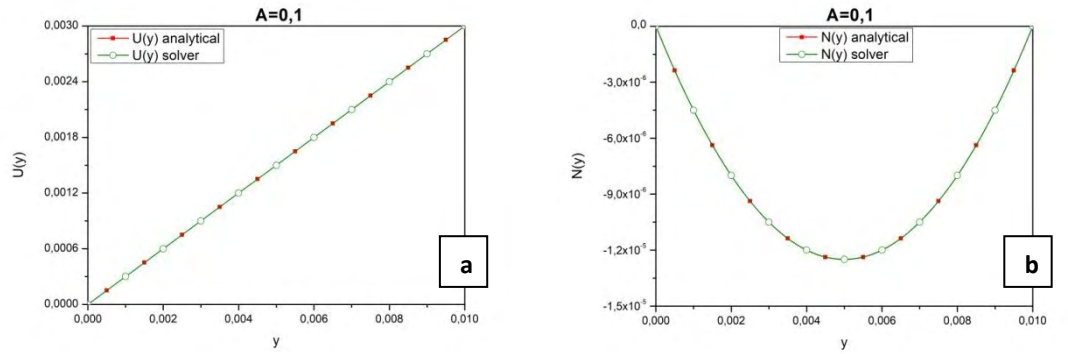

Figure 4.9. Solver and analytical profiles for velocity (a) and microrotation(b), case A=0,1

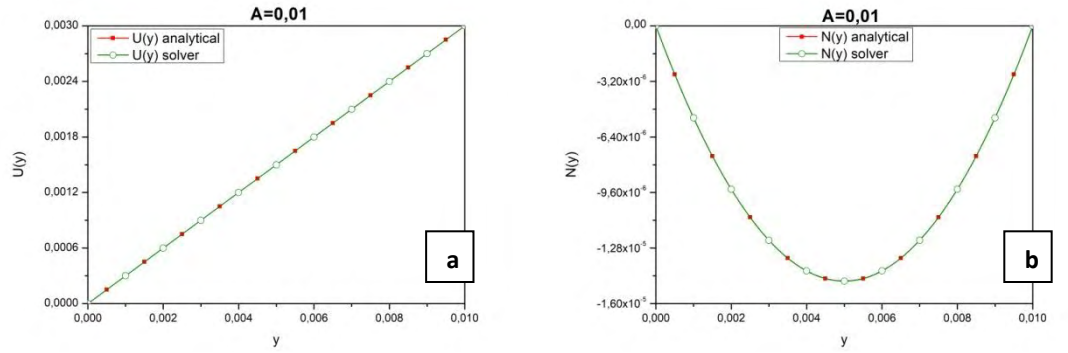

Figure 4.10. Solver and analytical profiles for velocity (a) and microrotation(b), case A=0.01

For these specific cases, the solver delivers results that effectively match the analytical solution.

4.4.2 B constant

To fully understand the change in fluid behavior, an independent analysis of the micropolar parameters was considered necessary. After removing the binding Ahmadi formula, B was

set to a constant value, while A was given selected values. This pattern can provide a clear impression of the effect of vortex viscosity k_v on the fluid.

Figures 4.11 and 4.12 present the change in profiles of microtation for varying values of the independent variable A, while B remains constant at 0,012.

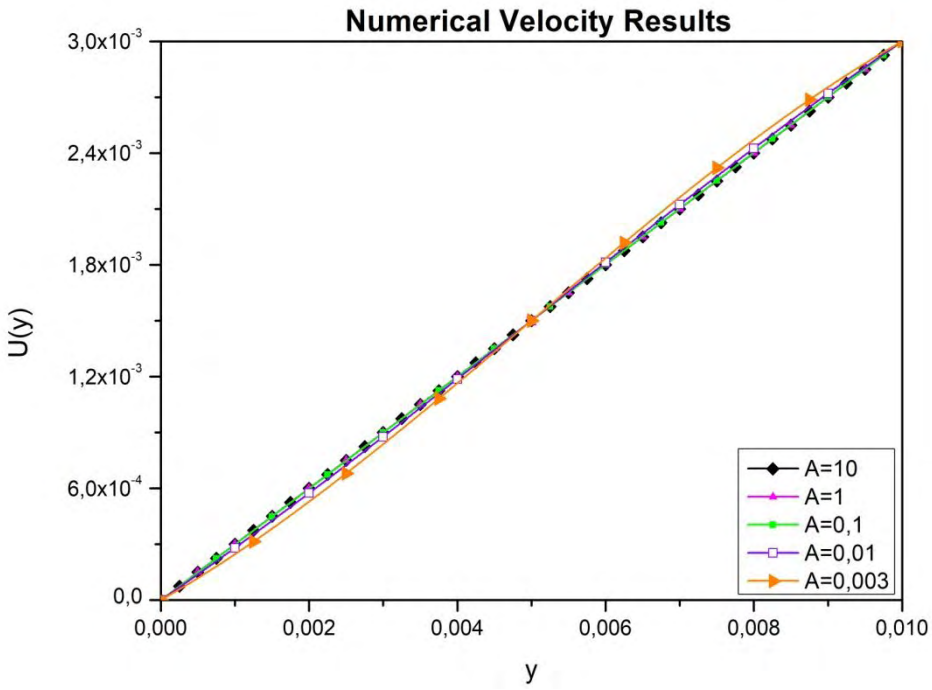

Figure 4.11. Numerical velocity for various values of variable A, with variable B=0,012. Units: y in $[m]$, $U(y)$ in $[m/s]$

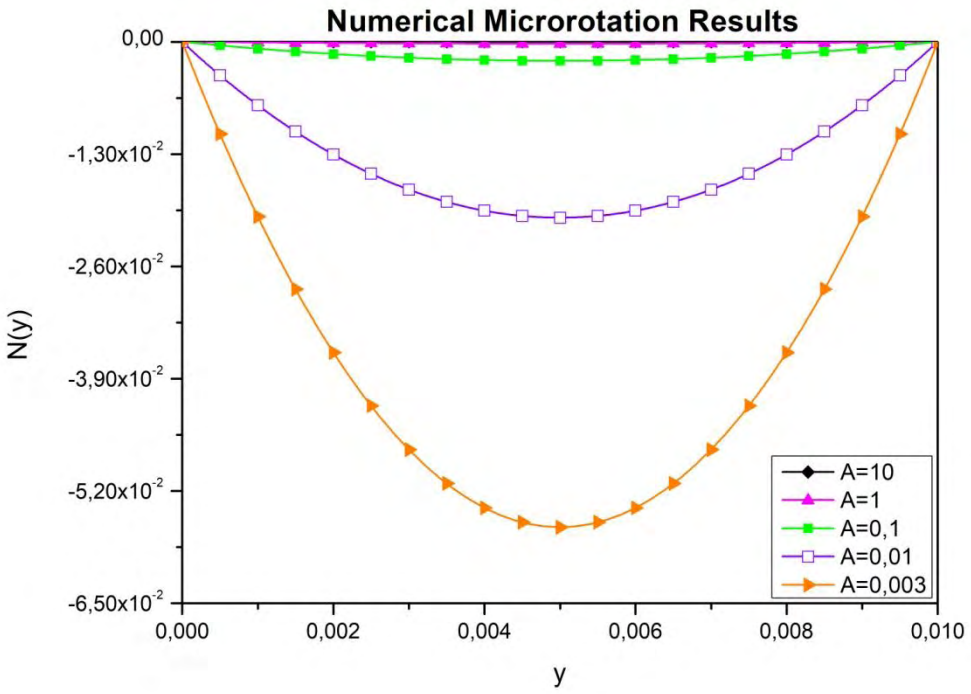

Figure 4.12. Numerical microrotation for various values of variable A, with variable B=0,012. Units: y in $[m]$, $N(y)$ in $[s^{-1}]$

It is instantly obvious that the range of microrotation is much wider, compared to the previous subset of cases, which incorporated the Ahmadi equation. In order to properly visualize the excessive variation of the output, the result is additionally presented in a logarithmic scale (Figure 4.13).

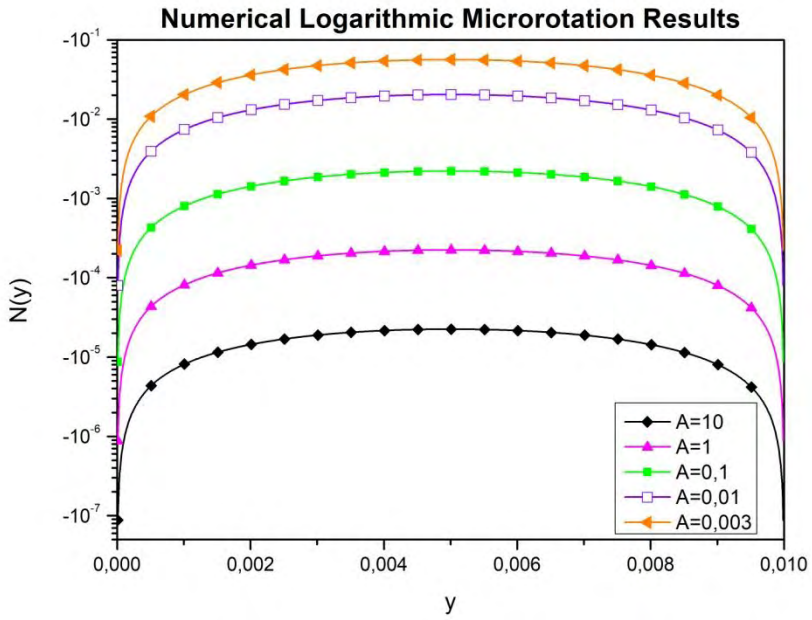

Figure 4.13. Numerical microrotation results in a logarithmic scale. Various values of variable A, variable B=0,012. Units: y in $[m]$, $N(y)$ in $[s^{-1}]$

It can be noted that the microrotation profiles reflect the exponentially changing values of the independent variable A, better than in the first measurement subset.

When A ranges from .0,01. to .0,003. , microrotation responds with notably high values, which in turn produce a distinct effect to the corresponding velocity profiles. For these extreme cases velocity exhibits a non-linear, sigmoid profile.

Figures 4.14 - 4.18 present the velocity and microrotation profiles of each individual case, as well as their corresponding analytical solutions. For all following profiles the units are: y in $[m]$, $U(y)$ in $[m/s]$, $N(y)$ in $[s^{-1}]$.

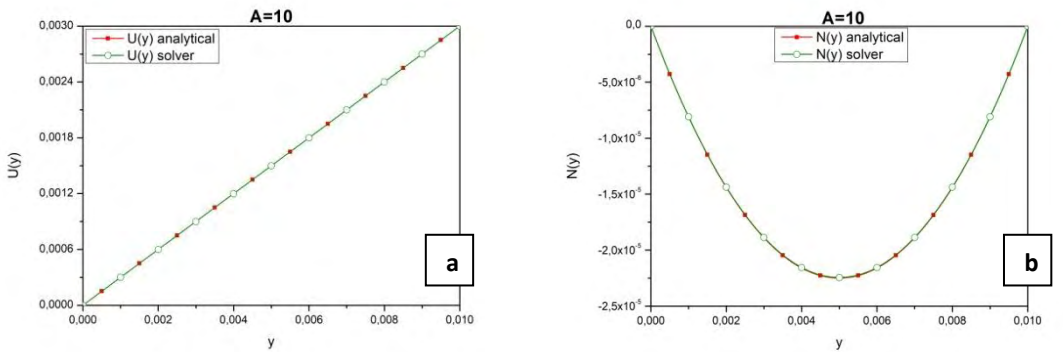

Figure 4.14. Solver and analytical profiles for velocity (a) and microrotation (b), case A=10

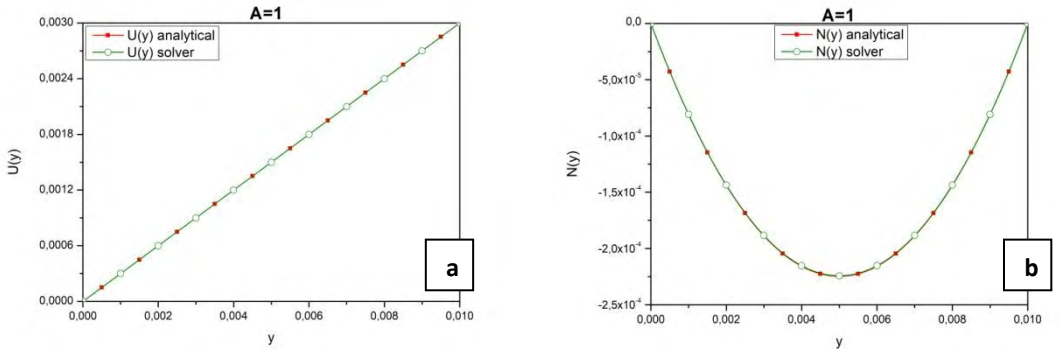

Figure 4.15. Solver and analytical profiles for velocity (a) and microrotation(b), case A=1

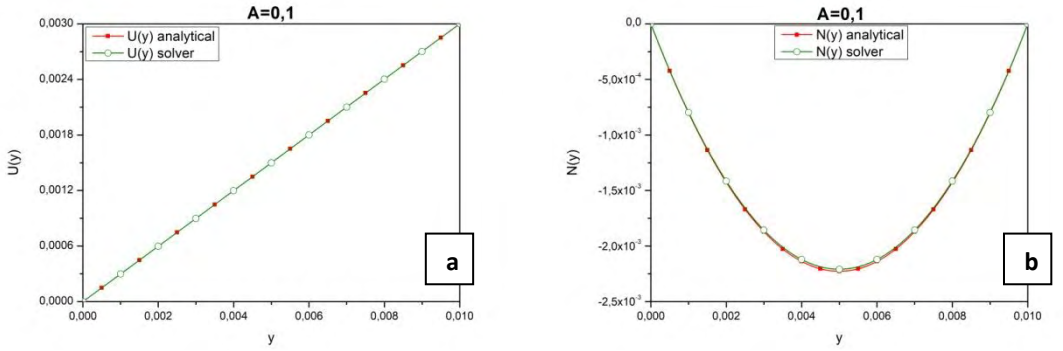

Figure 4.16. Solver and analytical profiles for velocity (a) and microrotation(b), case A=0,1

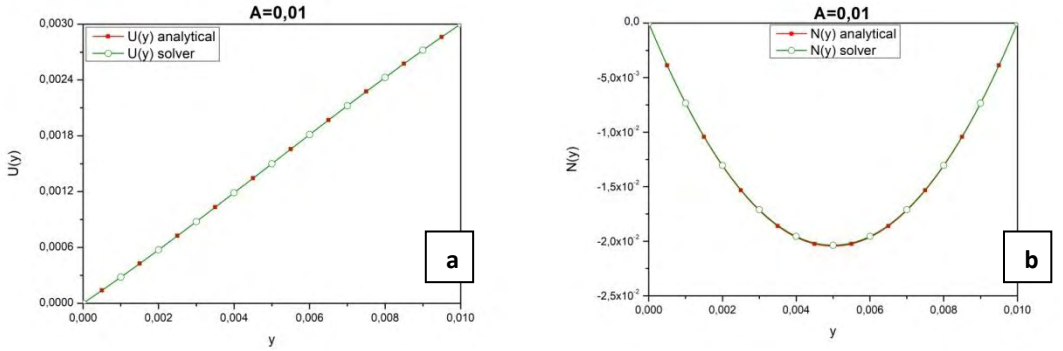

Figure 4.17. Solver and analytical profiles for velocity (a) and microrotation(b), case A=0,01

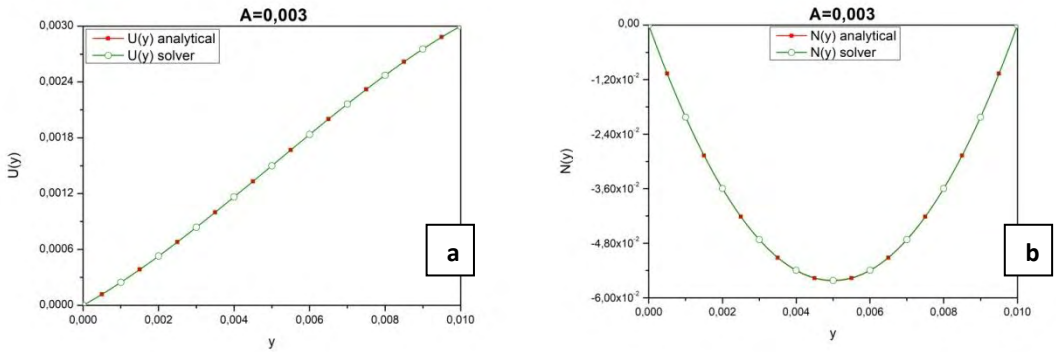

Figure 4.18. Solver and analytical profiles for velocity (a) and microrotation(b), case A=0,003

As with the first subset of cases, there is a sufficiently close correspondence between the numerical and analytical profiles. The sigmoid curve observed in the numerical velocity data is also apparent in the respective analytical solutions.

4.4.3 A constant

In the third subset of measurements, the effect of the gyration viscosity coefficient γ_v, was studied. For the analysis, A needs to be locked to a constant value, while B is given selected values.

Figures 4.19 and 4.20 depict the change in profiles of microtation for varying values of the independent variable B, while A remains constant at 0,01.

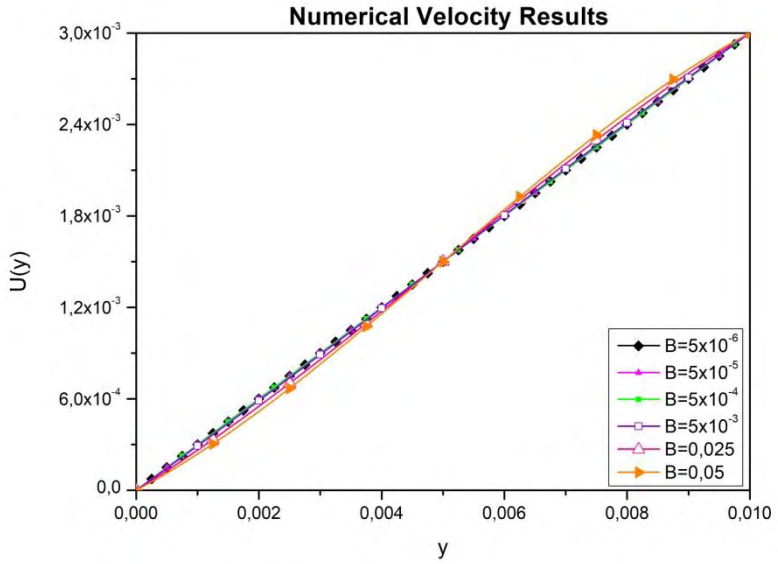

Figure 4.19. Numerical velocity for various values of variable B, with variable A=0,01. Units: y in $[m]$, $U(y)$ in $[m/s]$

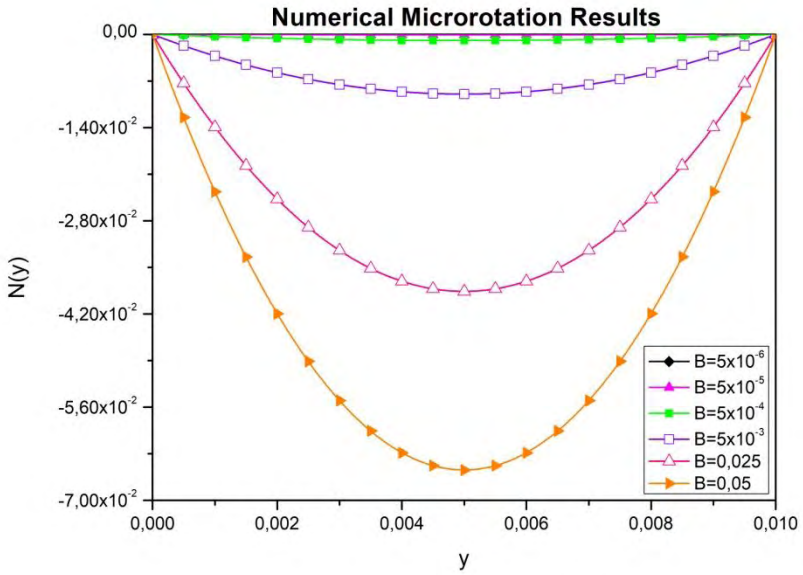

Figure 4.20. Numerical microrotation for various values of variable B, with variable A=0,01. Units: y in $[m]$, $N(y)$ in $[s^{-1}]$

It is evident that an increase in the values of B affects microrotation similarly to a decrease in variable A. In other words, the independent variables when set to act solely, produced

opposite outcomes. Again the microrotation values spread over a wide range and thus, a logarithmic scale is preferable. (Figure 4.21).

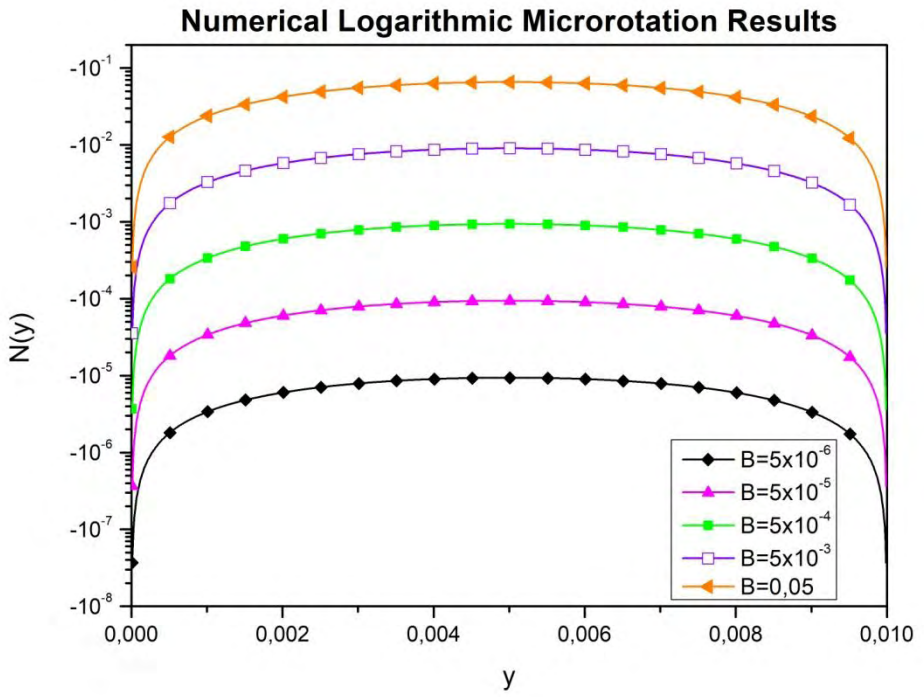

Figure 4.21. Numerical microrotation results in a logarithmic scale. Various values of variable B, variable A=0,01. Units: y in $[m]$, $N(y)$ in $[s^{-1}]$

The wide range of the microrotation values clearly follows the range of values given to variable B. The curved velocity profiles are again present and correspond to the highest values of microrotation, which in turn appear for high values of B, notably B=0,025 and B=0,05.

The velocity and microrotation profiles for each case, along with the corresponding analytical solutions, are presented below (Figures 4.22-4.27). For all following profiles the units are: y in $[m]$, $U(y)$ in $[m/s]$, $N(y)$ in $[s^{-1}]$.

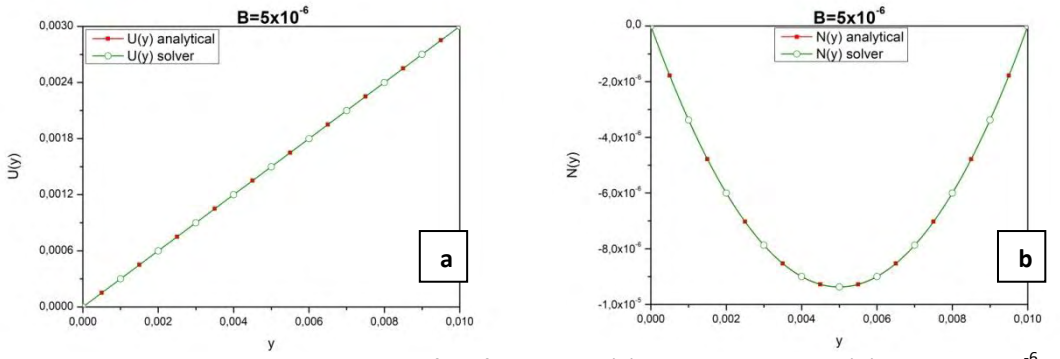

Figure 4.22. Solver and analytical profiles for velocity (a) and microrotation (b), case B=5x10^{-6}

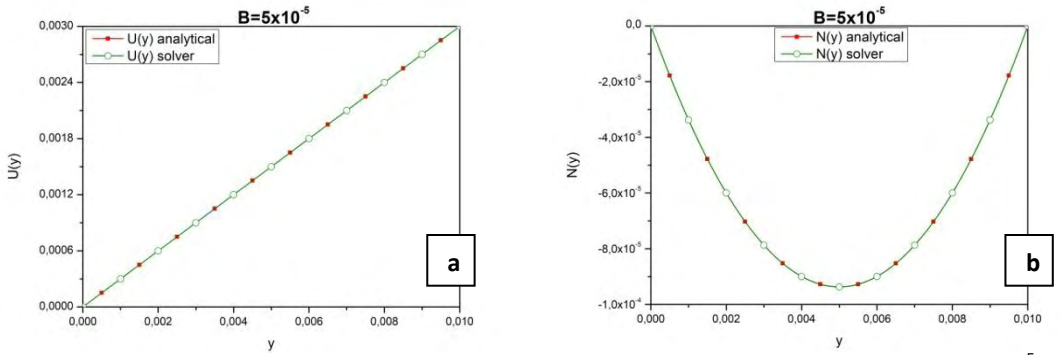

Figure 4.23. Solver and analytical profiles for velocity (a) and microrotation(b), case B=5x10^{-5}

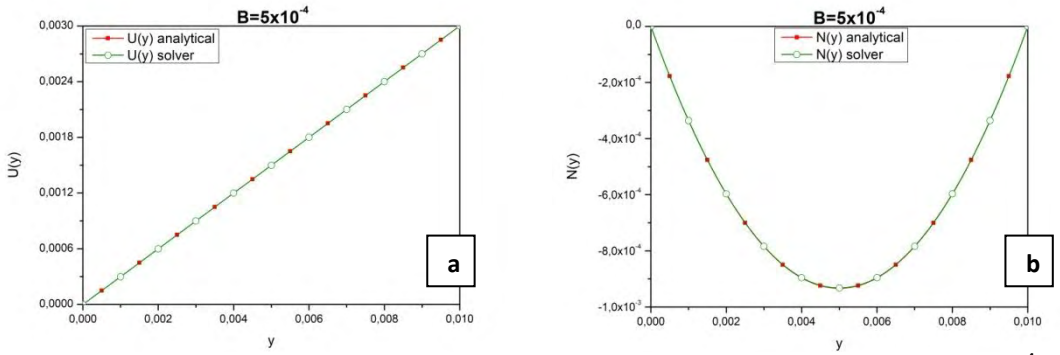

Figure 4.24. Solver and analytical profiles for velocity (a) and microrotation(b), case B=5x10^{-4}

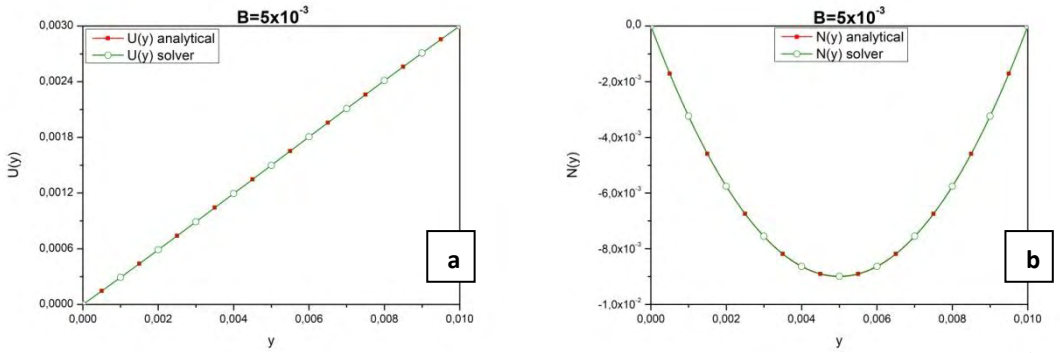

Figure 4.25. Solver and analytical profiles for velocity (a) and microrotation(b), case B=5x10^{-3}

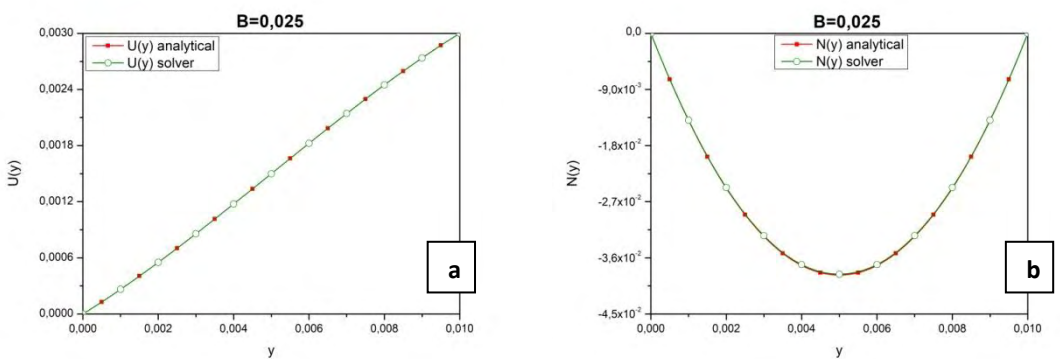

Figure 4.26. Solver and analytical profiles for velocity (a) and microrotation(b), case B=0,025

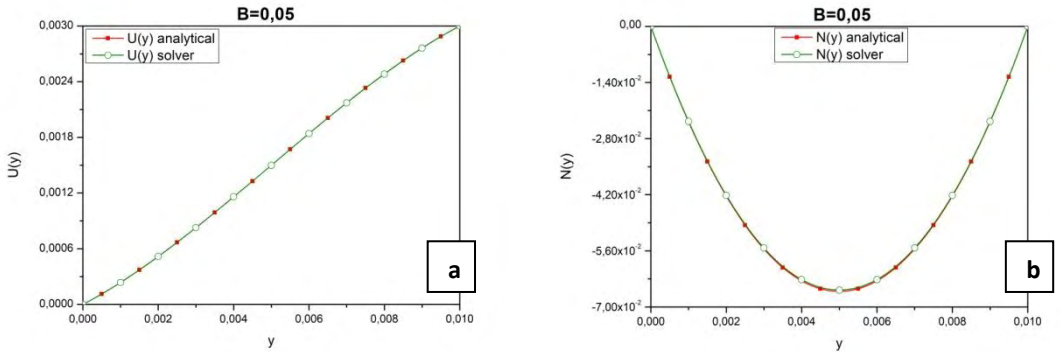

Figure 4.27. Solver and analytical profiles for velocity (a) and microrotation(b), case B=0,05

The agreement between the analytical and the numerical results can again be observed. As in the previous subsets of cases, the sigmoid velocity profile that was recorded, is verified by the analytical solution.

4.5 Shear Stress Analysis

The sigmoid response observed in some of the velocity profiles presented above, raises an issue regarding the effect on shear stress. In this subchapter, the analysis of two cases, exhibiting sigmoid velocity profiles, is expanded in regard to shear stress. Commonly, shear stress τ_{xy} is given by relationship:

$$\tau_{xy} = \mu \frac{dv_x}{dy}$$

It is widely known that the simple, fully developed, Newtonian Couette flow, corresponds to a constant shear stress. This value is calculated by dividing the wall velocity with the height of the channel, and then multiplying by the dynamic viscosity. By applying the above in a Newtonian Couette flow, analogous to the cases previously examined, the constant value was calculated.

$$\tau_{xy\ Newtonian} = \mu \frac{V}{h} = \mu \frac{0{,}003\ m/s}{0{,}01\ m} = 0{,}3\mu\ s^{-1}$$

In order to derive a final numerical value, the fluid, and more specifically its dynamic viscosity, must be defined. As this would limit the scope of the analysis, the shear rate $\dot{\gamma} = \frac{\tau_{xy}}{\mu}$ was instead measured in both the numerical results and the Newtonian fluid.

The two numerical cases in question are A=0,003, B=0,012 of the second subset, and B=0,05, A=0,01 of the third subset. The numerical derivative of velocity was obtained by the following numerical scheme:

$$\frac{df}{dx}_{x=x_i} = \frac{f_{i+1} - f_{i-1}}{x_{i+1} - x_{i-1}}$$

The result was then smoothed, in both cases, using a polynomial numerical fit. When placed alongside the fixed numerical value in Figure 4.28, the variation is easily noticeable.

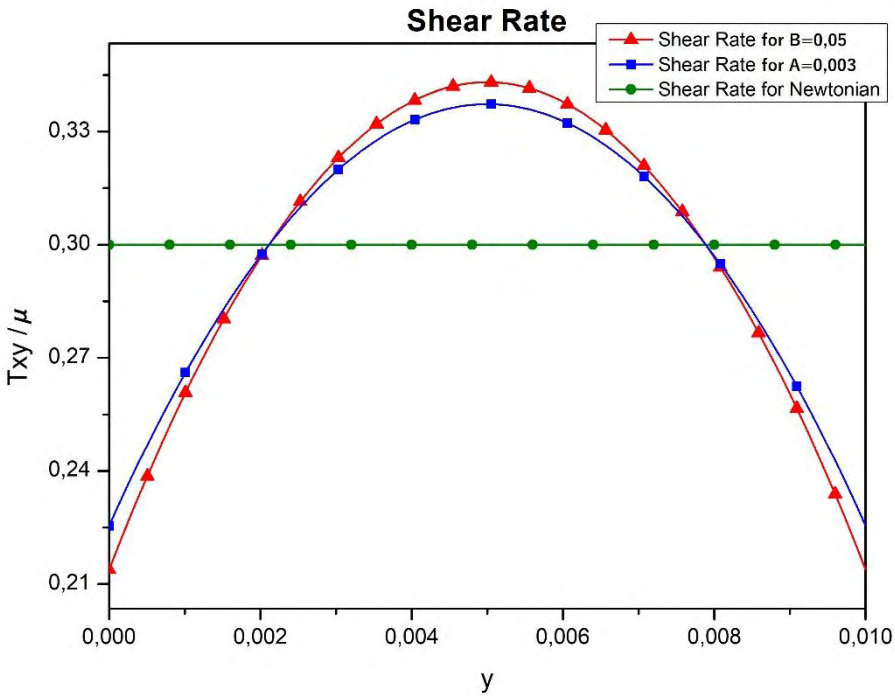

Figure 4.28. Shear Rate comparison of case A=0,003, case B=0,05 and Newtonian case. Units: y in $[m]$, τ_{yx}/μ in $[s^{-1}]$

The above comparison invites some interesting observations. As y increases from the bottom wall, the shear rate also increases, surpassing the Newtonian value. At the middle of the channel, the shear rate reaches its maximum value, then it proceeds to decrease as y increases further, mirroring the ascend. The low shear rate values near the solid walls are also worth mentioning.

The deviation from the fixed Newtonian line appears to increase as the sigmoid characteristic becomes more intense. This, as mentioned before, occurs for sufficiently high values of microrotation, which is in turn notably effected by A and B. Thus, there is a clear correlation between the values of the non dimensional parameters, and the shear rate profile. In this comparison, the shear rate profile for B=0,05 appears more intense than that of A=0,003, due to the highest values for microrotation in the former case.

CHAPTER 5 RESULTS PRESENTATION AND COMPARISON FOR POISEUILLE FLOW

5.1 Introduction

This chapter is dedicated to the analysis and comparison between results obtained by the execution of numerical simulations regarding Poiseuille flow. As a starting point, the different cases are formulated but also flow parameters closely related to flow characteristics are determined. In addition, the final grid density and consequently, the cell number is established. As a final step, all results were thoroughly examined and a parametric analysis is taking place.

5.2 Case Format

The equations of velocity and microrotation have been numerically solved for the case of poiseuille flow (flow between two parallel plates). In order to test the suitability of the micropolarFoam solver, comparison with the analytical results is performed on this chapter. Identification and correct representation of the parameters involved are of great importance, before the analysis take place. Accurate problem formulation, involves some set of initial and boundary conditions, thus, as a first estimation, the internal boundary velocity field was set to (0, 0, 0).

At this point, a distinct difference between the formulation of the exact problem and numerical simulations should be underlined. During the formulation of the problem in chapter 2.5.2 geometrical height of the channel was chosen as 2h (in order to be in agreement with the formulation of the problem proposed by Lukaszewicz. Taking that into consideration, all numerical simulations are based on a total channel height of $H_{tot} = 2h = 0{,}01\ (m)$. Also, the microinertia parameter was set at $j = 1\ (m^2)$. Last but far from least,

the boundary condition considered for microrotational parameter was set to $N_{wall} = 0\ (s^{-1})$. Inlet and outlet pressure was uniformly defined. A good starting point for setting the pressure boundary condition seem to be eq (40). Setting $\frac{-\frac{dp}{dx}h^2}{2\nu} = 1\ (\frac{m}{s})$, helps in both - definition of pressure drop inside the channel, as well as it offers an acceptable base line for results comparison, regarding velocity and microrotation measurement units.

The Reynolds number for poiseuille flow was first instroduced in the chapter 2 of theory. After the process of dimensionization it is proven to be:

$$Re_{total} = \frac{\rho v_0 L_0}{(\mu_v + k_v)} = \frac{v_{mean}\, H_{tot}}{(\nu + ku)} \frac{\boldsymbol{\nu}}{\boldsymbol{\nu}} = Re_h \cdot F_c$$

Since the value of the average velocity as well as parameter ku are different for every simulation, the Reynolds number cannot be assigned with a specific value. That formulation is mainly out of use, as it represents some sort of an effective Reynolds number (dynamically adjusted, as the parameter ku is involved). Due to the fact that the studied cases represent a fully developed, steady state, laminar flow, the hydrodynamically formulated Reynolds number is much more appreciated.

$$Re = \frac{\rho v_{mean} L_0}{\mu_v} = Re = \frac{\frac{2}{3} v_{max}^{parabolic} h_{tot,channel}}{v_v} = \frac{\frac{2}{3} \cdot 0.01}{0.003} \approx 2.22$$

With the objective to showcase any differences or similarities between the two models, an effort to use the same fluid material properties was in great need. All simulations were executed based on the non-dimensional parameters obtained in chapter 2.

5.3 Mesh Refinement

Mesh refinement may be the most crucial part of numerical results acquisition. The main purpose lies behind the fact that an increase in the mesh resolution can drastically improve

flow characteristics (accurately capture flow attributes). As it has previously been mentioned the generated mesh for the case studied was uniformly generated. There are many cases that involve multi grading of the mesh with a scaling factor. Besides the fact that many simulations have been performed with both meshes, non-significant results were acquired. The region that involves the formation of boundary layers is of great importance, due to the fact that viscosity phenomena greatly affect the flow characteristics. It is well known that the number of elements involved in the generated mesh greatly affect the numerical results. That idealized scenario with zero grid spacing is considered to be the finest. In order to find the appropriate grid, spatial convergence must be studied.

The typical case studied, involves the formulation of many meshes with a number of elements that gradually increases in the x and y directions. They have all been performed for a set of parameters $ku = 0.05$, $gu = 0.005$.

It is worth mentioning that the mesh density in the z-direction does not affect the results since microrotation is given in vectorial form as N=(0, 0, N(y)).

All the results obtained are graphically represented below:

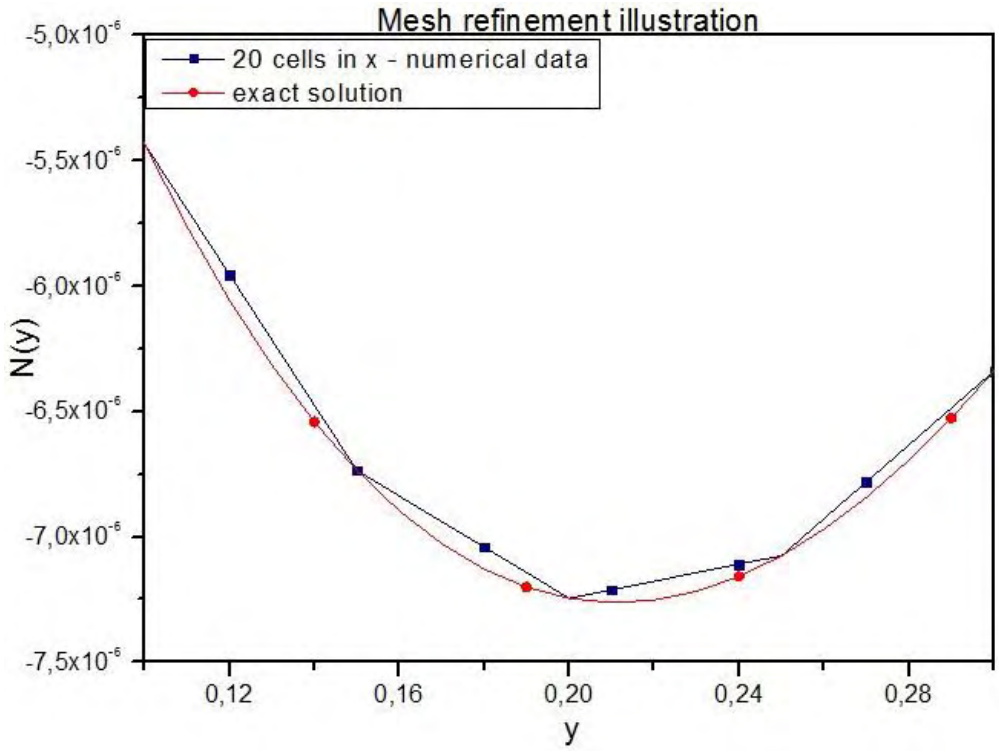

Figure 5.1: Numerical results deviation with regard to exact solution.

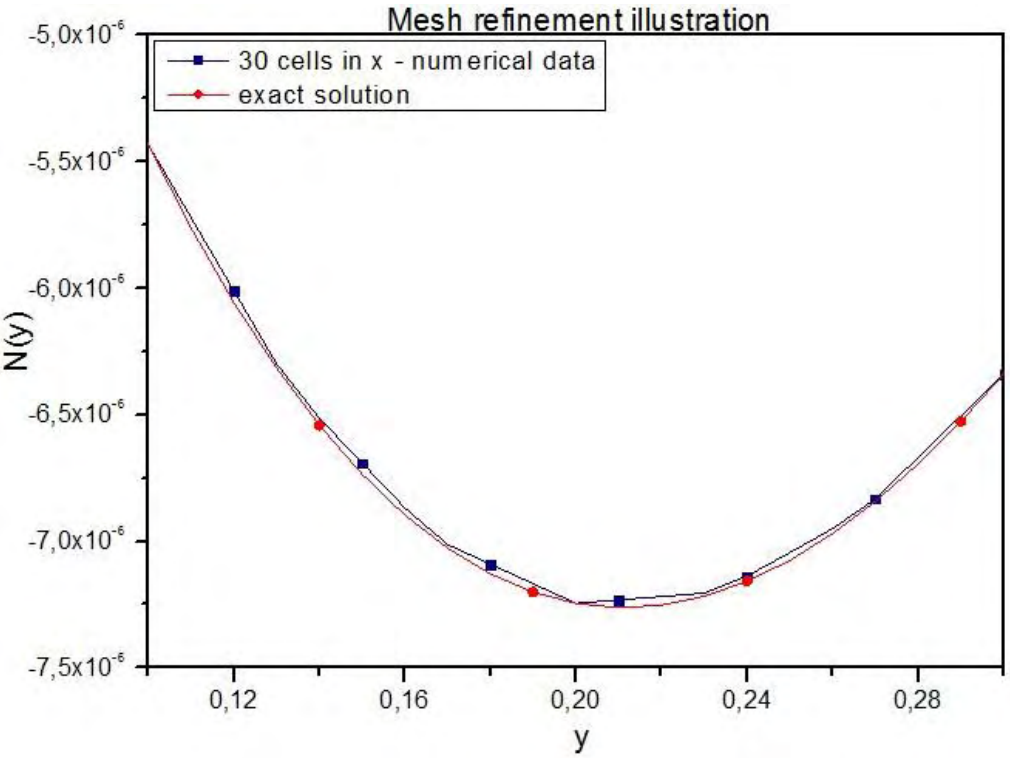

Figure 5.2: Numerical results deviation with regard to exact solution.

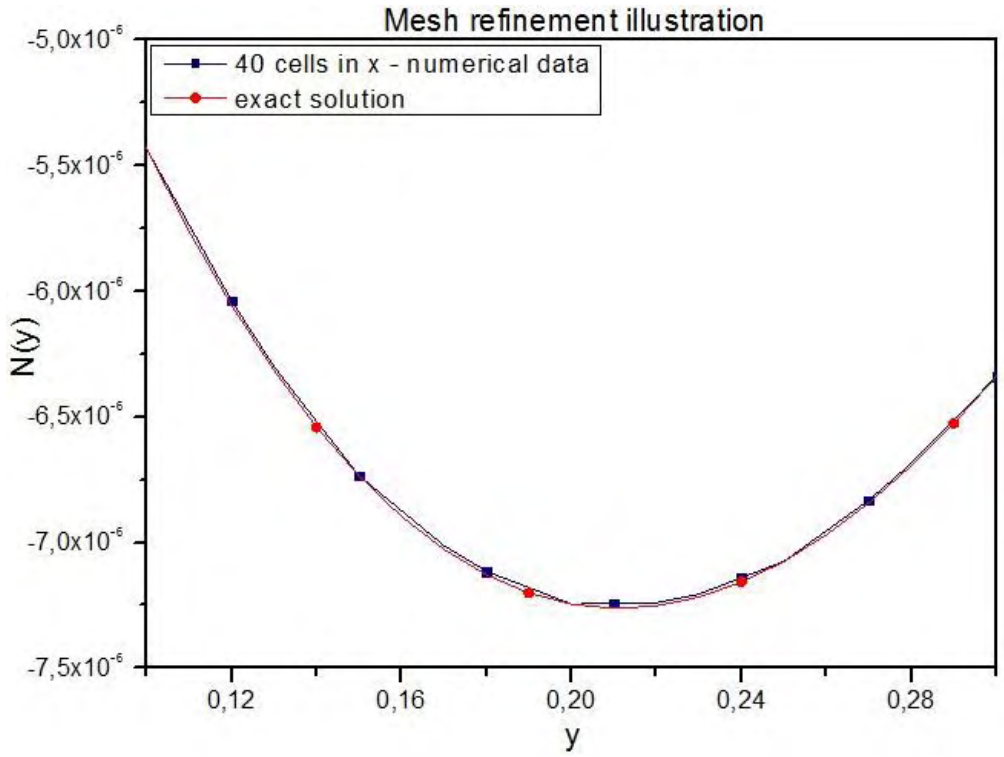

Figure 5.3: Numerical results deviation with regard to exact solution.

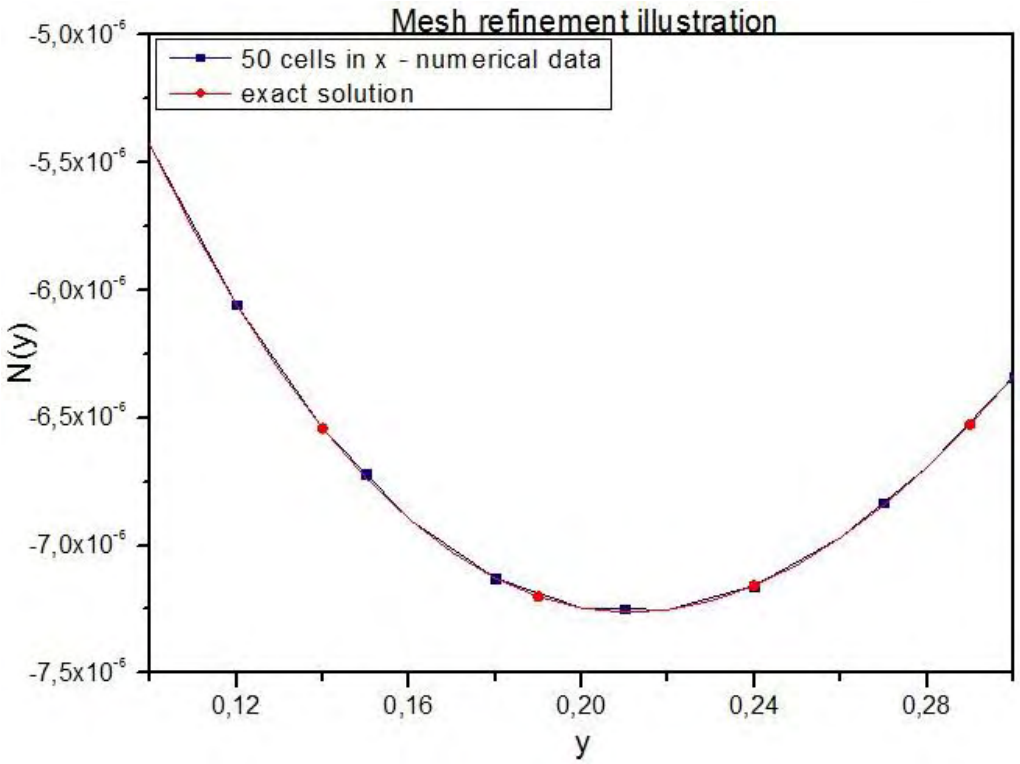

Figure 5.4: Numerical results deviation with regard to exact solution.

As it is clear, analytical and numerical results tend to coincide as the number of the cells increase. For finer meshes, it is obvious that the error between the two sets of results for the specific case studied, becomes negligible. Two types of data error, namely relative and absolute will be presented for each one the meshes above, using the following:

$$\epsilon_{abs,i} = \left| N_{i,analytical} - N_{i,numerical} \right|$$

And

$$\epsilon_{rel,tot} = \sum_{i=1}^{n} \frac{\epsilon_{abs,i}}{\left| N_{i,analytical} \right|}$$

Where n, is the total number of data for both, analytical and numerical results. In other words, it is preferably to say that the absolute error is the magnitude formulated, due to the difference among the analytical and numerical results. In addition to that, relative error is the ratio of absolute error to the magnitude of a specific numerical data point.

Bearing in mind these two formulas, the final results are summarized in the table below:

Table 5.1. Error values for the meshes used.

Mesh	$\epsilon_{abs,tot}$	$\epsilon_{rel,tot}$
20x20	4,52999028154108E − 6	0,84497368842139
30x30	2,07671028154108E − 6	0,61579741768601
40x40	1,13335028154107E − 6	0,341911770593257
50x50	5,6764272124369E − 7	0,176767157701199

As it was expected, all visual observations were confirmed. As the mesh becomes more dense, (each of the aforementioned cases consist of 1200, 2700, 4800, 7500 cells respectively), absolute as well as relative errors are getting closer to zero. In addition, relative error has to be compared to a physical ratio scale in order to be valid. Due to that, it

is compared to the magnitude of the microrotational field (10^{-5}). It is obvious that is adequate small. As a result, the mesh used for the execution of all numerical simulations, is the one, with a density of 7500 cells.

An alternative method used mainly for verification of the results, is affiliated with the solution to the volumetric flow rate of the studied poiseuille problem.

Flow rate of a fluid moving inside a square shaped cross sectional channel, is given by the integral of velocity with respect to the area perpendicular to the flow. Mathematically is presented by the following closed form integral:

$$\dot{V} = \oiint (\vec{u} \cdot \vec{n}) dA$$

Where the closed form integral, represents the cross section area of the channel. Since it is well known, that the velocity field is of the form $\vec{v} = (v_x(y), 0, 0)$, the formula above can be transformed into:

$$\dot{V} = \iint_{A_1}^{A_2} (\vec{u} \cdot \vec{n}) dA = \iint_0^h u_x\,(y) dy dz = Z(channel\ width) \times \int_0^h u_x(y) dy \qquad (45)$$

Bearing in mind that the only available data are that of the velocity field, a numerical approach needs to be established. Among many numerical schemes, Simpson's $\frac{1}{3}$ rule was used to approximate the integral form (45). Following the steps below we get:

$$\int_0^h u_x(y) dy \approx \frac{d}{3} (u_0 + 4u_1 + 2u_2 + \cdots + 2u_{n-2} + 4u_{n-1} + u_n)$$

The term d, denotes the preferable integration step, but also is in agreement with the total number of numerical data. It is determined as $= \frac{(upper\ limit) - (lower\ limit)}{n} = \frac{h-0}{100}$.

The main focus of the analysis, orbits around the fact that the problem is solved once again for a continuously increasing number of grid elements. Volumetric flow rate acquired by the exact data is set as the absolute target value. Three cases of $\pm 1\%$, $\pm 0.1\ \%$, and $\pm 0.01\%$ were graphically illustrated in figures (5.5)-(5.7) respectively.

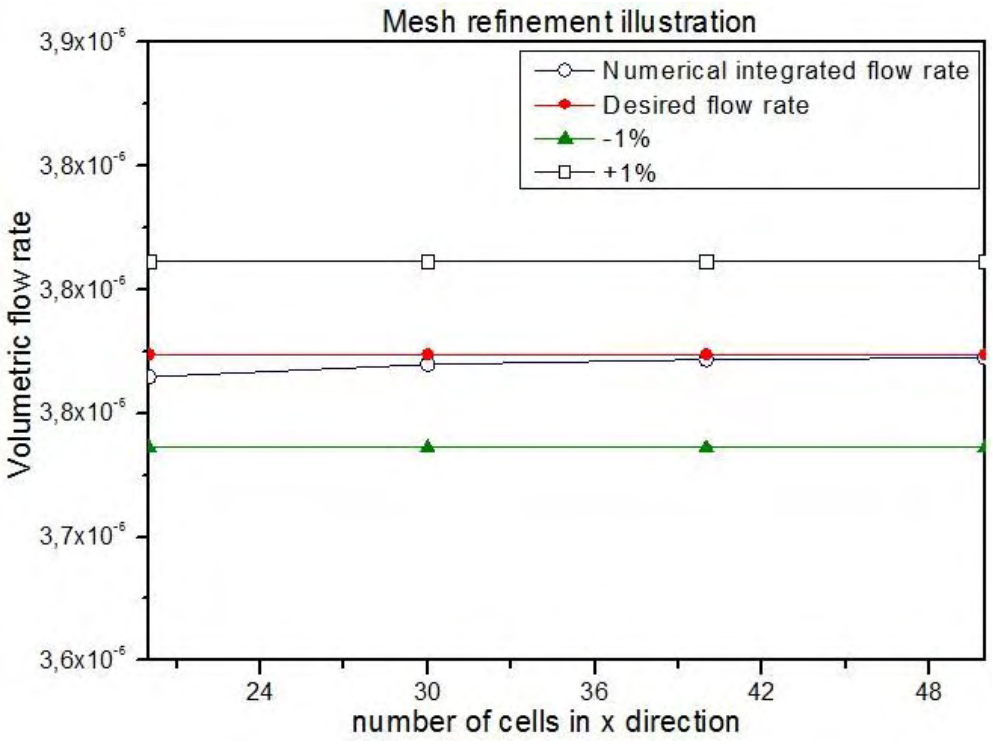

Figure 5.5: Numerical results deviation with regard to exact solution, for $\pm 1\%$

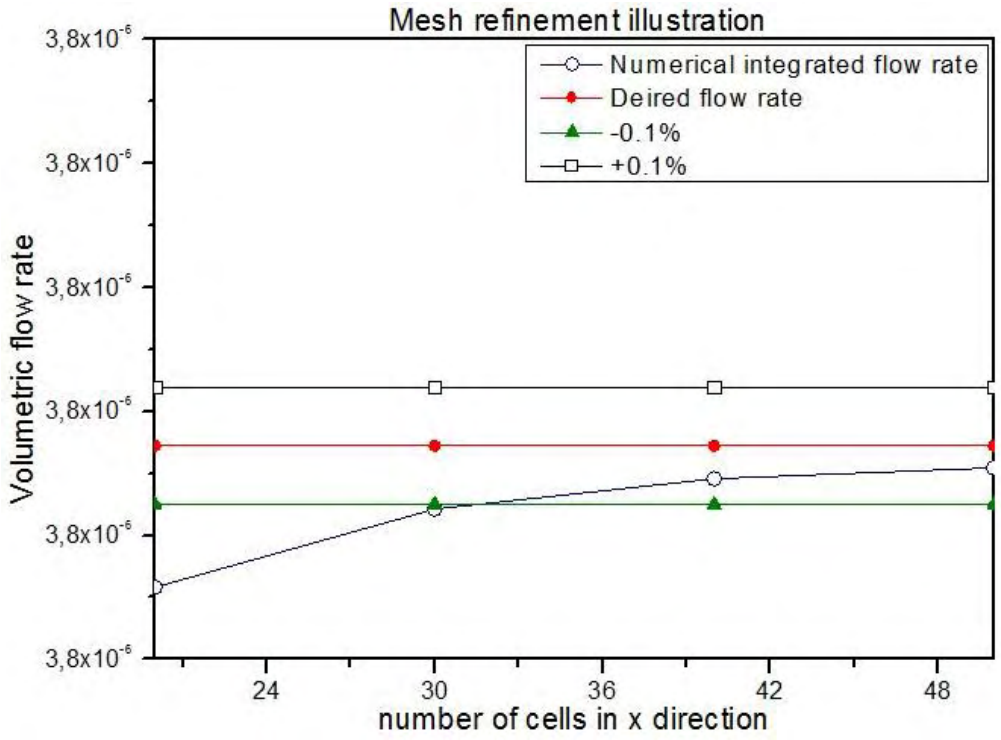

Figure 5.6: Numerical results deviation with regard to exact solution, for $\pm 0.1\ \%$

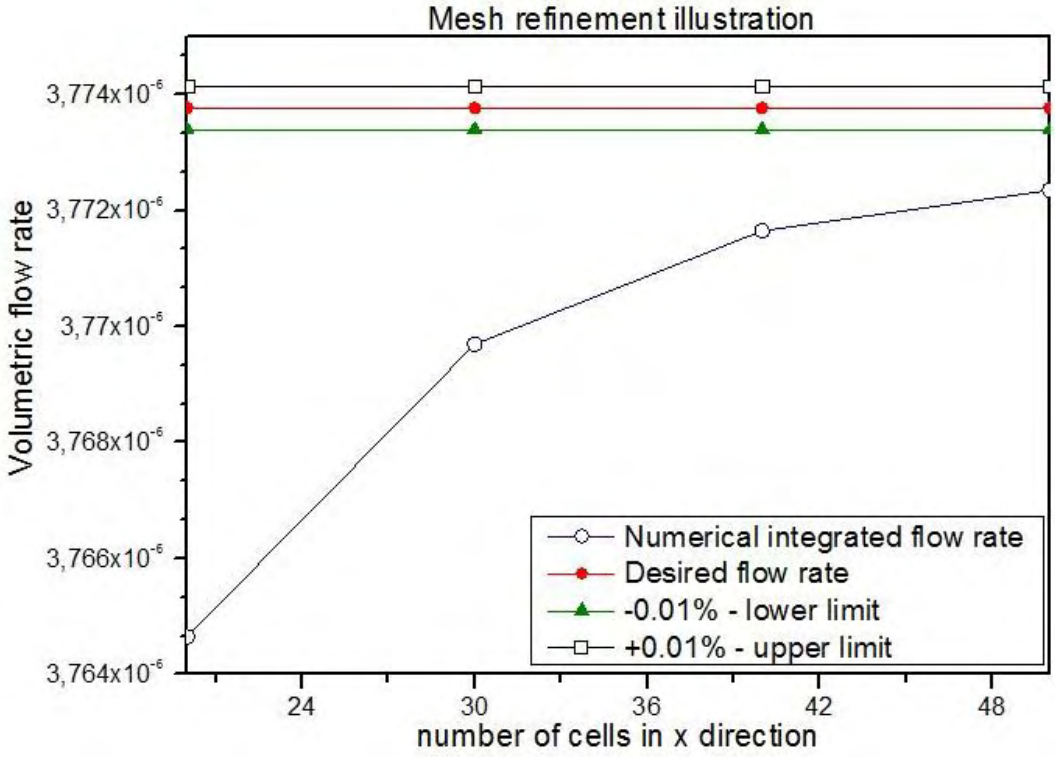

Figure 5.7: Numerical results deviation with regard to exact solution, for $\pm 0.01\%$

It is safe to say that all of the aforementioned results, were compared based on the previous reference levels. In many scientific papers, the criterion of acceptance is the same. Values in the range of $\pm 1\%$, of the convergence one, are considered acceptable. Hence, it is obvious, that the mesh used mainly consisted of 7500 elements is acceptable. Although, a more meticulous investigation, results to a more strict acceptance percentage.

Despite which one of these two methods will be adopted, it is concluded that the mesh used is in great agreement for both.

5.4 Presentation of Results

The quantities and the parameters used as independent variables in this examination are presented below:

Table 5.2. Representaion of parameters involved with respect to numerical simulations.

1st case (Ahmadi)	2nd case (gu=0.001 - L=0.054)	3rd case (ku=0.14 - N=0.99)
k=0.1 - ku=0.0003 - gu=0.00315	N=0.301 – k=0.1 – ku=0.003	L=0.09 - gu=0.000037
K=0.5 - ku=0.0015 - gu=0.00375	N=0.667 – k=0.8 – ku=0.0024	L=0.08 - gu=0.000046
K=1 - ku=0.03 - gu=0.0045	N=0.816 – k=2 – ku=0.006	L=0.06 - gu=0.000083
K=10 - ku=0.03 - gu=0.018	N=0.953 – k=10 – ku=0.03	L=0.04 - gu=0.000187
K=50 - ku=0.15 - gu=0.078	N=0.995 – k=100– ku=0.3	L=0.02 - gu=0.00075
K=100 - ku=0.3 - gu=0.3		

Once the mesh has been refined, and the total number of cells fully established, simulated cases have to be organized in such a way that the effects of the parameters introduced in chapter 2 (N and L), would be easily identified. In order to succeed that, the one factor at a time method was used. Along these lines, all simulations grouped in such way, involving the testing of parameters one at a time.

5.4.1 Ahmadi formula

As a starting point a connection between spin gradient γ_v and vortex k_v viscosities, was used. Proposed in the paper of Ahmadi [22], and simply states that:

$$\gamma_v = (\mu + \frac{k_v}{2})j$$

For the purpose of the non-dimensional parameters proposed in the previous chapter 2, a correlation between K, L and the above equation can be made. Setting $j = 1$, gives:

$$4\frac{h^2}{L^2} = 1 + \frac{K}{2}$$

Different results for microrotation and velocity are presented below for a wide range of material parameter values.

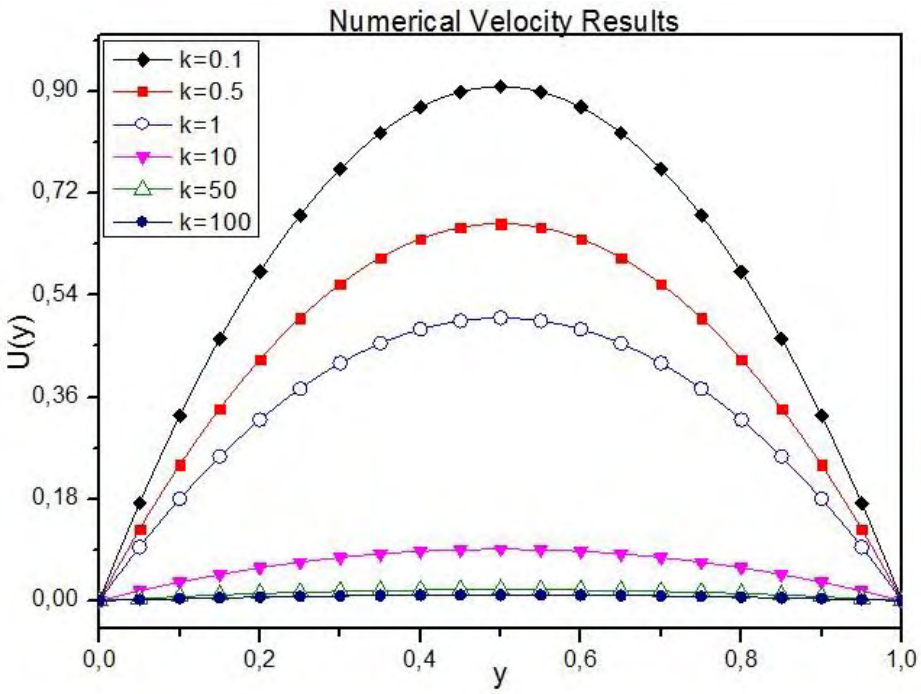

Figure 5.8. Numerical velocity for different material parameters K.

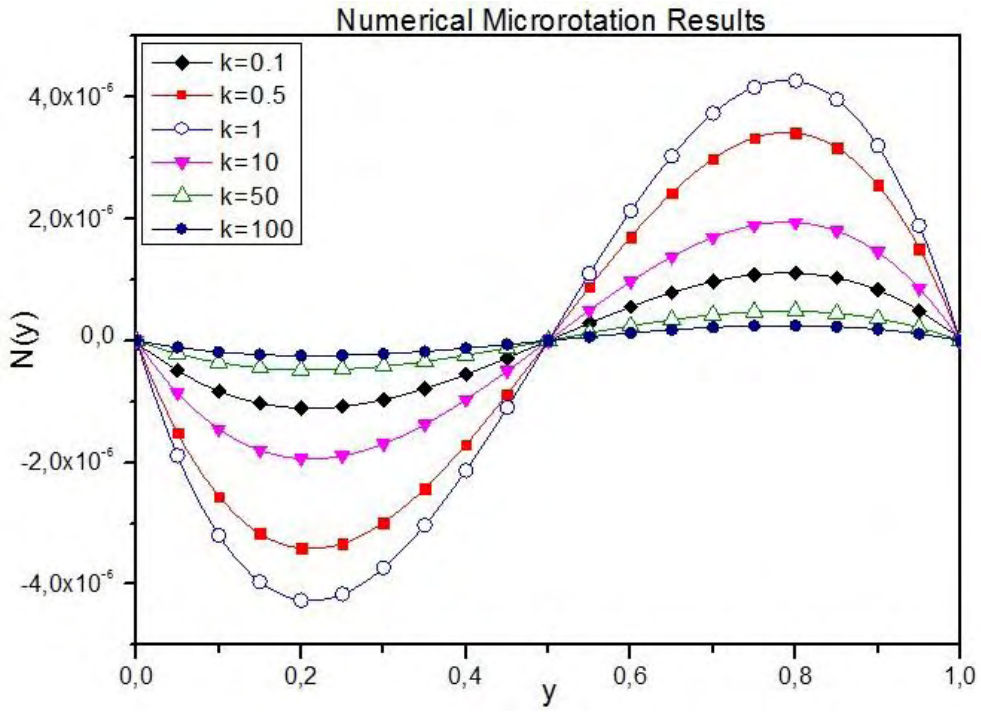

Figure 5.9. Numerical microrotation for different material parameters K.

It is clear that an increase of parameter K, respectively decreases the magnitude of the flow velocity. The changes are of significant importance in constrast to the results obtained by the couette case flow.

On the other hand, something extraordinary happens to the microrotation field. That monotonous behavior described previously does not take place here. As the parameter K increases, the magnitude of the microrotation respectively increases, but that suddenly changes at a specific point. To fully understand how microrotation responds to that change, another figure is presented below.

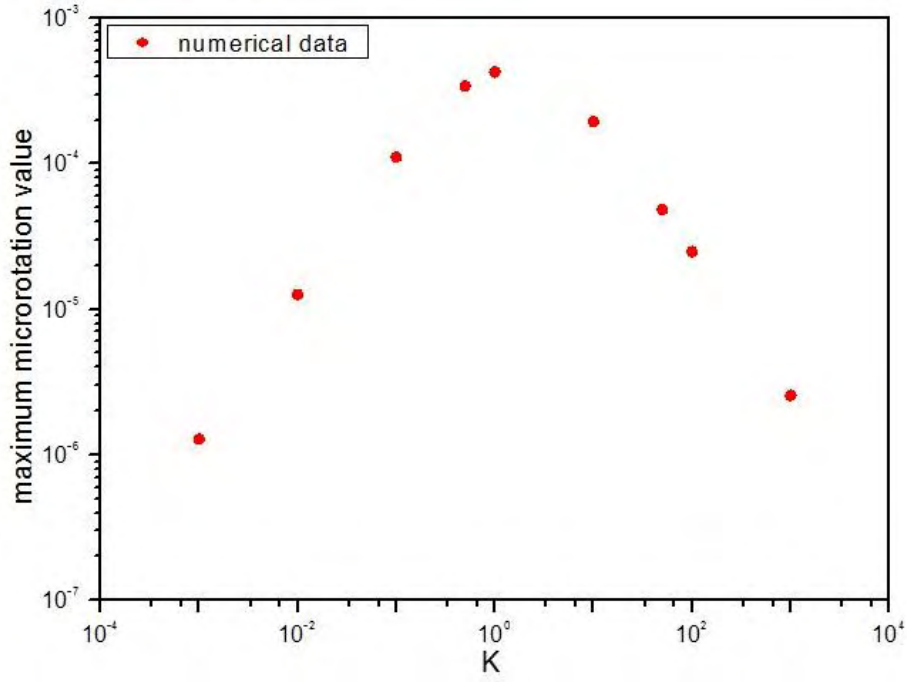

Figure 5.10. Maximum microrotation with respect to different material parameters K

The answer really lies behind the formula (). An increase in parameter K actually forces microrotational effects to be more substantial. Increase in K forces parameter L to decrease, reaching that point, where its significance becomes noticeable. A more thoroughly investigation of the effects of parameters will be performed in the next steps. Velocity and microrotation profiles for each value of the material parameter K, along with the corresponding analytical solutions obtained from exact solutions of chapter 2, are presented below.

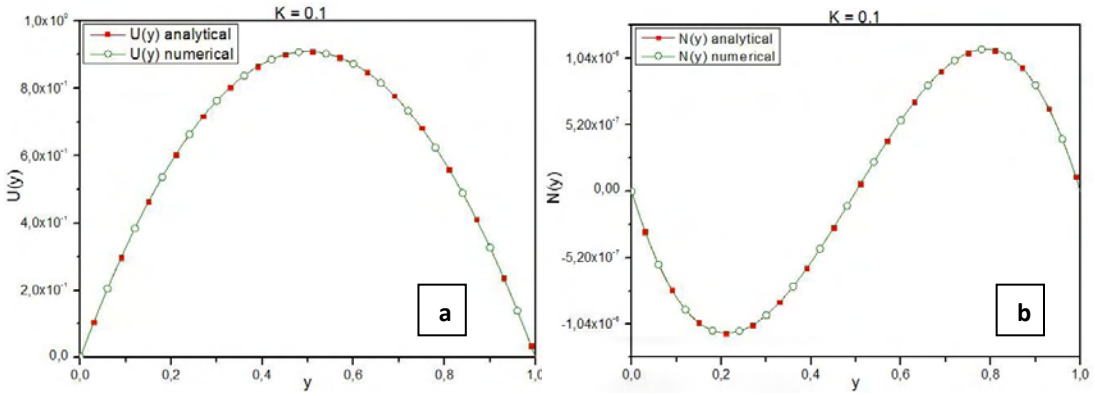

Figure 5.11. Solver and analytical profiles for velocity (a) and microrotation (b), case $K = 0{,}1$

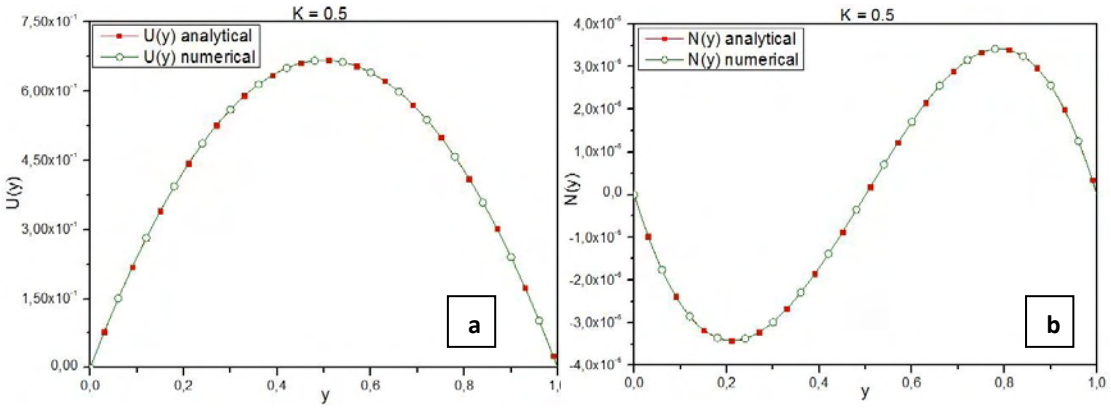

Figure 5.12. Solver and analytical profiles for velocity (a) and microrotation (b), case $K = 0{,}5$

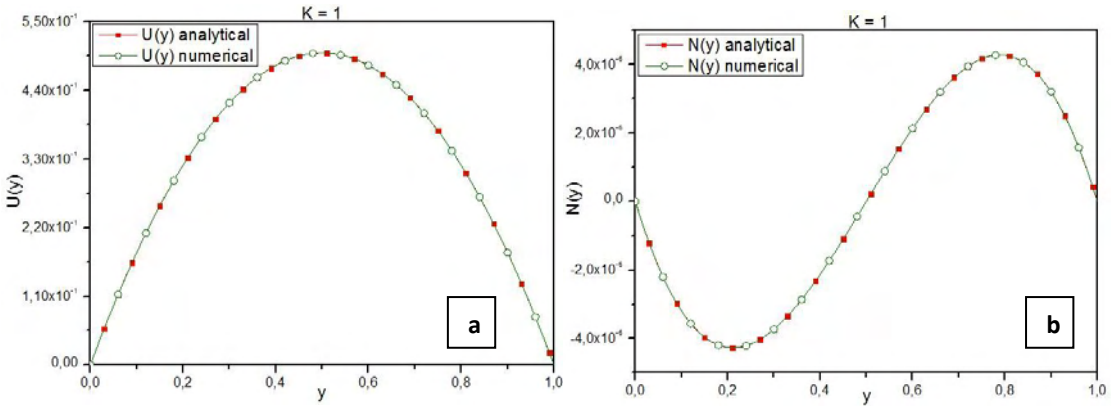

Figure 5.13. Solver and analytical profiles for velocity (a) and microrotation (b), case $K = 1$

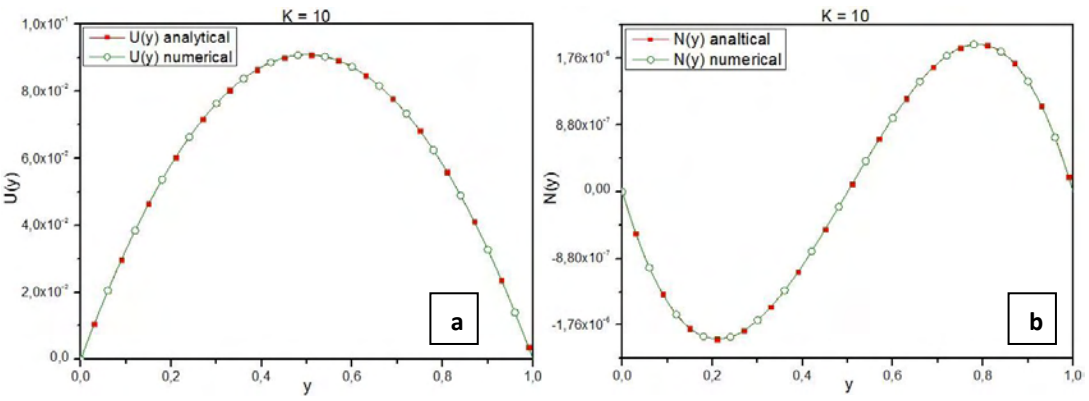

Figure 5.14. Solver and analytical profiles for velocity (a) and microrotation (b), case $K = 10$

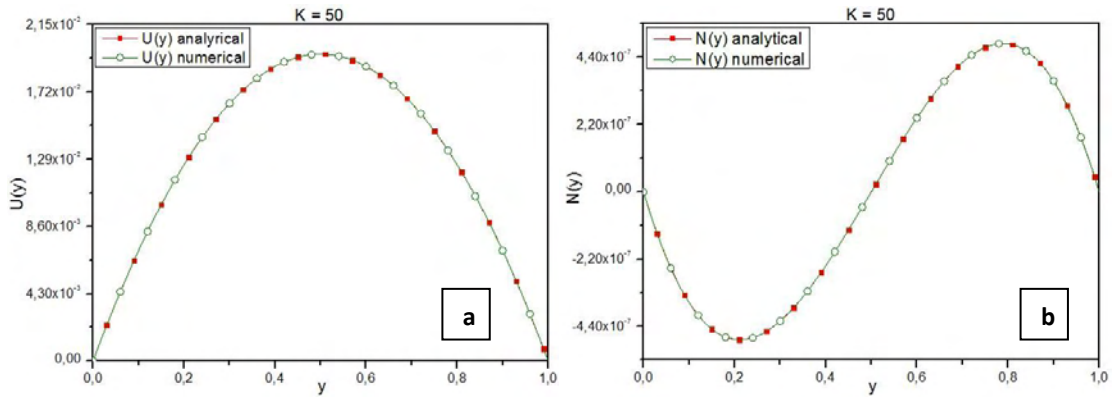

Figure 5.15. Solver and analytical profiles for velocity (a) and microrotation (b), case $K = 50$

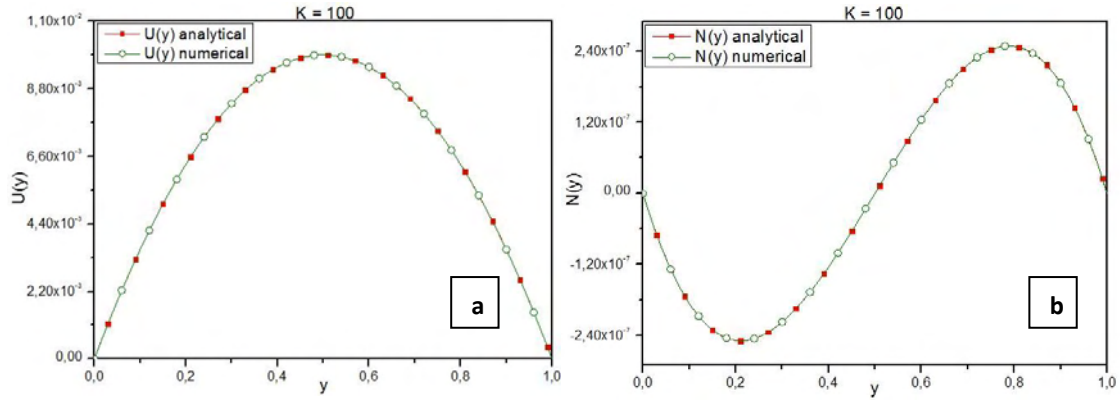

Figure 5.16. Solver and analytical profiles for velocity (a) and microrotation (b), case $K = 100$

All simulations above, are in complete agreement with the numerical results obtained by micropolarFoam solver.

5.4.2 L constant

As a second step to the analysis, a discrete examination of the parameters involved will take place. Following this procedure, L is set to a constant value, L=0.05 while simulations performed for different material parameters K. The effects of vortex viscosity on the fluid, will mainly examined, due to the fact that this is the only parameter affecting K, since kinematic viscosity is constant.

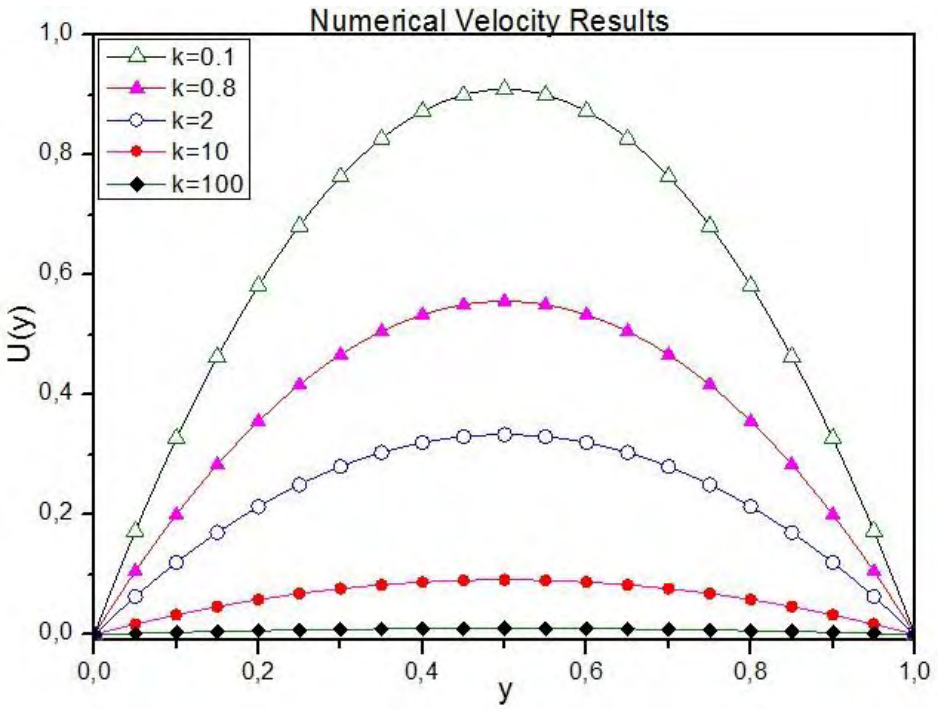

Figure 5.17. Numerical microrotation for different material parameters K.

As it an clearly be seen, the range of parameter K is the same one as in the previous simulations. There is no specific reason for this to happen. Mainly, that range of parameters actually provided with presentable results. The order of magnitude of the parameter nr

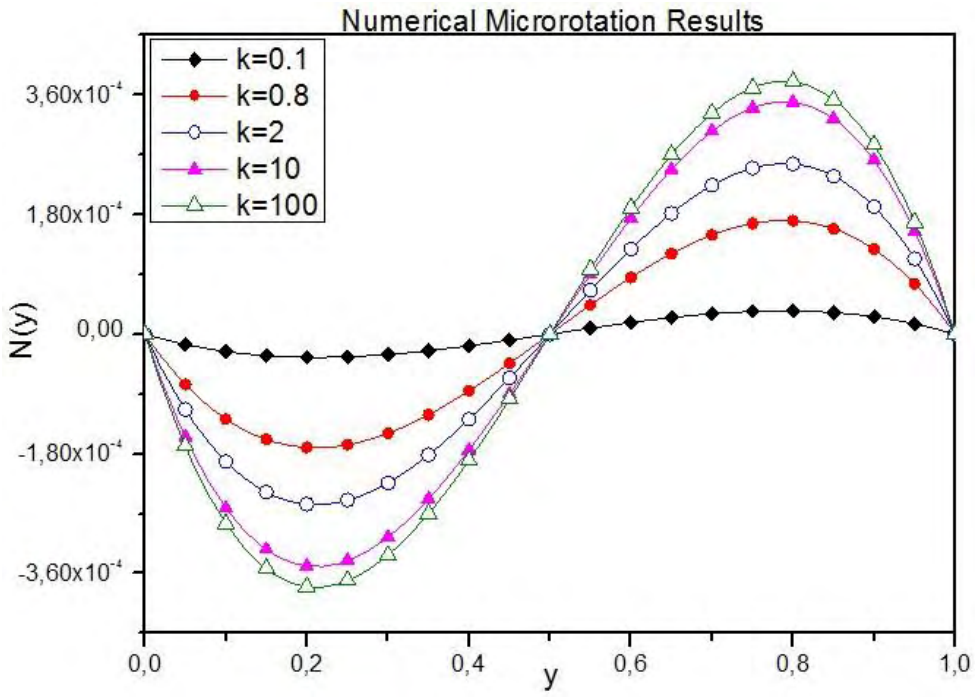

Figure 5.18. Numerical microrotation for different material parameters K.

It is observable the fact that the magnitude of velocity is much wider than that of microrotation. A rushed conclusion, is that the effects of material parameter and thus vortex viscosity k_v, have a greater impact on the velocity response than microrotation. This can be partially explained, if the non-dimensional form of the equation of momentum is taken into account. With this in mind, examining the last term, it is obvious that the parameter N is present.

Another thing is that an increase of K, actually triggers a decrease in the velocity magnitude. A truly fascinating way of describing what really happens is the one that follows. As K increases, also dimnsionless parameter N increases, which contributes to the microrotational phenomena to become more intense. As a result, particles contained in the fluid start rotating with higher angular velocity. A percentage of the actual fluid momentum is used to preserve that rotation and hence the total flow velocity decreases.

Moving along the same lines, microrotation and velocity profiles for different values of K are presented below:

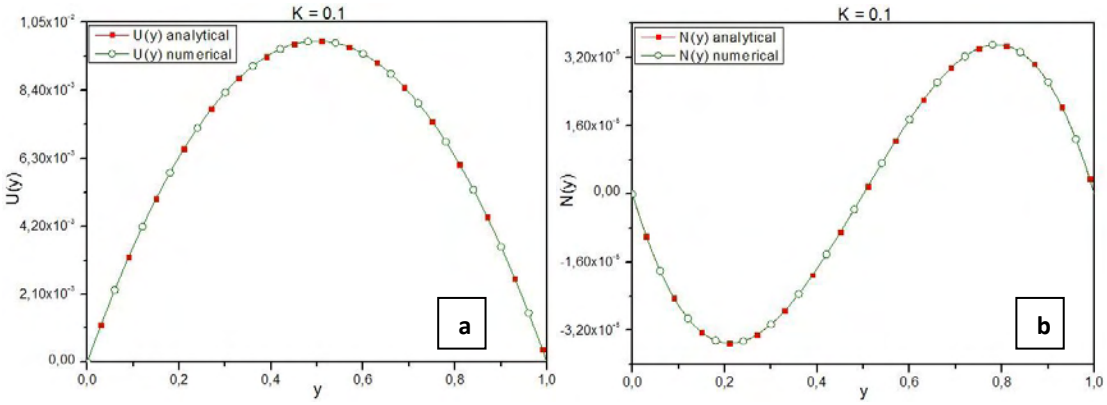

Figure 5.19. Solver and analytical profiles for velocity (a) and microrotation (b), case $K = 0{,}1$

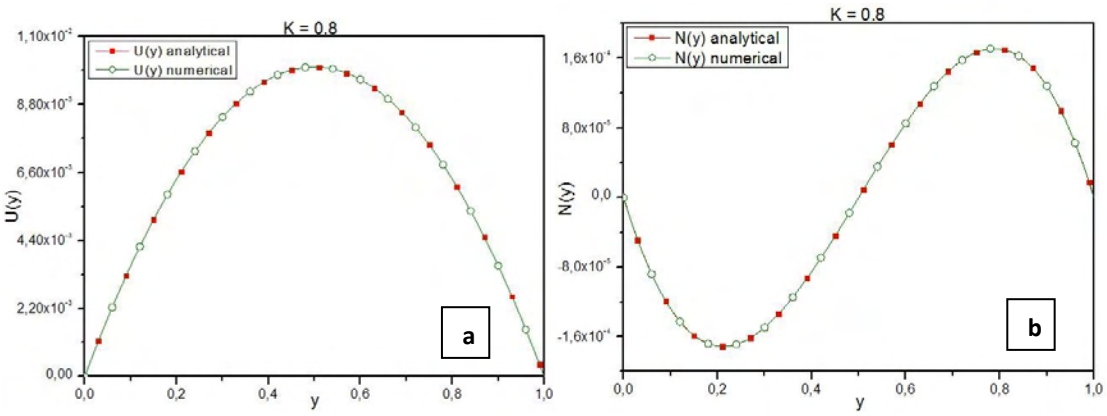

Figure 5.20. Solver and analytical profiles for velocity (a) and microrotation (b), case $K = 0{,}8$

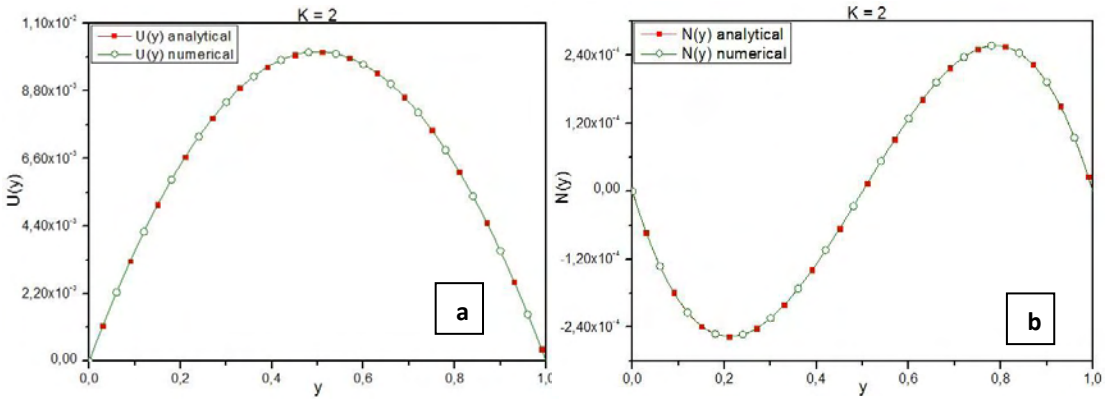

Figure 5.21. Solver and analytical profiles for velocity (a) and microrotation (b), case $K = 2$

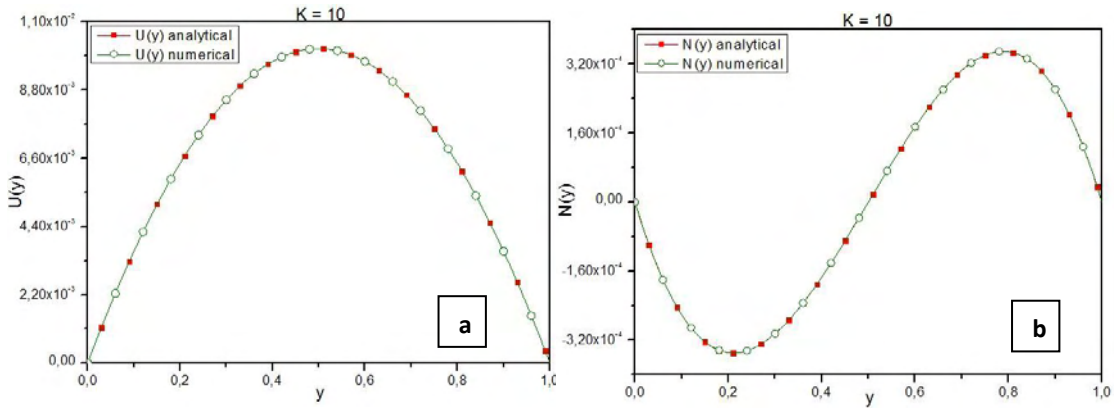

Figure 5.22. Solver and analytical profiles for velocity (a) and microrotation (b), case $K = 10$

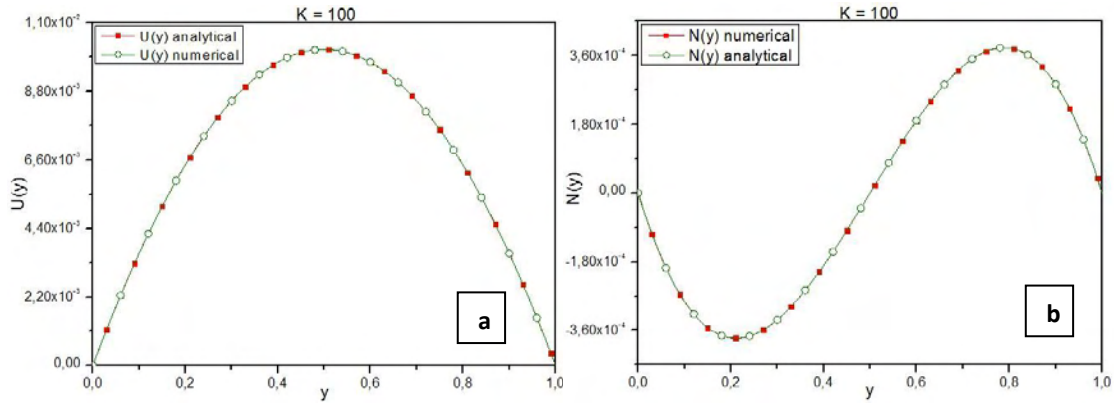

Figure 5.23. Solver and analytical profiles for velocity (a) and microrotation (b), case $K = 100$

As it is clear, numerical and exact results are also in complete agreement

5.4.3 N constant

For the third and final step to the analysis proposed, the effects of the gyration viscosity gu, was thoroughly investigated. Therefore, dimensionless parameter N was set to be a constant, while at the same time all simulations conducted for the parameter L, given a wide range of values.

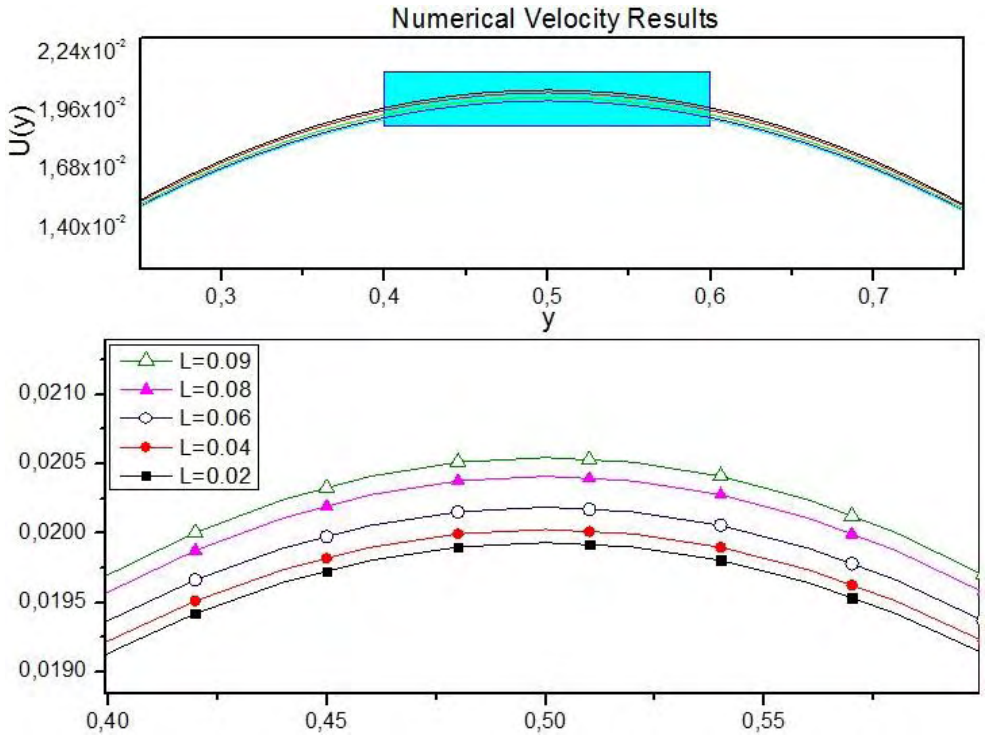

Figure 5.24. Numerical microrotation for different material parameters K.

It is actually observable the fact that, a change in the parameter L, have the opposite impact on the velocity behavior, since an increase of the L contributes to an increase of its magnitude. That change also does not follow the same rate as the one caused by the change in the material parameter K.

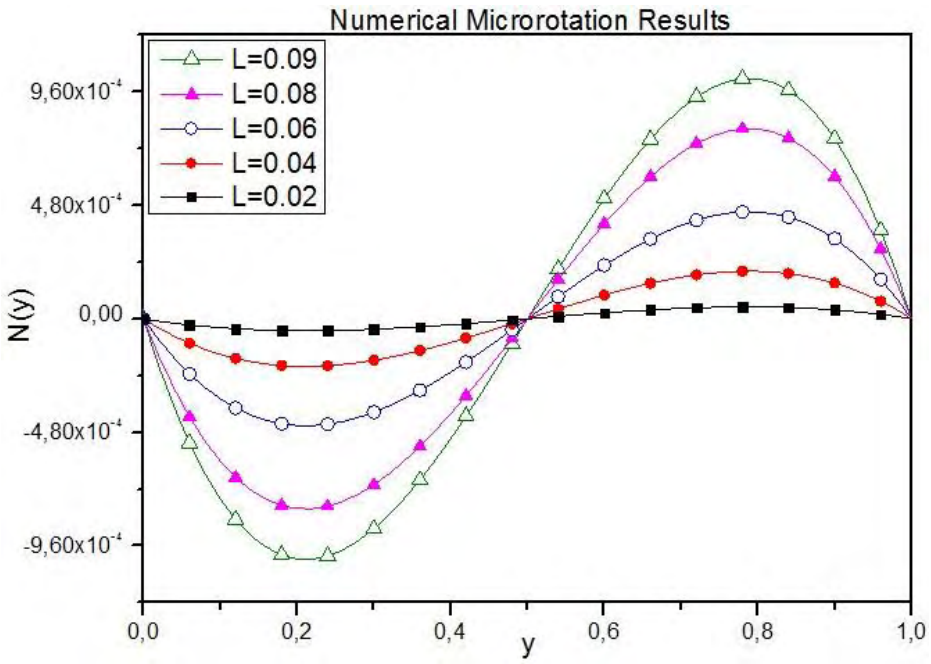

Figure 5.25. Numerical microrotation for different material parameters K.

In addition to the velocity field, it can be seen that an increase in L has also the same effects on microrotation. Among these two profiles it is clear that the magnitude of the velocity field seem to be a lot more restricted than that of microrotation. From the definition of micropolar fluids, it is well known that a part of their velocity originates from the couple stress tensor, introduced by the rotational motion of the particles. It is a reasonable conclusion that in the one dimensional fluid flow, velocity is affected by a small percentage. As it was mentioned above, the magnitude of microrotation seem to be more significant. Thus, it is fair to say that the effects of the parameter L, should be more perceptible on microrotation rather than velocity fields.

As it has been performed previously, all microrotation and velocity profiles obtained by the corresponding solver, are presented below, in contrast to the analytical ones.

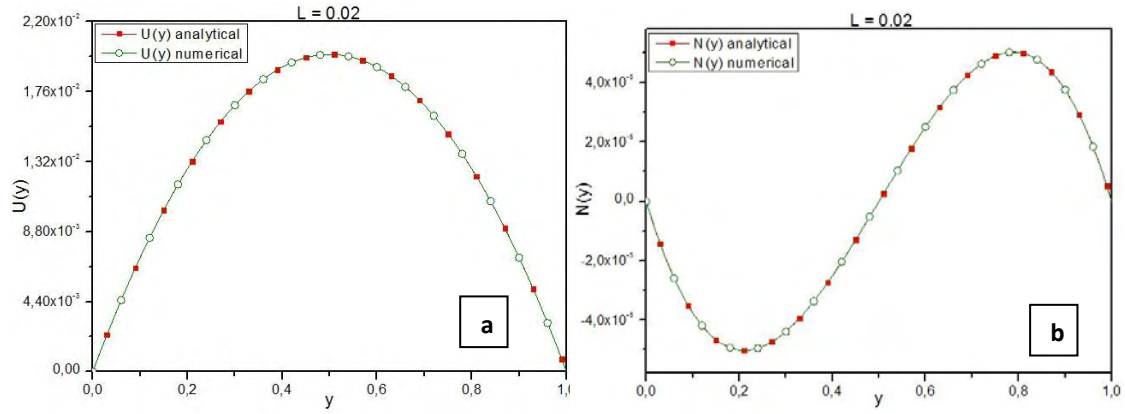

Figure 5.26. Solver and analytical profiles for velocity (a) and microrotation (b), case $L = 0{,}02$

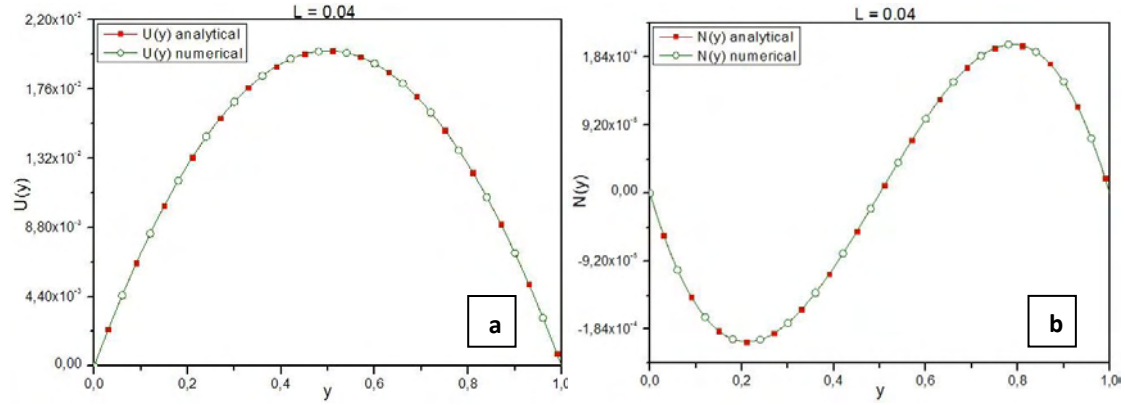

Figure 5.27. Solver and analytical profiles for velocity (a) and microrotation (b), case $L = 0{,}04$

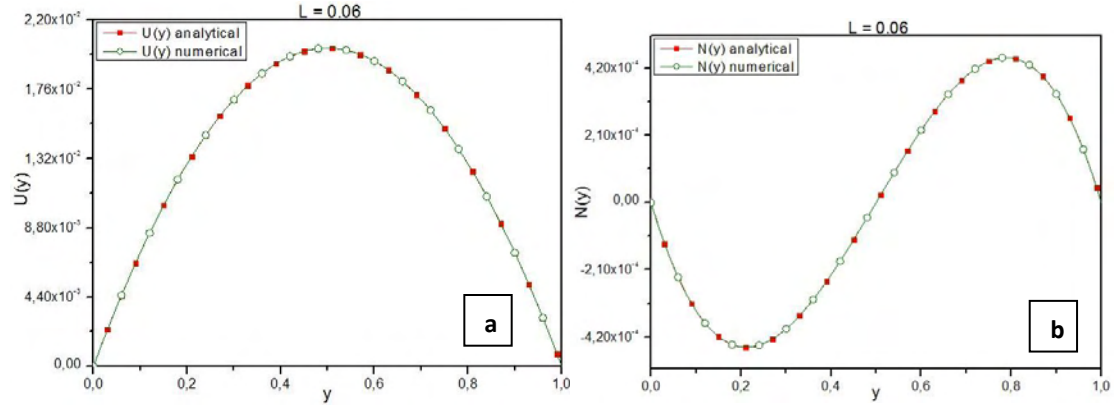

Figure 5.28. Solver and analytical profiles for velocity (a) and microrotation (b), case $L = 0{,}06$

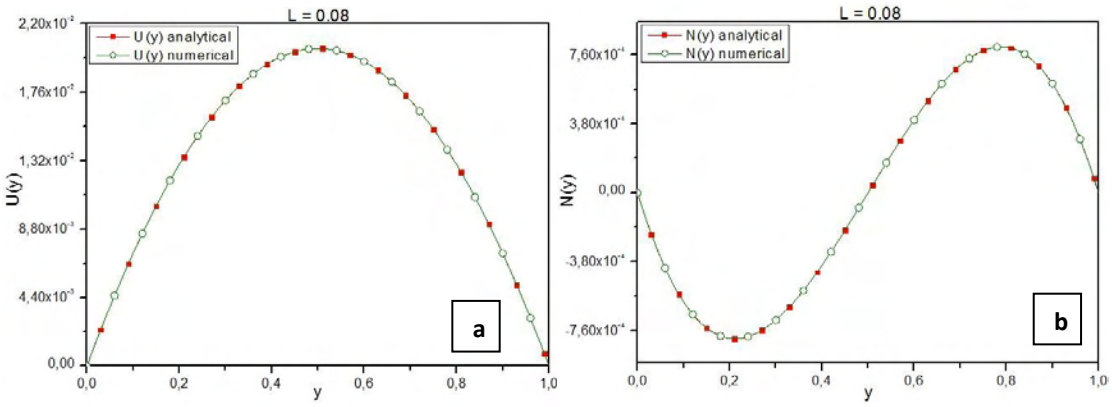

Figure 5.29. Solver and analytical profiles for velocity (a) and microrotation (b), case $L = 0{,}08$

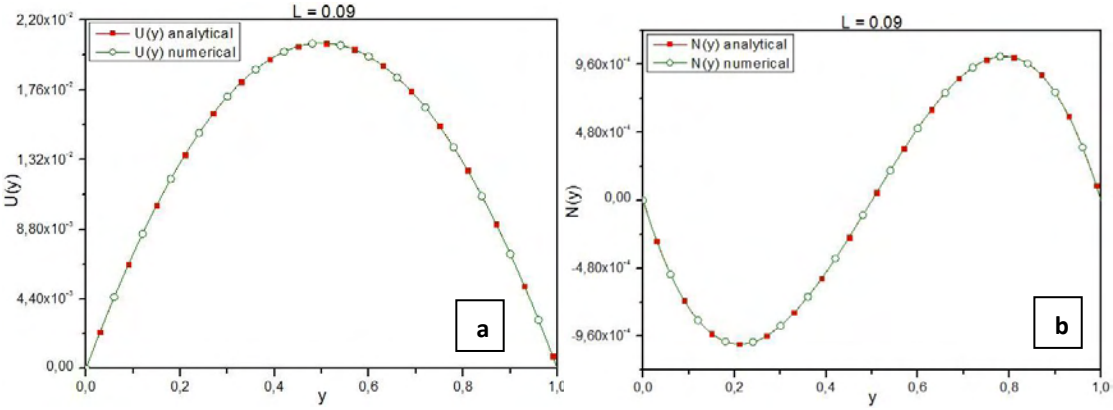

Figure 5.30. Solver and analytical profiles for velocity (a) and microrotation (b), case $L = 0{,}09$

One more time the agreement between the analytical and numerical data, can be perceived.

CHAPTER 6 CONCLUSIONS AND FUTURE SCOPE

6.1 Conclusions

As described in the present Chapter, Couette and Poiseuille flow models were developed, in order to examine the flow behavior of a micropolar fluid, and to test the validity of the micropolarFoam solver through comparison with corresponding analytical data. The process involved the parametric analysis of two micropolar variables, vortex viscosity (k_v) and spin gradient viscosity (γ_v) through several cases. The results were grouped in distinct categories and compared with the exact solutions.

By comparing the numerical and analytical data, a close agreement between them was observed for all cases. Thus, the solver proved valid in predicting the material behavior, for both flow types, and can be trusted for simulating analogous cases.

Based on the parametric analysis, for Couette flow, it was concluded that both vortex viscosity and spin gradient viscosity have a significant effect on flow behavior. Specifically, both an increase in parameter k_v and a decrease in parameter γ_v, resulted in higher absolute values of microrotation. The velocity profile was in turn affected and, especially for microrotation values exceeding $\sim 2{,}5 \times 10^{-2}\ s^{-1}$, exhibited a curved sigmoid profile. A shear stress analysis of this attribute showcased the non-Newtonian behavior of the fluids examined.

Similarly for poiseuille flow the effects of the aforementioned variables are also taking place in both velocity as well as microrotation profiles. More precisely, increasing in both vortex viscosity k_v, as well as spin gradient viscosity γ_v, contributes to a decrase of the velocity magnitude. In contrast to what was previously mentioned, microrotation profile exhibits a unique behavior. Mainly, an increase in vortex viscosity causes also microrotation magnitude

to increase. Last but far from least, a decrease in spin gradient viscosity causes microrotational effects to be more pronounced.

6.2 Implications for future research

Based on the above conclusions, and considering the limitations of the study, future investigations can be proposed, aiming to a more profound and complete understanding of the micropolar fluid behavior:

- ✓ Complete study of the the bell shaped velocity profile acquired, due to the increase of couple stress parameter L, is of great interest.
- ✓ Focused analysis of the Couette flow sigmoid velocity response is required, as well as an accompanying shear stress examination.
- ✓ Experimental results on real micropolar fluids could also aid in the confirmation of the observed phenomena.
- ✓ The micropolarFoam solver provides the option of studying micropolar fluid flow involving thermal aspects. This characteristic was not included in the present project, thus it can form the basis for a future work.
- ✓ Also, the analysis of microropolar flow under the influence of a magnetic field, is a field of great importance. In order to fulfill that goal equations of conservation ought to be transformed including Ampere's, Faraday's and Ohm's law.
- ✓ Another non-considered attribute of the micropolar fluid flow is the microrotation boundary condition. The full implementation of a Rees and Basson type boundary condition on the curved velocity profiles, as well as the derivation of an exact model describing poiseuille flow response, with regard to that change on the boundary, could be the objective for a future study.

CHAPTER 7 REFERENCES

[1] lumen learning.com (https://courses.lumenlearning.com/physics/chapter/11-1-what-is-a-fluid/) accessed on 25/06/2018

[2] Παπανίκας, Δ.Γ. (2010) *Εφαρμοσμένη Ρευστομηχανική*. Αθήνα: Εκδόσεις Media Guru.

[3]Stokes, V.K. (1966) Couple stresses in fluids, *Physics of Fluids,* **9**, 1709–1715.

[4] Devakar, M., Sreenivasu, D., and Shankar B. (2014) Analytical solutions of couple stress fluid flows with slip boundary conditions, *Alexandria Engineering Journal*, **53**, 723–30.

[5] Eringen, A.C. 1964 Simple microfluids, *International Journal of Engineering Science*, **2**, 205-217.

[6] Ashmawy, E.A. (2012) Unsteady Couette flow of a micropolar fluid with slip, *Meccanica*, **47**, 85–94.

[7] Lukaszewicz, G. (1999) *Micro-Polar Fluids. Theory and Applications*. New York: Springer Science+Business Media LLC.

[8] Verma, P.D.S., and Sehgal, M.M. (1968), Couette flow of micropolar fluids, *International Journal of Engineering Science*, **6**, 233-238.

[9] Eringen, A. C. (1966) Theory of micropolar fluids, *Journal of Mathematics and Mechanics*, **16**, 1-18. http://www.jstor.org/stable/24901466?seq=1#page_scan_tab_contents accessed on 25/06/2018

[10] Ariman, T., Turk, M.A., and Sylvester, N.D. (1974) Applications of microcontinuum fluid mechanics, *International Journal of Engineering Science*, **12**, 273-293.

[11] Eringen, A.C. (2001) *Microcontinuum Field Theories II. Fluent Media*. New York: Springer, USA.

[12] Zadravec, M., Hriberšek, M., and Škerget, L. (2008) Boundary element method for micropolar fluid flow in a channel, *WIT Transactions on Modelling and Simulation*, **47**, 33-42. www.witpress.com, ISSN 1743-355X (on-line)

[13] Ramana Murthy, J. V., and Srinivas, J. (2013) Second law analysis for Poiseuille flow of immiscible micropolar fluids in a channel, *International Journal of Heat and Mass Transfer*, **65**, 254–264.

[14] Kim, Y-J., and Kim, T-A. (2004) A study on the plane Couette flow using micropolar fluid theory, *KSME International Journal,* **18**, 491-498.

[15] Kucaba-Piętal, A. (2004) Microchannels flow modelling with the micropolar fluid theory, *Bulletin of the Polish Academy of Sciences-Technical Sciences,* 52, 209-214.

[16] Rees, D.A.S., and Basson, A.P. (1996) The Blasius boundary-layer flow of a micropolar fluid, *International Journal of Engineering Science*, **34**, 113-124.

[17] Jena, S.K., and Mathur, M.N. (1981) Similarity solutions for laminar free convection flow of a hermomicropolar fluid past a nonisothermal flat plate, *International Journal of Engineering Science*, **19**, 1431–1439.

[18] Peddieson, J. (1972) An Application of the Micropolar Fluid Model to the Calculation of Turbulent Shear Flow, *International Journal of Engineering Science*, **10**, 23-32.

[19] Ishak, A., Nazar, R., and Pop I. (2006) Flow of a micropolar fluid on a continuous moving surface, Archives of Mechanics, **58**, 529-541.

[20] Ariman, T., and Cakmak, A.S. (1968) Some basic viscous flows in micropolar fluids, *Rheololgica Acta*, **7**, 236–242.

[21] Openfoam User Guide, Openfoam Foundation, Version 2.1.2 , 2012

[22] Ahmadi, G. (1976) Self-similar solution of incompressible micropolar boundary layer flow over a semi-infinite flat plate, *International Journal of Engineering Science*, **14**, 639-646.